DMD Fast Forward. Published on August 30, 2021 as DOI: 10.1124/dmd.121.000493
This article has not been copyedited and formatted. The final version may differ from this version.

Elucidation of Metabolic and Disposition Pathways for Maribavir in Non-human Primates Through Mass Balance and Semi-Physiologically Based Modeling Approaches

Kefeng Sun and Devin Welty*

Global Drug Metabolism and Pharmacokinetics, Takeda Development Center Americas, Inc., Lexington, MA, USA

*D.W. is currently an employee of Nuventra Pharma Sciences, Broomfield, CO, USA.

Primary laboratory of origin: United States

Conflict of interest: K.S. is an employee of Takeda Development Center Americas, Inc. D.W. was an employee of Shire Human Genetic Therapies, Inc. (now Takeda Development Center Americas, Inc.) at the time of the study.

DMD Fast Forward. Published on August 30, 2021 as DOI: 10.1124/dmd.121.000493
This article has not been copyedited and formatted. The final version may differ from this version.

Running Title: Maribavir DMPK data and modeling in cynomolgus monkeys

Corresponding author: Kefeng Sun

Address: 300 Shire Way, Lexington, MA 02421

Telephone: +1 617 893 8791

Email: kefeng.sun@takeda.com

Co-author email: dwelty@nuventra.com

Text pages: 18

Tables: 5 (+8 supplemental)

Figures: 7 (+29 supplemental)

References: 41

Abstract: 246/250 words

Introduction: 643/750 words

Discussion: 1487/1500 words

ABBREVIATIONS

AUC, area under the curve; b.i.d., twice daily; BDC, bile duct-cannulated; BLQ, below the limit of quantitation; C_{max}, peak concentration; CMV, cytomegalovirus; C_{Obs}, observed plasma concentration at each time point; C_{Pred}, simulated concentration at corresponding time points; CL, clearance; CYP, cytochrome P450; DMPK, drug metabolism and pharmacokinetics; EHR, enterohepatic recirculation; f_m, fraction metabolized; f_m(Gluc), fraction metabolized by direct glucuronidation; GI, gastrointestinal; GUS, β-glucuronidase; HPLC, high-performance liquid chromatography; i.v., intravenous; LC-MS/MS, liquid chromatography–tandem mass spectrometry; LSC, liquid scintillation counters; PBPK, physiologically based pharmacokinetic(s); P_{eff}, effective

DMD Fast Forward. Published on August 30, 2021 as DOI: 10.1124/dmd.121.000493
This article has not been copyedited and formatted. The final version may differ from this version.

permeability; PK, pharmacokinetic(s); p.o., orally; SITT, small intestine transit time; Vd, volume of distribution; V_{ss}, volume of distribution at steady state.

DMD Fast Forward. Published on August 30, 2021 as DOI: 10.1124/dmd.121.000493
This article has not been copyedited and formatted. The final version may differ from this version.

ABSTRACT (246/250)

Maribavir is in phase 3 clinical development for treatment of cytomegalovirus infection/disease in transplant recipients. Previous research, conducted using only intact cynomolgus monkeys, indicated biliary secretion as the primary elimination pathway for maribavir and that maribavir undergoes enterohepatic recirculation (EHR). To clarify the exact mechanisms of maribavir's EHR behavior, we studied its clearance pathways using intravenously administered ^{14}C-labeled maribavir in intact and bile duct-cannulated (BDC) monkeys and constructed a semi-physiologically based pharmacokinetic (semi-PBPK) model. Total radioactivity metabolite profiles in plasma and excreta were quantitatively determined, along with plasma maribavir concentrations. Intact animals showed significantly lower clearance and longer half-lives in both total radioactivity and parent concentration in plasma than BDC monkeys. The primary in vitro and in vivo metabolic pathway for maribavir in monkey is direct glucuronidation; *N*-dealkylation and renal clearance are minor pathways. In BDC monkeys, 73% of dose was recovered as maribavir glucuronides in bile and 3% of dose was recovered as parent in bile and feces; in intact animals' feces, 58% of dose was recovered as parent and no glucuronides were detected. Therefore, EHR of maribavir occurs through biliary secretion of maribavir glucuronides, followed by hydrolysis of glucuronides in the gut lumen and subsequent reabsorption of parent. A semi-PBPK model, constructed from physiological, in vitro, and in vivo BDC monkey data, is capable of projecting maribavir's pharmacokinetic and EHR behavior in intact animals after intravenous or oral dosing, and could be applied to modeling other xenobiotics that are subject to similar EHR processes.

DMD Fast Forward. Published on August 30, 2021 as DOI: 10.1124/dmd.121.000493
This article has not been copyedited and formatted. The final version may differ from this version.

Keywords

physiologically-based pharmacokinetic modeling/PBPK; metabolite disposition; pharmacokinetics; animal/nonclinical/preclinical

SIGNIFICANCE STATEMENT (76/80)

Through both mass balance and semi-physiologically based pharmacokinetic (semi-PBPK) modeling approaches, we mechanistically and quantitatively elucidated maribavir's enterohepatic recirculation (EHR) behavior in monkeys, which occurs via extensive direct glucuronidation, biliary secretion of these glucuronides, luminal hydrolysis of glucuronides to parent, and subsequent reabsorption of the parent. We also identified important drug- and animal-specific parameters that determine the EHR kinetics, and the semi-PBPK model is readily applicable to other drugs that undergo similar metabolic and recirculation mechanisms.

DMD Fast Forward. Published on August 30, 2021 as DOI: 10.1124/dmd.121.000493
This article has not been copyedited and formatted. The final version may differ from this version.

Introduction

Cytomegalovirus (CMV) infection is a serious complication that frequently occurs in recipients of hematopoietic cell or solid organ transplantations (Teira et al., 2016; Hakimi et al., 2017). Treatment with the currently available antiviral therapies has limitations such as drug toxicities and lack of efficacy against drug-resistant strains of CMV (Venton et al., 2014; Kotton et al., 2018). Maribavir (5,6-dichloro-2-(isopropylamino)-1, β-L-ribofuranosyl-1-H-benzimidazole; structure shown in Fig. 1) is a potent and selective, orally bioavailable benzimidazole riboside, and is active against human CMV (Biron et al., 2002; Williams et al., 2003) by blocking nuclear egress of viral capsids through protein kinase UL97 inhibition (Krosky et al., 2003; Hamirally et al., 2009); this mechanism of action stands in contrast to that of DNA polymerase inhibitors (ganciclovir, valganciclovir, cidofovir, and foscarnet) and terminase inhibitor (letermovir) approved for management of CMV (Marty et al., 2017; Kotton et al., 2018). In two phase 2 studies, the majority of solid organ transplant and hematopoietic stem cell transplant recipients with CMV infection achieved viremia clearance following maribavir treatment across all doses studied (400, 800, and 1,200 mg twice daily [b.i.d.]); maribavir exhibited comparable efficacy to valganciclovir and recipients of maribavir experienced low incidences of neutropenia and renal toxicity (Maertens et al., 2019; Papanicolaou et al., 2019). The ongoing clinical development program for maribavir for the treatment of transplant recipients with CMV includes two phase 3 trials (NCT02927067, NCT02931539) (National Library of Medicine, 2020b; National Library of Medicine, 2020a).

The pharmacokinetics (PK), metabolism and disposition of maribavir in nonclinical species have been previously reported (Koszalka et al., 2002). After intravenous or oral administration of ^{14}C-labeled maribavir to both intact rat and monkey, a large proportion of radioactivity (≥89% in rat and up to 57% in monkey) was recovered as unchanged parent in feces, suggesting that biliary excretion may be the predominant route of elimination in these species. Renal clearance was thought to be a minor elimination pathway for maribavir, as indicated by the relatively low percentage dose recovered in urine, at <6% total dose in rat and <18% total dose in monkey; a portion of the radioactivity in urine was attributed to the *N*-dealkylated metabolite VP44469 (4% to 7% total dose in both rat and monkey after intravenous [i.v.] or oral [p.o.] dosing) (Koszalka et al., 2002). VP44469 was also detected in feces of monkeys (11% i.v. dose and 15.5% p.o dose).

DMD Fast Forward. Published on August 30, 2021 as DOI: 10.1124/dmd.121.000493
This article has not been copyedited and formatted. The final version may differ from this version.

Additionally, in these monkeys, a prolonged elimination phase was observed, suggesting that maribavir may undergo enterohepatic recirculation (EHR) before excretion. Biliary clearance was thus deemed the major clearance pathway and oxidative metabolism to VP44469 as the primary metabolic pathway, as indicated by parent and metabolite profiles in plasma, urine, and feces of intact animals (Koszalka et al., 2002).

Characterization of clearance pathways of xenobiotics is commonly evaluated using bile duct-cannulated (BDC) animals, most often in rats, but also larger animal species (Kimoto et al., 2017). The use of only intact animals in previous research (Koszalka et al., 2002) that pointed to biliary secretion being the primary elimination pathway for maribavir confounds determination of the mechanisms of its EHR. A lack of understanding on such mechanisms presents inherent uncertainty pertaining to evaluation of drug–drug interaction risks and factors driving inter-individual variability in maribavir PK. Here we conducted additional definitive studies in monkeys, which were selected due to their relative closeness in physiology to humans, particularly in organs such as liver and the gastrointestinal tract, and present quantitative evidence on the clearance pathways of maribavir in both intact and BDC monkeys, as well as the mechanism of EHR in intact monkeys. We then constructed a semi-physiologically based pharmacokinetic (semi-PBPK) model and demonstrated that the PK of maribavir in intact monkeys could be projected with physiologically based modeling and simulations, and also identified important parameters that drive the extent and kinetics of EHR of maribavir with implications in both non-human primates and humans.

Materials and Methods

Materials

Maribavir was provided by Carbogen AMCIS AG (Bubendorf, Switzerland). ^{14}C-maribavir (2.43 μCi/mg) and d_7-maribavir were provided by Almac Sciences (Craigavon, Northern Ireland, United Kingdom). The chemical and radioactive purity of ^{14}C-maribavir (lot SJJ-0004E-010-01) were >98%. Cryopreserved mixed-gender pooled human hepatocytes (20 donors) and cynomolgus monkey hepatocytes (6 donors) were purchased from BioreclamationIVT (Baltimore, MD, USA). All

DMD Fast Forward. Published on August 30, 2021 as DOI: 10.1124/dmd.121.000493
This article has not been copyedited and formatted. The final version may differ from this version.

buffers and chemicals used in in vitro studies were obtained from Sigma-Aldrich (St Louis, MO, USA) or EMD Chemicals (Gibbstown, NJ, USA).

Animal Preparation and Dosing

Animals. All animal housing and care conformed to the standards recommended by the Guide for the Care and Use of Laboratory Animals as adopted and promulgated by the U.S. National Institutes of Health, and were approved by the Institution's Animal Care and Use Committee or local equivalent. Male cynomolgus monkeys were from the Covance (Princeton, NJ, USA) stock colony. Animals were acclimated to study conditions for 5 weeks prior to dose administration. At dosing, animals weighed between 3.7 and 4.2 kg and were 3–4 years of age. Animals were assigned to either Group 1 (intact, *n* = 3) or Group 2 (BDC, *n* = 3). BDC surgery was done under sterile conditions, using appropriate sedation and inhalation anesthetic. The bile duct was cannulated to allow collection of bile, and a second cannula was placed in the duodenum for the infusion of bile salts replacement solution or other fluids (Kimoto et al., 2017). Further details on animal husbandry and surgical procedures are provided in the Supplemental Materials.

Dosing. ^{14}C-maribavir dosing solution was prepared on the day of dosing. Animals were dosed with 13 mg/kg ^{14}C-maribavir (corresponding to a mean 31.5 µCi/kg; prepared in 7% ethanol and 15% propylene glycol in sterile saline vehicle) via i.v. infusion followed by a 2 mL flush of saline. Details on the preparation and administration of ^{14}C-maribavir are provided in the Supplemental Materials.

Pharmacokinetics and Excretion Balance

Sample Collection. Blood was collected from both groups (intact and BDC) at pre-dose and at 5, 15, and 30 minutes, followed by 2, 6, 24, 48, 72, 96, 120, 144, and 168 hours post-dose. At each time point, blood samples were collected from each animal for radioanalysis and metabolite profiling (1 mL), and plasma extraction (1.5 mL).

Blood samples were processed using standard techniques (Supplemental Materials) and stored at −70 °C until analysis. Urine and feces from both groups and bile (Group 2) were collected at 0–8 and 8–24 hours post-dose and at 24-hour intervals through to at least 168 hours post-dose.

DMD Fast Forward. Published on August 30, 2021 as DOI: 10.1124/dmd.121.000493
This article has not been copyedited and formatted. The final version may differ from this version.

Non-biological samples (cage rinse, cage debris, cage wash, cage wipe, jacket extract, and urine wipe; bile duct cannulae for Group 2) were also collected. Further details can be found in the Supplemental Materials.

Radioactivity Measurement. Radioactivity in samples was measured using Model 2900TR and 2910TR liquid scintillation counters (LSC; Packard Instrument Company, Downers Grove, IL, USA) with Ultima Gold XR scintillation cocktail (PerkinElmer, Waltham, MA, USA) for at least 5 minutes or 100,000 counts. Blood and fecal samples were further processed before analysis (see Supplemental Materials). Other samples (including bile, urine, and plasma) were analyzed directly. To obtain disintegration per minute (dpm) data, scintillation counting data (in cpm) were automatically corrected for counting efficiency using the external standardization technique and an instrument stored quench curve generated from a series of sealed quenched standards. The representative lower limit of quantitation (LLOQ) for radioactivity in blood and plasma were 40 ng-equivalent/g for 72-hour samples in Group 1 and 24-hour samples in Group 2, and 78 ng-equivalent/g for all other blood and plasma samples.

Metabolite Profiling

Radioactivity Extraction Recovery. Extraction recoveries for each excreta were determined as described in the Supplemental Materials.

Plasma. Plasma samples were pooled by group and at each time point. Radioactivity in each pooled sample was determined by LSC. Reconstituted samples (see Supplemental Materials) were analyzed by liquid chromatography–tandem mass spectrometry (LC-MS/MS) with eluent fractions collected at 10-second intervals into 96-well plates containing solid scintillant. Radioactivity in each well was determined using TopCount analysis for the generation of radioactive profiles.

Urine. Pre-dose to 144-hour samples from Group 1 and pre-dose to 48-hour samples from Group 2 were analyzed using LC-MS with eluent fractions collected at 10-second intervals into 96-well plates containing solid scintillant. Radioactivity in each well was determined using TopCount analysis, and radiochemical profiles were generated based on radioactivity counts. Due to low levels of radioactivity, Group 1 samples from 144 hour onwards and Group 2 samples from 48 hour onwards were analyzed by LC-MS/MS only.

DMD Fast Forward. Published on August 30, 2021 as DOI: 10.1124/dmd.121.000493
This article has not been copyedited and formatted. The final version may differ from this version.

Bile*.* Bile samples from Group 2 were pooled by collection interval. Radioactivity in each pooled sample was determined by LSC. Samples were analyzed by LC-MS/MS and radioactivity determined as described above.

Feces. Feces from Group 1 were pooled to generate one 0–120-hour pooled sample. Samples from Group 2 were pooled to generate one 0–72-hour pool. Radioactivity in each pooled sample was determined by LSC. Reconstituted samples (see Supplemental Materials) were analyzed by LC-MS/MS with eluent fractions collected at 10-second intervals into 96-well plates containing solid scintillant. The radioactivity in each well was determined through TopCount analysis, and radioactive profiles were generated based on radioactivity counts.

LC/MS-MS Instrumentation and Conditions. Processed tissue matrices samples were injected with a Shimadzu Nexera SIL-30ACMP autoinjector (10 °C) equipped with a Prominence CBM-20A controller and Nexera LC-30AD pumps (Shimadzu Scientific Instruments, Columbia, MD) that was coupled to a Phenomenex 3 x 4 mm C18 guard column (Phenomenex, Torrance, CA), a Waters Atlantis T3 HPLC column (4.6 x 250 mm, 5 µm; Waters Corporation, Milford, MA) and a LEAP Technologies PAL HTC-xt fraction collector (LEAP Technologies Inc., Morrisville, NC). Mobile phase A was 0.1% formic acid in water and mobile phase B was acetonitrile. MS/MS was performed in a Thermo Fisher Scientific Q Exactive mass spectrometer (Thermo Fisher Scientific, Waltham, MA) with a positive/negative heated electrospray interface (HESI). Detailed LC-MS/MS conditions are listed in Supplemental Materials.

Data Analysis for Mass Balance Study in Monkey

Pharmacokinetic and Mass Balance Analyses. Radioanalysis data tables were generated by Debra, version 6.1.1.87 (LabLogic Systems Ltd., Sheffield, UK). PK parameters for both total radioactivity and plasma concentrations of parent were calculated using Phoenix WinNonlin, version 6.4 or higher (Certara USA, Inc., Princeton, NJ, USA) with a non-compartmental approach.

Metabolite Identification. To describe and quantify peaks, a background of 3 cpm was applied to all chromatograms and the net radioactivity in each peak was expressed as a percent of total radioactivity in the chromatogram or sample. Metabolite profiles in plasma were reported as a

DMD Fast Forward. Published on August 30, 2021 as DOI: 10.1124/dmd.121.000493
This article has not been copyedited and formatted. The final version may differ from this version.

percent total sample radioactivity and as concentration (ng equivalents/g). For excreta, the percent of the administered dose excreted as the component represented by the peak was calculated using the following equation: % of dose = % of radioactivity in peak × % of dose in sample. The percent dose and concentration of the peak were corrected for extraction and reconstitution recoveries, as applicable. M numbers were assigned to peaks as M1 through M6 to match previously reported metabolites along with additional metabolites found in this study assigned up to M17.

Pharmacokinetics of Unlabeled Maribavir in Intact Monkeys After a Single Intravenous or Oral Administration

Male cynomolgus monkeys of Chinese origin aged 3–4 years (*n* = 3) were used. On Day 1 each animal received a single i.v. dose of maribavir at 5 mg/kg in a dose volume of 1 mL/kg in saline containing 10% ethanol and 40% propylene glycol 400. Blood was collected for plasma at pre-dose and at 0.083, 0.25, 0.5, 0.75, 1, 2, 4, 8, 24, 36, 48, 72, and 96 hours post-dose. On Day 15, the same animals received a single oral gavage dose of maribavir at 10 mg/kg in a dose volume of 5 mL/kg with the same vehicle as i.v. dosing. The feeding tube was flushed with 2–3 mL of water after gavage dosing. Blood was collected for plasma once pre-dose and at 0.25, 0.5, 0.75, 1, 2, 4, 6, 8, 24, 36, 48, 72, and 96 hours post-dose. Monkey plasma samples added with the internal standard (d_7-maribavir) were extracted using protein precipitation with organic solvent. Plasma samples were analyzed by high-performance liquid chromatography (HPLC) equipped with an AB SCIEX API 4000™ triple quadrupole mass spectrometer using an electrospray ionization source. Negative ions were monitored in the multiple reaction monitoring mode. Quantitation was determined using a weighted linear regression analysis ($1/concentration^2$) of peak area ratios of the maribavir and internal standard. Additional details are in the Supplemental Materials. Non-compartmental PK analysis was performed for both the i.v. and p.o. arms with Phoenix WinNonlin version 6.4 or higher. The same non-compartmental analysis was also used to calculate PK parameters for previously published studies with maribavir.

DMD Fast Forward. Published on August 30, 2021 as DOI: 10.1124/dmd.121.000493
This article has not been copyedited and formatted. The final version may differ from this version.

In Vitro Metabolism of ^{14}C-maribavir in Hepatocytes

The in vitro metabolism of maribavir was evaluated in cryopreserved hepatocytes isolated from cynomolgus monkeys or humans. ^{14}C-maribavir (10 μM) was incubated in 1 mL at 10^6 cells/mL for 4 hours and metabolite profiles were obtained by analyzing hepatocyte extracts by LC/UV/MS and LC/UV/radioactivity flow detector. Further details are described in the Supplemental Materials.

Permeability of Maribavir Across Caco-2 Cell Monolayer

Caco-2 cell monolayers were grown to confluence on collagen-coated, microporous, polycarbonate membranes in 12-well Transwell plates (Corning Life Sciences, Tewksbury, MA, USA). Transepithelial electrical resistance (TEER) was measured with standard procedures before and after the study (Benson et al., 2013); the average TEER was 553 Ω·cm^2. Compounds tested were maribavir as well as Lucifer Yellow, atenolol, and propranolol. Cells were dosed on the apical or basolateral side and incubated at 37 °C. At 1 and 2 hours, a 200-μL aliquot was taken from the receiver chamber and replaced with fresh assay buffer. Concentrations of test article were determined by LC/MS in ES+ mode. Further details are described in the Supplemental Materials.

Semi-PBPK Model for Disposition of Maribavir in Monkeys

Based on findings from the mass balance study in BDC and intact monkeys, a semi-PBPK model was developed to describe the kinetics of maribavir in plasma, and that of maribavir and its glucuronides in the gastrointestinal (GI) tract. The model construction, parameter estimation, simulations, and sensitivity analyses were conducted with SimBiology® version 5.7 hosted in MATLAB® R2017b with Optimization Toolbox version 8.0 (The Mathworks Inc., Natick, MA, USA).

Model Construction. The semi-PBPK model comprised a compartmental absorption and transit module for the GI tract (Yu and Amidon, 1999) and three systemic compartments (peripheral, central, and liver) (Fig. 2 and Supplemental Fig. 1, and Supplemental Tables 1 and 2). The GI model consists of 13 total luminal compartments: stomach (1 compartment), duodenum (1), jejunum (2), ileum (4), and colon (5). Within each luminal segment, maribavir is absorbed with first-order kinetics, with the rate (k_a) determined by effective permeability (P_{eff}) specific to each segment (see Supplemental Methods and Supplemental Table 3). Human jejunal P_{eff} of maribavir was

DMD Fast Forward. Published on August 30, 2021 as DOI: 10.1124/dmd.121.000493
This article has not been copyedited and formatted. The final version may differ from this version.

estimated from its measured Caco-2 apparent permeability, which was calibrated by assay controls (atenolol and propranolol), and log-linear regression of P_{eff}-P_{app} (apparent permeability) data (see Supplemental Methods, Supplemental Table 4, and Supplemental Fig. 2). Monkey jejunal P_{eff} was assumed to be the same as human. The observed plasma concentrations were assumed to resemble that of the central compartment. The liver compartment was necessary to model the first-pass metabolism as well as the metabolic and biliary elimination of maribavir as glucuronides or others. Luminal conversion of maribavir glucuronides to maribavir was assumed to occur in the distal small intestine and throughout the colon, and that the entirety of regenerated maribavir is available for reabsorption. All system parameters such as intestinal transit times, intestinal radii, and hepatic blood flow were obtained from literature; drug-specific parameter values were either determined in in vitro studies, measured from excreta contents of the BDC group, or estimated from the plasma concentration time course of the BDC group (Table 1 and Supplemental Table 5). Further details are described in the Supplemental Materials.

Parameter Estimation. Four systemic PK parameters (drug clearance from the liver compartment [Drug_Liver_CL], central to peripheral transfer clearance [Drug_Q12], and volumes of the central and peripheral compartments [Drug_Vc_Ref and Drug_Vp_Ref]) were estimated by fitting the BDC group plasma concentrations of maribavir to the central compartment concentration using the constrained non-linear least-squares method. The observed plasma concentrations were pooled at each time point (due to BDC animal #2 having fewer available plasma concentrations) and an exponential error model was chosen. Termination tolerance on the estimated coefficients, objective function value, and first-order optimality were all set at 10^{-12} and maximum iterations at 5,000. The performance of fitting was evaluated and confirmed with coefficient of variation (%CV) of the estimated values (Table 1) and the observed data versus predictions and residuals versus predictions plots (Supplemental Fig. 3A and B).

Model Qualification and Simulations. By varying the doses and routes of administration (i.v. bolus or oral), plasma concentration versus time profiles of maribavir in intact animals were simulated, using the semi-PBPK model, for 13 mg/kg i.v. dosing in mass balance study, 5 mg/kg i.v. and 10 mg/kg p.o. dosing in the unlabeled PK study, and for 20, 60, and 180 mg/kg/day

DMD Fast Forward. Published on August 30, 2021 as DOI: 10.1124/dmd.121.000493
This article has not been copyedited and formatted. The final version may differ from this version.

reported in a historical toxicokinetic study (Koszalka et al., 2002). The SUNDIALS solver was used and absolute tolerance set at 1.0^{-9}; dimension analysis was enabled. Observed data were overlaid to and graphically compared with simulated results. Quantitative comparisons included area under the curve (AUC) (i.v. and p.o.), peak concentration (C_{max}), time to peak concentration (T_{max}), and bioavailability (p.o. only) as well as the median percent predictive error (%PE, defined by Equation 1):

$$\%PE = \frac{C_{\mathrm{Pred}} - \bar{C}_{\mathrm{Obs}}}{\bar{C}_{\mathrm{Obs}}} \times 100\% \qquad \text{Equation 1}$$

where $\bar{C}_{\mathrm{Obs}}$ is the mean observed plasma concentration at each time point and C_{Pred} is the simulated concentration at corresponding time points. A median %PE between −50% and 100%, which corresponds to the predicted value being within the two-fold range of the mean observed value, generally indicates a PBPK model with good predictability (Khalil and Laer, 2014; Zhou et al., 2016; Matsumoto et al., 2019).

Sensitivity Analysis. Sensitivity analyses of the plasma PK time profile of maribavir after a single 10 mg/kg p.o. administration with respect to parameters in Table 1 were conducted within SimBiology® by varying each designated parameter within a range around the final model value. Four drug- and system-specific parameters, i.e. P_{eff} in the jejunum, clearance from the liver compartment (Drug_Liver_CL), fraction metabolized (f_m) by the direct glucuronidation pathway (f_m(Gluc)), and transit rate within the colonic lumen (k_T_Colon), were found to confer the most impact on the exposure of maribavir.

Results

Metabolic Pathway of ^{14}C-maribavir After a Single Intravenous Bolus Injection to Cynomolgus Monkeys

Following a single 13 mg/kg i.v. dose of ^{14}C-maribavir to male intact monkeys (Group 1), radioactivity in plasma declined after the first time point (5 minutes) and was below the limit of quantitation (BLQ) after 72 hours (Fig. 3A and Supplemental Fig. 4). Mean clearance and terminal

DMD Fast Forward. Published on August 30, 2021 as DOI: 10.1124/dmd.121.000493
This article has not been copyedited and formatted. The final version may differ from this version.

half-life ($t_{1/2}$) for radioactivity in plasma was 1,700 g/h and 19.7 hours, respectively (Table 2). In BDC monkeys (Group 2), after a single 13 mg/kg i.v. dose of ^{14}C-maribavir, radioactivity in plasma declined more rapidly than in Group 1, and was BLQ by 24 hours post-dose (Fig. 3A and Supplemental Fig. 4). In Group 2, the clearance of radioactivity in plasma, at 3,010 g/h, was 77% higher than in Group 1; mean $t_{1/2}$ (2.71 hours) was also much shorter than in Group 1 (Table 2).

The major route of elimination of radioactivity in intact monkeys (Group 1) was via feces, with a mean of 75.2% excreted over 336 hours (Fig. 4A). The mean percentage of radioactivity recovered in urine was 14.1% over 336 hours, with the majority of the radioactivity being excreted by 96 hours. The major route of elimination of radioactivity in BDC monkeys (Group 2) was via bile, with a mean of 84.0% excreted over 168 hours post-dose (Fig. 4B). The mean percentages of the administered radioactivity recovered in urine and feces from BDC monkeys were 5.16% and 2.36%, respectively, over 168 hours. The majority of the radioactivity was excreted by 8 hours post-dose; radioactivity levels in bile were BLQ by 72 hours. The mean combined radioactivity in all non-biological samples was less than 5% of dose for both groups. The mean overall recovery of the dose administered was 95.3% and 97.0% in Groups 1 and 2, respectively.

Pharmacokinetics of ^{14}C-Maribavir in Plasma After Intravenous Bolus Injection to Monkeys

The PK profiles of maribavir in plasma after a single i.v. bolus administration in monkeys are depicted in Fig. 3B (individually plotted in Supplemental Fig. 4) and the PK properties are listed in Table 3. The mean clearance in intact animals (2.99 L/h) was about half of that in BDC animals (5.72 L/h). Intact animals also displayed a much more pronounced terminal phase (mean $t_{1/2}$ of 12.5 hours) than their BDC counterparts ($t_{1/2}$ 2.5 hours). These results were consistent with the aforementioned observations on total radioactivity (Table 2, Fig. 3A, and Supplemental Fig. 4).

Identification and Quantitation of Metabolites of ^{14}C-Maribavir in Monkey Plasma and Excreta

Eleven metabolites of maribavir (Table 4; structures shown in Supplemental Table 6; MS/MS spectra and structural assignment for each fragment ion detailed in Supplemental Figs 5–17) were tentatively identified from the collected biological matrices (reconstructed ion chromatograms and

DMD Fast Forward. Published on August 30, 2021 as DOI: 10.1124/dmd.121.000493
This article has not been copyedited and formatted. The final version may differ from this version.

radiochromatograms detailed in Supplemental Figs 18–27). A comprehensive illustration of metabolic pathways of maribavir in monkeys is depicted in Fig. 5. For plasma from both intact and BDC animals, parent was the predominant species associated with radioactivity in circulation at almost all time points, accounting for more than 80% of all radioactivity in plasma (Supplemental Table 7). Much lower concentrations of the *N*-dealkylated metabolite M4 (also known as VP44469 (Goldwater et al., 2008)), two glucuronides of M4 (M7 and M17), and two direct glucuronides of parent (M11 and M12) were also detected at some time points in plasma, but the combined percentages of these metabolites generally amounted to less than 15% of circulating radioactivity. At all time points, no individual metabolite accounted for more than 8% of circulating radioactivity in plasma.

A pronounced difference in the composition of metabolites in excreta was observed between intact and BDC animals. In the excreta from intact animals (Group 1), the bulk of radioactivity (58%–60% of the administered dose) was recovered as the unchanged parent compound in feces. The dealkylation product, M4, generated from cytochrome P450 (CYP)-mediated pathways (Koszalka et al., 2002; Goldwater et al., 2008), represented approximately 9% of the total dose in pooled feces; in pooled urine, M4 and its glucuronides in total also comprised up to 9% of administered dose (Table 4). Metabolites M11 and M12, direct glucuronides of maribavir, were present in the urine from intact animals at a combined 3% total dose. No maribavir glucuronides nor M4 glucuronides were detected in the feces of intact animals. In contrast, in BDC animals, the majority (73%) of administered dose was recovered as M11 and M12 in bile. Biliary secretion of the parent compound itself only accounted for a small fraction (1.3%) of the dose; the amount of parent in pooled feces of BDC animals was also small (1.5% total dose). In the urine of BDC monkeys, 0.22% of the dose was identified as parent, and M4 and its glucuronides combined were 3.6% of administered dose; thus, both values were numerically lower than the respective 0.89% and >7.1% observed in intact animals (Table 4). M15, a dechlorinated and cysteine-conjugated metabolite, was unique to BDC animals and detected only in bile samples, but it cumulatively represented only 1.4% of the total dose. Two other metabolites were also detected at low amounts: metabolite M5,

DMD Fast Forward. Published on August 30, 2021 as DOI: 10.1124/dmd.121.000493
This article has not been copyedited and formatted. The final version may differ from this version.

with oxidation on N-isopropyl, at <0.43% of the total dose, and M2, the deribosylated and glucuronidated metabolite, at <2.5% of the total dose in both groups (Table 4).

In Vitro Metabolism of Maribavir in Cryopreserved Hepatocytes

After a 4-hour incubation with cynomolgus monkey hepatocytes, ^{14}C-maribavir was almost completely metabolized. Major metabolites included M11 and M12 (direct glucuronides), as well as the multiple glucuronides to M4 (*N*-dealkylation). M11 and M12 combined and M4-glucuronides represented 85.3% and 10.4% of total radioactive peak areas, respectively. After a 4-hour incubation with human hepatocytes, parent, M4, M4-glucuronides, and one of the direct glucuronides to parent (M11 or M12) represented 47.2%, 31.1%, 10.2%, and 10% of total radioactive peak areas, respectively; M4 plus its glucuronides and M11/M12 represented 78% and 19% of metabolism of maribavir in human hepatocytes. Other metabolites were present at trace amounts (each <1%) for both monkey and human hepatocyte incubations.

Permeability of Maribavir Across Cultured Caco-2 Cell Monolayer.

The apparent permeability for maribavir in the apical-to-basolateral and basolateral-to-apical directions were 5.9×10^{-6} cm/s and 33.7×10^{-6} cm/s, respectively. The apical-to-basolateral apparent permeability for Lucifer Yellow, atenolol, and propranolol were 0.26×10^{-6} cm/s, 0.36×10^{-6} cm/s, and 17.1×10^{-6} cm/s, respectively.

Semi-PBPK Model for EHR of Maribavir in Monkeys

Parameter Estimations. The final PK parameters derived from fitting the semi-PBPK model to the observed plasma concentration over time from BDC monkeys (Group 2) are listed in Table 1 (see also Supplemental Results and Discussion). The fitted concentration and observed data over time are shown in Fig. 6A; observed versus predicted and residual versus prediction graphs in Supplemental Fig. 3A and B. The overall residual error of the fitting was 0.256.

Simulations for Intravenous Bolus Dosing of Maribavir in Monkeys. Two f_m(Gluc) values were used in simulations: 0.853 from the in vitro hepatocyte data or 0.728 from the metabolite content in the pooled bile of BDC monkeys. Graphic results for simulated and observed plasma concentrations of maribavir in intact monkeys administered with ^{14}C-maribavir (13 mg/kg mass

equivalent) or 5 mg/kg unlabeled maribavir are shown in Fig. 6B and derived PK properties in Table 5. At both doses, the simulations were able to predict the initial phase of rapid decline (0 to 4–6 hours post-dose) as well as the prolonged terminal phase (after 4–6 hours post-dose) in maribavir plasma concentrations. The observed inter-group difference in predictability of the time course could potentially be explained by the contribution of glucuronidation in the overall clearance: simulation with f_m(Gluc) = 0.853 and 0.728 seemingly presented a better match for terminal phase and AUC for the 13 mg/kg i.v. group and the 5 mg/kg i.v. group, respectively. The median %PE for 13 mg/kg i.v. were 12% at f_m(Gluc) = 0.853 and −49% at f_m(Gluc) = 0.728; median %PE for 5 mg/kg i.v. was 81% at f_m(Gluc) = 0.853 and 30% at f_m(Gluc) = 0.728. The overall median %PE for all available PK data points after i.v. dosing in intact animals was 38% at f_m(Gluc) = 0.853 and 1% at f_m(Gluc) = 0.728. The f_m(Gluc) of 0.728 was eventually selected for all follow-up simulations because it is a direct in vivo measurement and also produced a slightly better overall %PE and predictive profile across the concentration range (Supplemental Fig. 28).

Simulations for Oral Dosing of Maribavir and Qualification of the Semi-PBPK Model in Monkeys. The semi-PBPK model with f_m(Gluc) = 0.728 was able to capture the plasma concentration profiles after a single 10 mg/kg p.o. dose to intact monkeys (Fig. 6C) during both the apparent absorption and terminal phases; median %PE was 38%. Derived PK parameters such as AUC, C_{max} and bioavailability (F) were also well predicted (Table 5). The fraction absorbed (F_a) was estimated at 67% after a single p.o. dose. For multiple dosing, observed plasma profiles of maribavir after b.i.d. dosing at 10, 30, and 90 mg/kg (20, 60, and 180 mg/kg/day total) were all reasonably characterized by model predictions (Fig. 6 D and E) and median %PE were 17%, 20%, and 29% for 10, 30, and 90 mg/kg b.i.d. regimens, respectively.

Sensitivity Analyses. Important determinants for systemic exposure of maribavir after a single p.o. dose include the overall f_m(Gluc) (Fig. 7A), k_T_Colon (Fig. 7B), P_{eff} in the small intestine (Supplemental Fig. 29A; Supplemental Results and Discussion), and Drug_Liver_CL (Supplemental Fig. 29B). The AUC in plasma could be increased by increasing f_m(Gluc), increasing colonic transit time, increasing P_{eff}, or decreasing Drug_Liver_CL. Of note, a change in Drug_Liver_CL would result in little change in the terminal slope; the latter is largely determined by

DMD Fast Forward. Published on August 30, 2021 as DOI: 10.1124/dmd.121.000493
This article has not been copyedited and formatted. The final version may differ from this version.

f_m(Gluc), k_T_Colon, and, to a lesser degree, P_{eff}. This phenomenon demonstrates the prominent effects of the EHR on systemic exposure of maribavir in monkeys. Systemic C_{max}, on the other hand, is largely driven by P_{eff} and Drug_Liver_CL but not by the other two major parameters. Variations in other parameters, such as small intestine transit time (SITT), rate of hydrolysis of maribavir glucuronides (Gluc_k_hydrolysis), and intercompartmental drug clearance (Drug_Q12), also lead to changes in plasma exposures of maribavir, but their effects are comparatively minor (Supplemental Fig. 29C–E).

Discussion

We thoroughly investigated the biotransformation and clearance pathways of maribavir in cynomolgus monkeys by utilizing intact and bile-duct cannulated models and in vitro approaches. We demonstrated that in monkeys, maribavir is primarily metabolized by direct glucuronidation and that these glucuronides, after biliary secretion, can be efficiently converted to maribavir and reabsorbed into circulation. Consequently, in intact animals, maribavir present in gut lumen after i.v. dosing resulted in a higher apparent volume of distribution (Vd) than in BDC animals (Table 2). Conversely, in the BDC group, both the faster clearance due to lack of recirculation and a smaller Vd led to a much shorter maribavir $t_{1/2}$ (Fig. 3B and Table 2). A semi-PBPK model was then constructed with data from literature, in vitro and in vivo BDC animals (Table 1 and Supplemental Table 5); this qualified model captured the pharmacokinetics of maribavir in intact monkeys after either i.v. or oral administration and also identified important compound- and animal-related parameters that impact the kinetics of recirculation.

A previous mass balance study in intact monkeys (Koszalka et al., 2002) found a large amount of radioactivity in feces as parent and concluded that maribavir was secreted into the bile and subsequently reabsorbed. It may be tempting to claim that the biliary secretion was facilitated through efflux of parent compound at the canalicular surface of hepatocytes (Patel et al., 2016). In this study, we clarified that biliary section of parent drug was actually a minor pathway despite maribavir being a substrate of efflux transporters (Welty et al., 2018; Song et al., 2019a), and that the biliary secretion is primarily facilitated through various glucuronides of maribavir. We assumed

DMD Fast Forward. Published on August 30, 2021 as DOI: 10.1124/dmd.121.000493
This article has not been copyedited and formatted. The final version may differ from this version.

that the liver is the primary organ where glucuronidation of maribavir occurs because of the low percentage of total (%dose) recovered in urine as maribavir glucuronides (Table 4) and because maribavir is an in vitro substrate of human UGT1A1, UGT1A3, and UGT2B7 (unpublished data). Additionally, in monkeys the liver expresses the highest levels of UGT1A and UGT2B, and displays much stronger glucuronidation activities than do other organs (Albert et al., 2000).

The hydrolysis of glucuronides by the gut microbiome is mediated by β-glucuronidases (GUSs) (Zenser et al., 1999). Bacterial GUSs are known to metabolize glucuronides, which occurs in the lumen of distal ileum and colon (Zenser et al., 1999; Koppel et al., 2017; Tropini et al., 2017). The degradation rate constant of typical *O*-glucuronides by colonic microbiota was estimated at 3.1 h^{-1} in monkeys (derived from (Kim and Jin, 2001; Peters, 2012; Sender et al., 2016); see Supplemental Methods). Even considering uncertainty related to different *O*-glucuronide substrates, the GUS-mediated hydrolysis of glucuronides is still significantly faster than the typical colon transit rate in monkeys (0.042 h^{-1}). After biliary secretion likely mediated by transporters (Patel et al., 2016), maribavir glucuronides travel along the GI lumen to the distal ileum and colon, where GUS-expressing bacteria reside. Indeed, between intact and BDC groups, maribavir plasma concentration time courses diverged between 2 and 6 hours post-i.v. dose (Fig. 3B), matching SITT around 2.7 hours in monkeys (Table 1) (Ikegami et al., 2003). It is of note that the “second peak” of plasma concentration commonly observed for other enterohepatically recirculated compounds was not apparent in the mass balance study (Fig. 3), but was evident in another study (Fig. 6B, 5 mg/kg group) at ~8-hour post-dose; this may be attributed to different blood collection schedules of the two studies.

Given the abundant knowledge of GI tract physiology and its successful usage for modeling drug absorption (Yu and Amidon, 1999), we created a customized semi-PBPK model to integrate in vivo and in vitro data for maribavir and its metabolites in monkeys. A previous PBPK model (Wu, 2012) provided a theoretical basis on the impact of glucuronide bioconversion to PK of the aglycone, especially on the latter’s terminal half-life and bioavailability; however, the model did not consider the difference between the small and large intestine (radii, transit time, and location of the gut microbiota), nor were any measured drug or metabolite PK data included to validate the model.

DMD Fast Forward. Published on August 30, 2021 as DOI: 10.1124/dmd.121.000493
This article has not been copyedited and formatted. The final version may differ from this version.

In our work, the GI tract was compartmentalized with representations of different physiology within each segment; in particular, the colon into five compartments to represent the spatial and temporal transit of both maribavir and its glucuronides. This compartmentalization is a simplification of the continuous transit model of drug-containing intestinal fluid that requires much more complex mathematical methods, but is also an improvement over models that did not focus on drug absorption and transit in the colon (Yu and Amidon, 1999; Wu, 2012). As a result, the novel semi-PBPK model is able to characterize the segmental (re)absorption of maribavir after either i.v. or p.o. dosing (Supplemental Table 8). Of note, we did not model drug dissolution because of maribavir's aqueous solubility profiles (0.8 mg/mL in water; 34 and 0.67 mg/mL at pH 3 and 6.6, respectively; unpublished data) and because all dosing formulations were in solution; it was also deemed unnecessary to model metabolism of maribavir within the gut wall because of its high permeability and low CYP-driven intrinsic clearance.

In the semi-PBPK model, four parameters were fitted from the BDC animals' parent PK profiles, whereas all other parameters were either directly from literature or derived from in vitro data or in vivo metabolite data from BDC animals. We then demonstrated that this model captured PK profiles in intact monkeys following single i.v., single p.o., or multiple p.o. administrations. Through sensitivity analyses, we identified important parameters determining the AUC, C_{max}, and terminal elimination rate for maribavir in plasma. The terminal slope is mostly driven by f_m(Gluc) and colon transit rate, rather than by hepatic clearance, although the latter still drives the overall exposure of maribavir in terms of AUC and C_{max}. In contrast, SITT and luminal hydrolytic rates of the maribavir glucuronides have much smaller impacts on maribavir exposure in intact animals (Supplemental Fig. 29). This semi-PBPK model is applicable to other xenobiotics exhibiting similar phenomena, aiding in comprehension and projection of EHR in preclinical/translational settings; in particular, sensitive drug- and species-related parameters should be given the most attention (Fig. 7 and Supplemental Fig. 29).

The fraction metabolized (f_m) contributed by each potential clearance pathway is a key drug metabolism and PK metric for small molecular drug candidates due to its implications in the lead optimization process, species translation, clinical study design, and population variability (Di,

2017). For maribavir, it is clear that a higher f_m(Gluc) will lead to more apparent EHR and higher systemic exposure, as more glucuronides will be generated by hydrolysis in the gut lumen and releasing parent drug for reabsorption. The f_m(Gluc) for maribavir in monkey was high at 73% (in vivo) to 85% (hepatocytes), but only around 20% in human hepatocytes. Hence, in theory, humans should demonstrate a less significant EHR compared with monkeys. Indeed, in humans, ^{14}C-maribavir was primarily eliminated through CYP3A-mediated metabolism with renal clearance as a minor pathway; M4 (VP44469) was the principal metabolite observed in urine and feces (Song et al., 2019b) and no direct glucuronides were detected in feces (unpublished data). No apparent recirculation was observed for plasma profiles of maribavir in humans (Wang et al., 2003) and the $t_{1/2}$ observed in humans, at around 3.5–7 hours (Wang et al., 2003; Ma et al., 2006; Goldwater et al., 2008; Song et al., 2019a), also mimicked sensitivity analyses wherein f_m(Gluc) was changed to 20% (Fig. 7C), at which scenario the simulated $t_{1/2}$ became ~6 hours (versus ~15 hours at f_m(Gluc) of 80%). The much lower f_m(Gluc) for maribavir in humans thus confers not only a lower risk of drug–drug interaction for increased systemic concentrations of maribavir and its glucuronides when maribavir is co-administered with inhibitors of canalicular efflux transporters (Zamek-Gliszczynski et al., 2014; Patel et al., 2016) or with inhibitors of UDP-glucuronosyltransferases (UGTs) (Zhang et al., 2015), but also less risk of reduced systemic concentrations of maribavir due to potential induction of UGTs (Court, 2010). In addition, inter-subject variabilities in intrinsic factors such as UGT polymorphism (Court, 2010) and colonic transit time (Vinarov et al., 2021) should have less impact on maribavir exposure in humans due to the lower f_m(Gluc). Therefore, for drugs that undergo EHR through formation and degradation of conjugative metabolites, species differences in metabolism should be considered when extrapolating PK properties from nonclinical species to humans (Kimoto et al., 2017).

In conclusion, using both intact and bile duct-cannulated animals to measure the metabolism and disposition of maribavir, we quantitatively demonstrated that the primary in vivo clearance pathway of maribavir in monkeys was direct glucuronidation. In intact animals, maribavir undergoes enterohepatic recirculation through biliary secretion of maribavir glucuronides, followed by hydrolysis of these glucuronides in the gut lumen and subsequent reabsorption of parent. Finally, the overall pharmacokinetics and disposition of maribavir was mechanistically modeled

using semi-physiologically-based approaches; the novel model captured maribavir's pharmacokinetic and EHR behavior in intact animals, and is indicative of lack of EHR in humans when species differences are incorporated.

Acknowledgments

The authors would like to acknowledge Aiqun Li, Dan Cui, and Haojing Rong, who at the time of the study were employees of Shire (now Takeda Development Center Americas, Inc.), for their contribution to the experimental studies, and Varun Aggarwal, who was an employee of Shire Human Genetic Therapies, Inc. (now Takeda Development Center Americas, Inc.), for technical aspects related to MATLAB® and SimBiology®. Additionally, the authors thank Matthew Crouthamel, an employee of Takeda Development Center Americas, Inc., and Swapan K. Chowdhury, Cindy Q. Xia, Michael Zientek, and Xiaochun Zhu, who are employees of Takeda, for scientific and editorial inputs during preparation of this manuscript. Additionally, Elizabeth Spencer, Justine Oswald, Sara Leitz, and Mark Gohdes (all employees of Covance, which received funding from Takeda Development Center Americas, Inc., for contracted research) are acknowledged for conducting experiments. Medical writing services were provided by Robert Coover, MPH, formerly of Caudex, and Amy Holloway, DPhil, of Caudex, funded by Takeda Development Center Americas, Inc.

Authorship Contributions

Participated in research design: Sun and Welty.

Conducted experiments: Sun.

Contributed new reagents or analytic tools: Sun.

Performed data analysis: Sun.

Wrote or contributed to the writing of the manuscript: Sun and Welty.

DMD Fast Forward. Published on August 30, 2021 as DOI: 10.1124/dmd.121.000493
This article has not been copyedited and formatted. The final version may differ from this version.

References

Albert C, Barbier O, Vallee M, Beaudry G, Belanger A, and Hum DW (2000) Distribution of uridine diphosphate-glucuronosyltransferase (UGT) expression and activity in cynomolgus monkey tissues: evidence for differential expression of steroid-conjugating UGT enzymes in steroid target tissues. *Endocrinology* **141**: 2472-2480.

Benson K, Cramer S, and Galla HJ (2013) Impedance-based cell monitoring: barrier properties and beyond. *Fluids Barriers CNS* **10**: 5.

Biron KK, Harvey RJ, Chamberlain SC, Good SS, Smith AA, III, Davis MG, Talarico CL, Miller WH, Ferris R, Dornsife RE, Stanat SC, Drach JC, Townsend LB, and Koszalka GW (2002) Potent and selective inhibition of human cytomegalovirus replication by 1263W94, a benzimidazole L-riboside with a unique mode of action. *Antimicrob Agents Chemother* **46**: 2365-2372.

Court MH (2010) Interindividual variability in hepatic drug glucuronidation: studies into the role of age, sex, enzyme inducers, and genetic polymorphism using the human liver bank as a model system. *Drug Metab Rev* **42**: 209-224.

Di L (2017) Reaction phenotyping to assess victim drug-drug interaction risks. *Expert Opin Drug Discov* **12**: 1105-1115.

Goldwater DR, Dougherty C, Schumacher M, and Villano SA (2008) Effect of ketoconazole on the pharmacokinetics of maribavir in healthy adults. *Antimicrob Agents Chemother* **52**: 1794-1798.

Hakimi Z, Aballea S, Ferchichi S, Scharn M, Odeyemi IA, Toumi M, and Saliba F (2017) Burden of cytomegalovirus disease in solid organ transplant recipients: a national matched cohort study in an inpatient setting. *Transpl Infect Dis* **19**: e12732.

Hamirally S, Kamil JP, Ndassa-Colday YM, Lin AJ, Jahng WJ, Baek MC, Noton S, Silva LA, Simpson-Holley M, Knipe DM, Golan DE, Marto JA, and Coen DM (2009) Viral

mimicry of Cdc2/cyclin-dependent kinase 1 mediates disruption of nuclear lamina during human cytomegalovirus nuclear egress. *PLoS Pathog* **5**: e1000275.

Ikegami K, Tagawa K, Narisawa S, and Osawa T (2003) Suitability of the cynomolgus monkey as an animal model for drug absorption studies of oral dosage forms from the viewpoint of gastrointestinal physiology. *Biol Pharm Bull* **26**: 1442-1447.

Khalil F and Laer S (2014) Physiologically based pharmacokinetic models in the prediction of oral drug exposure over the entire pediatric age range-sotalol as a model drug. *AAPS J* **16**: 226-239.

Kim DH and Jin YH (2001) Intestinal bacterial beta-glucuronidase activity of patients with colon cancer. *Arch Pharm Res* **24**: 564-567.

Kimoto E, Bi YA, Kosa RE, Tremaine LM, and Varma MVS (2017) Hepatobiliary Clearance Prediction: Species Scaling From Monkey, Dog, and Rat, and In Vitro-In Vivo Extrapolation of Sandwich-Cultured Human Hepatocytes Using 17 Drugs. *J Pharm Sci* **106**: 2795-2804.

Koppel N, Maini Rekdal V, and Balskus EP (2017) Chemical transformation of xenobiotics by the human gut microbiota. *Science* **356**: eaag2770.

Koszalka GW, Johnson NW, Good SS, Boyd L, Chamberlain SC, Townsend LB, Drach JC, and Biron KK (2002) Preclinical and toxicology studies of 1263W94, a potent and selective inhibitor of human cytomegalovirus replication. *Antimicrob Agents Chemother* **46**: 2373-2380.

Kotton CN, Kumar D, Caliendo AM, Huprikar S, Chou S, Danziger-Isakov L, Humar A, and The Transplantation Society International CMVCG (2018) The third international consensus guidelines on the management of cytomegalovirus in solid-organ transplantation. *Transplantation* **102**: 900-931.

Krosky PM, Baek MC, and Coen DM (2003) The human cytomegalovirus UL97 protein kinase, an antiviral drug target, is required at the stage of nuclear egress. *J Virol* **77**: 905-914.

Ma JD, Nafziger AN, Villano SA, Gaedigk A, and Bertino JS, Jr. (2006) Maribavir pharmacokinetics and the effects of multiple-dose maribavir on cytochrome P450 (CYP) 1A2, CYP 2C9, CYP 2C19, CYP 2D6, CYP 3A, N-acetyltransferase-2, and xanthine oxidase activities in healthy adults. *Antimicrob Agents Chemother* **50**: 1130-1135.

Maertens J, Cordonnier C, Jaksch P, Poire X, Uknis M, Wu J, Wijatyk A, Saliba F, Witzke O, and Villano S (2019) Maribavir for preemptive treatment of cytomegalovirus reactivation. *N Engl J Med* **381**: 1136-1147.

Marty FM, Ljungman P, Chemaly RF, Maertens J, Dadwal SS, Duarte RF, Haider S, Ullmann AJ, Katayama Y, Brown J, Mullane KM, Boeckh M, Blumberg EA, Einsele H, Snydman DR, Kanda Y, DiNubile MJ, Teal VL, Wan H, Murata Y, Kartsonis NA, Leavitt RY, and Badshah C (2017) Letermovir Prophylaxis for Cytomegalovirus in Hematopoietic-Cell Transplantation. *N Engl J Med* **377**: 2433-2444.

Matsumoto Y, Cabalu T, Sandhu P, Hartmann G, Iwasa T, Yoshitsugu H, Gibson C, and Uemura N (2019) Application of Physiologically Based Pharmacokinetic Modeling to Predict Pharmacokinetics in Healthy Japanese Subjects. *Clin Pharmacol Ther* **105**: 1018-1030.

National Library of Medicine (2020a) Efficacy and Safety Study of Maribavir Compared to Valganciclovir for the Treatment of Cytomegalovirus (CMV) Infection in Hematopoietic Stem Cell Transplant Recipients. https://clinicaltrials.gov/ct2/show/NCT02927067.

National Library of Medicine (2020b) Efficacy and Safety Study of Maribavir Treatment Compared to Investigator-assigned Treatment in Transplant Recipients With Cytomegalovirus (CMV) Infections That Are Refractory or Resistant to Treatment With

Ganciclovir, Valganciclovir, Foscarnet, or Cidofovir. https://clinicaltrials.gov/ct2/show/NCT02931539.

Papanicolaou GA, Silveira FP, Langston AA, Pereira MR, Avery RK, Uknis M, Wijatyk A, Wu J, Boeckh M, Marty FM, and Villano S (2019) Maribavir for Refractory or Resistant Cytomegalovirus Infections in Hematopoietic-cell or Solid-organ Transplant Recipients: A Randomized, Dose-ranging, Double-blind, Phase 2 Study. *Clin Infect Dis* **68**: 1255-1264.

Patel M, Taskar KS, and Zamek-Gliszczynski MJ (2016) Importance of Hepatic Transporters in Clinical Disposition of Drugs and Their Metabolites. *J Clin Pharmacol* **56 Suppl 7**: S23-39.

Peters SA (2012) Appendix A: Physiological Parameters in Preclinical Species, in: *Physiologically-Based Pharmacokinetic (PBPK) Modeling and Simulations: Principles, Methods, and Applications in the Pharmaceutical Industry*, pp 408-413, John Wiley & Sons, Inc., New Jersey.

Sender R, Fuchs S, and Milo R (2016) Revised Estimates for the Number of Human and Bacteria Cells in the Body. *PLoS Biol* **14**: e1002533.

Song I, Ilic K, Sun K, and Martin P (2019a) Clinical Pharmacology of maribavir (SHP620): A comprehensive overview, in: *Biol Blood Marrow Transplant*, pp S342, Transplantation and Cellular Therapy (TCT) Meeting, Houston, TX.

Song I, Sun K, Ilic K, and Martin P (2019b) Summary of Maribavir (SHP620) Drug–Drug Interactions Based on Accumulated Clinical and Nonclinical Data, in: *Biol Blood Marrow Transplant*, pp S370-S371, Transplantation and Cellular Therapy (TCT) Meeting, Houston, TX.

Teira P, Battiwalla M, Ramanathan M, Barrett AJ, Ahn KW, Chen M, Green JS, Saad A, Antin JH, Savani BN, Lazarus HM, Seftel M, Saber W, Marks D, Aljurf M, Norkin M, Wingard JR, Lindemans CA, Boeckh M, Riches ML, and Auletta JJ (2016) Early

cytomegalovirus reactivation remains associated with increased transplant-related mortality in the current era: a CIBMTR analysis. *Blood* **127**: 2427-2438.

Tropini C, Earle KA, Huang KC, and Sonnenburg JL (2017) The Gut Microbiome: Connecting Spatial Organization to Function. *Cell Host Microbe* **21**: 433-442.

Venton G, Crocchiolo R, Furst S, Granata A, Oudin C, Faucher C, Coso D, Bouabdallah R, Berger P, Vey N, Ladaique P, Chabannon C, le Merlin M, Blaise D, and El-Cheikh J (2014) Risk factors of ganciclovir-related neutropenia after allogeneic stem cell transplantation: a retrospective monocentre study on 547 patients. *Clin Microbiol Infect* **20**: 160-166.

Vinarov Z, Abdallah M, Agundez JAG, Allegaert K, Basit AW, Braeckmans M, Ceulemans J, Corsetti M, Griffin BT, Grimm M, Keszthelyi D, Koziolek M, Madla CM, Matthys C, McCoubrey LE, Mitra A, Reppas C, Stappaerts J, Steenackers N, Trevaskis NL, Vanuytsel T, Vertzoni M, Weitschies W, Wilson C, and Augustijns P (2021) Impact of gastrointestinal tract variability on oral drug absorption and pharmacokinetics: An UNGAP review. *Eur J Pharm Sci* **162**: 105812.

Wang LH, Peck RW, Yin Y, Allanson J, Wiggs R, and Wire MB (2003) Phase I safety and pharmacokinetic trials of 1263W94, a novel oral anti-human cytomegalovirus agent, in healthy and human immunodeficiency virus-infected subjects. *Antimicrob Agents Chemother* **47**: 1334-1342.

Welty D, Sun K, Rong H, and Song I (2018) In vitro metabolic and transporter profiling for marabavir (SHP620), in: *22nd North American ISSX meeting*, Montreal, Canada.

Williams SL, Hartline CB, Kushner NL, Harden EA, Bidanset DJ, Drach JC, Townsend LB, Underwood MR, Biron KK, and Kern ER (2003) In vitro activities of benzimidazole D- and L-ribonucleosides against herpesviruses. *Antimicrob Agents Chemother* **47**: 2186-2192.

Wu B (2012) Use of physiologically based pharmacokinetic models to evaluate the impact of intestinal glucuronide hydrolysis on the pharmacokinetics of aglycone. *J Pharm Sci* **101**: 1281-1301.

Yu LX and Amidon GL (1999) A compartmental absorption and transit model for estimating oral drug absorption. *Int J Pharm* **186**: 119-125.

Zamek-Gliszczynski MJ, Chu X, Polli JW, Paine MF, and Galetin A (2014) Understanding the transport properties of metabolites: case studies and considerations for drug development. *Drug Metab Dispos* **42**: 650-664.

Zenser TV, Lakshmi VM, and Davis BB (1999) Human and Escherichia coli beta-glucuronidase hydrolysis of glucuronide conjugates of benzidine and 4-aminobiphenyl, and their hydroxy metabolites. *Drug Metab Dispos* **27**: 1064-1067.

Zhang N, Liu Y, and Jeong H (2015) Drug-Drug Interaction Potentials of Tyrosine Kinase Inhibitors via Inhibition of UDP-Glucuronosyltransferases. *Sci Rep* **5**: 17778.

Zhou W, Johnson TN, Xu H, Cheung S, Bui KH, Li J, Al-Huniti N, and Zhou D (2016) Predictive Performance of Physiologically Based Pharmacokinetic and Population Pharmacokinetic Modeling of Renally Cleared Drugs in Children. *CPT Pharmacometrics Syst Pharmacol* **5**: 475-483.

Footnote

This research was funded by Takeda Development Center Americas, Inc.

DMD Fast Forward. Published on August 30, 2021 as DOI: 10.1124/dmd.121.000493
This article has not been copyedited and formatted. The final version may differ from this version.

Figure Legends

Fig. 1. Structure of maribavir (also known as TAK-620, SHP620, VP41263, and 1263W94). The position of the ^{14}C atom is marked with an asterisk.

Fig. 2. Simplified diagram for the semi-PBPK model of maribavir disposition in cynomolgus monkeys. Numbers in the graph denote physiologic and biological processes: (1) transit of substance from stomach to duodenum, (2) transit within the small intestine, (3) transit within the colon and to feces, (4) absorption from the small intestine, (5) conversion of glucuronides to parent, which occurs in the last two compartments of the ileal lumen and throughout the colon, (6) absorption from the colon, (7) biliary excretion of parent, (8) glucuronidation of parent and secretion to duodenal lumen, (9) excretion of glucuronides in urine, (10) transport between the liver and central compartment, (11) transport between the central and peripheral compartments, (12) renal excretion of parent, and (13) all other pathways for parent. The two segments of the jejunum, four segments of the ileum, and five of the colon were not separately depicted in this diagram; the detailed diagram in MATLAB® SimBiology® is shown in Supplemental Fig. 1.

MBV, maribavir (parent); MBV-Gluc, maribavir glucuronides; Met, other metabolites of maribavir; PBPK, physiologically based pharmacokinetic.

Fig. 3. (A) Total radioactivity in plasma versus time profile after a single i.v. bolus administration of 13 mg/kg ^{14}C-maribavir to intact animals (Group 1, circles) or BDC animals (Group 2, squares) as determined by LSC, (B) concentration of maribavir in plasma versus time profile after a single i.v. bolus administration of 13 mg/kg ^{14}C-maribavir to intact animals (Group 1, circles) or BDC animals (Group 2, squares) as determined by LC-MS/MS. Insets show a zoomed-in view of the time course from zero to 6 hours post-dose. Missing samples are not plotted and BLQ data are treated as zeros. *N* = 3 for both groups and error bars denote standard deviation and *N* = 2 for Group 2's 24-hour sample in panel (B).

DMD Fast Forward. Published on August 30, 2021 as DOI: 10.1124/dmd.121.000493
This article has not been copyedited and formatted. The final version may differ from this version.

BDC, bile duct-cannulated; BLQ, below the limit of quantitation; i.v., intravenous; LC-MS/MS, liquid chromatography–tandem mass spectrometry; LSC, liquid scintillation counters.

Fig. 4. Mean cumulative recovery percentages in urine, feces, cage rinse, and bile (Group 2 only) as well as in all matrices combined ("TOTAL") in (A) intact animals (Group 1) and (B) bile-duct cannulated animals (Group 2) after a single intravenous bolus administration of ^{14}C-maribavir. *N* = 3 for both groups and error bars denote standard deviation.

Fig. 5. Metabolic pathways of maribavir in cynomolgus monkeys. Italicized letters in parentheses denote matrices where each metabolite was detected and numbers next to the arrows denote distinct pathways: (1) *N*-dealkylation (to M4, also known as VP44469), (2) oxidation, (3) glucuronide conjugation, (4) deribosylation, (5) dechlorination, (6) glutathione (GSH) conjugation, and (7) amide hydrolysis after GSH conjugation.

b, bile; *f*, feces; Gluc, glucuronide; *p*, plasma; *u*, urine.

Fig. 6. Observed plasma concentration versus time profiles of maribavir in cynomolgus monkey overlaid with fitted curves (BDC only, panel A) or simulations (intact animals, panels B, C, D, and E) in MATLAB® SimBiology®. (A) observed data in individual BDC animals overlaid with fitted curve; (B) simulated data with a single i.v. administration in intact animals, using f_m(Gluc) at 0.728 or 0.853 at both 5 mg/kg and 13 mg/kg doses, overlaid with individually observed data; (C) simulated data with a single p.o. administration in intact animals, using f_m(Gluc) at 0.728 at 10 mg/kg dose, overlaid with individually observed data; (D) simulated data with repeated b.i.d. p.o. administration at 10, 30, or 100 mg/kg in intact male animals within the first 8 hours on Day 2, using f_m(Gluc) at 0.728, overlaid with individually observed data (Koszalka et al., 2002); (E) simulated data with repeated b.i.d. p.o. administrations at 10, 30, or 100 mg/kg in intact male animals within the first 8 hours on Day 27, using f_m(Gluc) at 0.728 , overlaid with individually observed data (Koszalka et al., 2002).

DMD Fast Forward. Published on August 30, 2021 as DOI: 10.1124/dmd.121.000493
This article has not been copyedited and formatted. The final version may differ from this version.

BDC, bile duct-cannulated; b.i.d., twice daily; f_m(Gluc), fraction metabolized by glucuronidation; i.v., intravenous; p.o., oral.

Fig. 7. Sensitivity analyses of effects of (A) fraction metabolized by glucuronidation (f_m(Gluc)) and (B) transit rate in the colon lumen (k_T_Colon) on pharmacokinetic profile of maribavir after a 10 mg/kg single oral administration to cynomolgus monkeys.

DMD Fast Forward. Published on August 30, 2021 as DOI: 10.1124/dmd.121.000493
This article has not been copyedited and formatted. The final version may differ from this version.

Tables

TABLE 1

Key system parameters and drug-specific parameters used in construction of the customized semi-physiologically based pharmacokinetic model for maribavir in cynomolgus monkeys.

Parameter in SimBiology®	Description	Value	Notes
Key system parameters			
k_T_Stomach	Rate of transit from stomach to duodenum	2.0 h^{-1}	From fasted state, gastric emptying time of 30 min
SITT	Small intestine transit time	2.7 h	Ikegami et al., 2003
k_T_Colon	Colon transit rate	0.042 h^{-1}	Peters et al., 2012
Key drug-specific parameters from in vitro data or in vivo BDC group data			
Drug_Peff	Effective permeability in jejunum	1.3×10^{-4} cm/s	Calculated from Caco-2 cell data; see Supplemental Methods
Drug_ka_Jejunum	First-order absorption rate in jejunum	2.3 h^{-1}	Calculations in Supplemental Methods
Drug_ka_Colon	First-order absorption rate in colon	0.056 h^{-1}	Calculations in Supplemental Methods
Drug_fm_gluc	Fraction metabolized by the direct glucuronidation pathway	0.73 or 0.85	0.728 from in vivo data in BDC group (Table 5); 0.853 from in vitro hepatocyte data
Gluc_k_hydrolysis	Rate of hydrolysis of maribavir glucuronides	3.1 h^{-1}	Calculations in Supplemental Methods
Drug_CL_Renal	Renal clearance of parent from central compartment	0.013 L/h	From BDC mean systemic CL × %dose in urine: 5.72 L/h × 0.224% (Tables 3 and 4)
Drug_CL_Biliary	Biliary clearance of parent from central compartment	0.072 L/h	From BDC systemic CL × %dose in bile: 5.72 L/h × 1.26% (Tables 3 and 4)

DMD Fast Forward. Published on August 30, 2021 as DOI: 10.1124/dmd.121.000493
This article has not been copyedited and formatted. The final version may differ from this version.

Drug-specific parameters from fitting the model to the observed plasma concentration time course in BDC animals			
Drug_Q12	Central to peripheral transfer CL	0.66 L/h	S.E. 0.0049
Drug_Liver_CL	Drug clearance from the liver compartment	16 L/h	S.E. 0.24
Drug_Vc_Ref	Volume of the central compartment	6.3 L	S.E. 0.085
Drug_Vp_Ref	Volume of peripheral compartment	2.8 L	S.E. 0.046

For a full list of parameters, refer to Supplemental Table 5. “Drug” refers to maribavir.

BDC, bile-duct cannulated; CL, clearance; S.E., standard error.

DMD Fast Forward. Published on August 30, 2021 as DOI: 10.1124/dmd.121.000493
This article has not been copyedited and formatted. The final version may differ from this version.

TABLE 2

Non-compartmental PK parameters for radioactivity in plasma collected from male cynomolgus monkeys after a single intravenous administration of ^{14}C-maribavir (both groups at 13 mg/kg). Group 1: intact monkeys (n = 3), Group 2: BDC monkeys (n = 3).

PK parameter on total radioactivity in plasma	**Group 1 (Intact), Mean ± S.D.**	**Group 2 (BDC), Mean ± S.D.**
AUC_{0-t} (ng maribavir equivalent·h/g)	28,000 ± 5,770	17,100 ± 4,050
$AUC_{0-\infty}$ (ng maribavir equivalent·h/g)	30,300 ± 5,900	17,900 ± 3,470
$t_{1/2}$ (h)	19.7 ± 3.4	2.71 ± 1.4
CL (g/h)	1,700 ± 347	3,010 ± 528
V_{ss} (g)	27,700 ± 3,910	6,010 ± 1,110

AUC_{0-t}, area under the concentration–time curve from time zero to the last measurable time point; $AUC_{0-\infty}$, area under the concentration–time curve from zero to infinity; BDC, bile duct-cannulated; CL, clearance; PK, pharmacokinetic; S.D., standard deviation; $t_{1/2}$, half-life; V_{ss}, volume of distribution at steady state.

DMD Fast Forward. Published on August 30, 2021 as DOI: 10.1124/dmd.121.000493
This article has not been copyedited and formatted. The final version may differ from this version.

TABLE 3

Non-compartmental PK parameters for concentrations of maribavir in plasma from male cynomolgus monkeys after a single intravenous bolus administration of ^{14}C-maribavir (Groups 1 [*n* = 3] and 2 [*n* = 3], 13 mg/kg).

PK parameter on maribavir concentration in plasma	**Group 1 (Intact), Mean ± S.D.**	**Group 2 (BDC), Mean ± S.D.**
AUC_{0-t} (h·mg/L)	17.4 ± 3.9	9.33 ± 1.7
$AUC_{0-\infty}$ (h·mg/L)	17.4 ± 3.9	9.36 ± 1.6
C_0 (mg/L)	9.96[a]	10.4 ± 1.3
$t_{1/2}$ (h)	12.5 ± 1.1	2.49 ± 1.2
CL (L/h)	2.99 ± 0.73	5.72 ± 0.90
V_{ss} (L)	35.4 ± 6.5	7.09 ± 1.5

[a]For C_0, only two animals in Group 1 were involved in calculating the mean, due to one animal missing the 5-minute PK time point.

AUC_{0-t}, area under the concentration–time curve from time zero to the last measurable time point; $AUC_{0-\infty}$, area under the concentration–time curve from zero to infinity; BDC, bile duct-cannulated; C_0, initial concentration; CL, clearance; PK, pharmacokinetic; S.D., standard deviation; $t_{1/2}$, half-life; V_{ss}, volume of distribution at steady state.

TABLE 4

Descriptions and cumulative percentages of dose recovered in each pooled biological matrix for maribavir and its metabolites, after a single intravenous bolus administration to intact (Group 1) or BDC (Group 2) cynomolgus monkeys.

Metabolite	Description	Percentage of dose administered to Group 1		Percentage of dose administered to Group 2		
		Urine (0–144 h)	Feces (0–168 h)[a]	Urine (0–48 h)	Feces (0–48 h)	Bile (0–24 h)
M15	Loss of chlorine + cysteine conjugate	ND	ND	ND	ND	1.42
M1	Glucuronide conjugate to M4	2.16	ND	1.19	ND	ND
M7	Glucuronide conjugate to M4	2.62	ND	1.14	ND	3.77
M16	Glucuronide conjugate to M4	0.297	ND	ND	ND	0.992
M17[b]	Glucuronide conjugate to M4	0–1.85	ND	0–0.596	ND	0–1.83
M2[b]	Loss of ribose + glucuronide	0–1.85	ND	0–0.596	0.0282	0–1.83
M10	Glucuronide conjugate to parent	0.402	ND	ND	ND	ND
M4	Loss of propyl	2.0	8.80–9.34	0.678	0.511	ND
M5	Oxidation on propyl	ND	0.416–0.433	0.0457	ND	ND
M11	Glucuronide conjugate to parent	1.2	ND	0.334	ND	34.2
M12	Glucuronide conjugate to parent	2.01	ND	0.551	ND	38.6
Maribavir	Parent	0.823	57.9–60.3	0.224	1.45	1.26

[a] The lower dose percentage value was based on pooled fecal samples from all three animals from 0 to 120 hours. Only one animal generated feces from 120 to 168 hours; the upper value reflected the addition of dose percentage from this single animal after 120 hours to the group's pre-120-hour

value. [b] When M17 and M2 are both present in the same matrix, they are indistinguishable in the radio- and ion chromatogram as a single peak. Dose percentage values derived from this combined peak were therefore reported.

BDC, bile duct-cannulated; ND, not detected or below the limit of quantitation (1% of run and 10 cpm peak height).

DMD Fast Forward. Published on August 30, 2021 as DOI: 10.1124/dmd.121.000493
This article has not been copyedited and formatted. The final version may differ from this version.

TABLE 5

PK properties observed in in vivo studies with maribavir in cynomolgus monkeys and estimated from the semi-PBPK model. The f_m(Gluc) was set as 0.728 unless specified otherwise. The twice-daily doses were administered 8 hours apart within each dosing day.

PK properties on maribavir in plasma	**Observed, Mean ± S.D.**	**Estimated/predicted by semi-PBPK model**
13 mg/kg ^{14}C-maribavir intravenous bolus, single dose		
AUC_{0-t} (mg·h/L)	17.4 ± 3.9	12.5 (f_m(Gluc) = 0.728) 15.1 (f_m(Gluc) = 0.853)
CL (L/h)	2.99 ± 0.73	4.02 (f_m(Gluc) = 0.728) 3.33 (f_m(Gluc) = 0.853)
V_{ss} (L)	35.4 ± 6.5	35.2 (f_m(Gluc) = 0.728) 45.8 (f_m(Gluc) = 0.853)
5 mg/kg maribavir intravenous bolus, single dose		
AUC_{0-t} (mg·h/L)	4.55 ± 0.71	5.05
CL (L/h)	4.47 ± 0.18	4.06
V_{ss} (L)	36.8 ± 14.7	35.4
10 mg/kg maribavir oral gavage, single dose		
AUC_{0-t} (mg·h/L)	6.13 ± 3.6	6.21
C_{max} (mg/L)	1.50 ± 1.0	1.01
T_{max} (h)	2 ± 0	1.31
F	0.661 ± 0.33	0.615
F_a	N/A	0.671
10 mg/kg twice-daily maribavir oral gavage, multiple dose		
AUC (mg·h/L), Day 2, 0–8 h	3.60 ± 1.2	4.41
C_{max} (mg/L), Day 2, 0–8 h	0.97 ± 0.39	1.13
AUC (mg·h/L), Day 27, 0–8 h	4.60 ± 0.33	4.83
C_{max} (mg/L), Day 27, 0–8 h	0.90 ± 0.05	1.20
30 mg/kg twice-daily maribavir oral gavage, multiple dose		
AUC (mg·h/L), Day 2, 0–8 h	8.70 ± 1.2	13.2
C_{max} (mg/L), Day 2, 0–8 h	2.55 ± 0.63	3.40

DMD Fast Forward. Published on August 30, 2021 as DOI: 10.1124/dmd.121.000493
This article has not been copyedited and formatted. The final version may differ from this version.

AUC (mg·h/L), Day 27, 0–8 h	12.8 ± 1.4	14.5
C_{max} (mg/L), Day 27, 0–8 h	2.63 ± 0.38	3.59
90 mg/kg twice-daily maribavir oral gavage, multiple dose		
AUC (mg·h/L), Day 2, 0–8 h	32.1 ± 11	39.7
C_{max} (mg/L), Day 2, 0–8 h	7.3 ± 3.5	10.2
AUC (mg·h/L), Day 27, 0–8 h	30.6 ± 3.2	43.5
C_{max} (mg/L), Day 27, 0–8 h	6.9 ± 1.1	10.8

AUC_{0-t}, area under the concentration–time curve from time zero to the last measurable time point; CL, clearance; C_{max}, peak concentration; F, bioavailability; F_a, fraction absorbed; f_m(Gluc), fraction metabolized by glucuronidation; N/A, not available; PBPK, physiologically based pharmacokinetic; PK, pharmacokinetics; S.D., standard deviation; T_{max}, time to peak concentration; V_{ss}, volume of distribution at steady state.

Figure 1

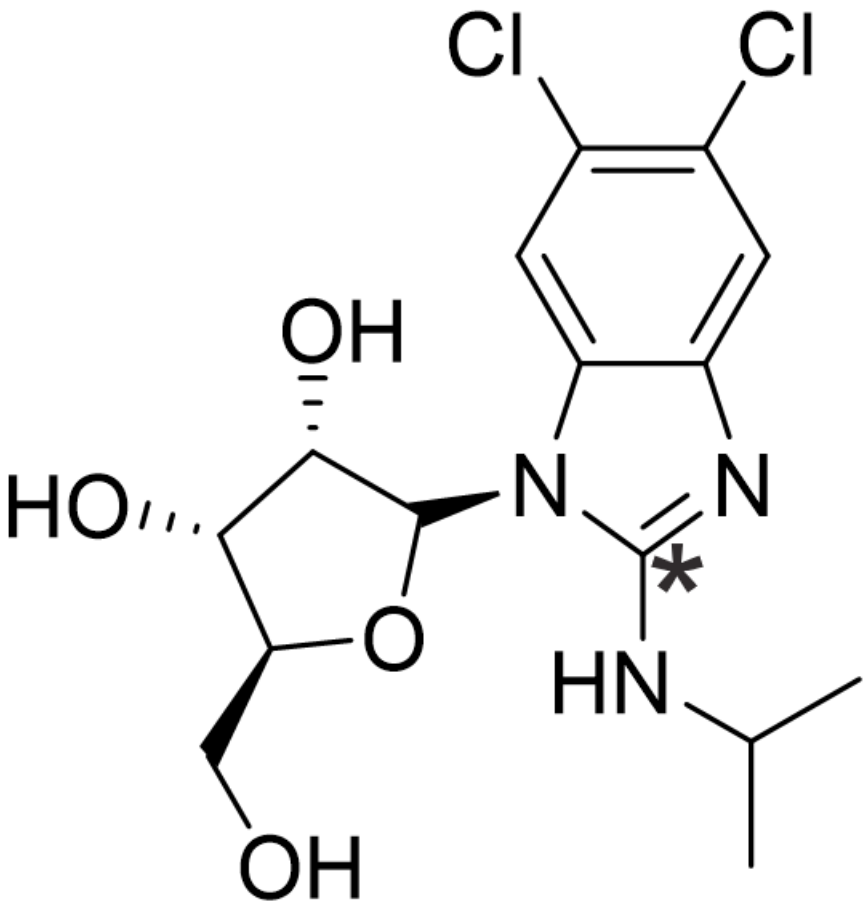

Figure 2

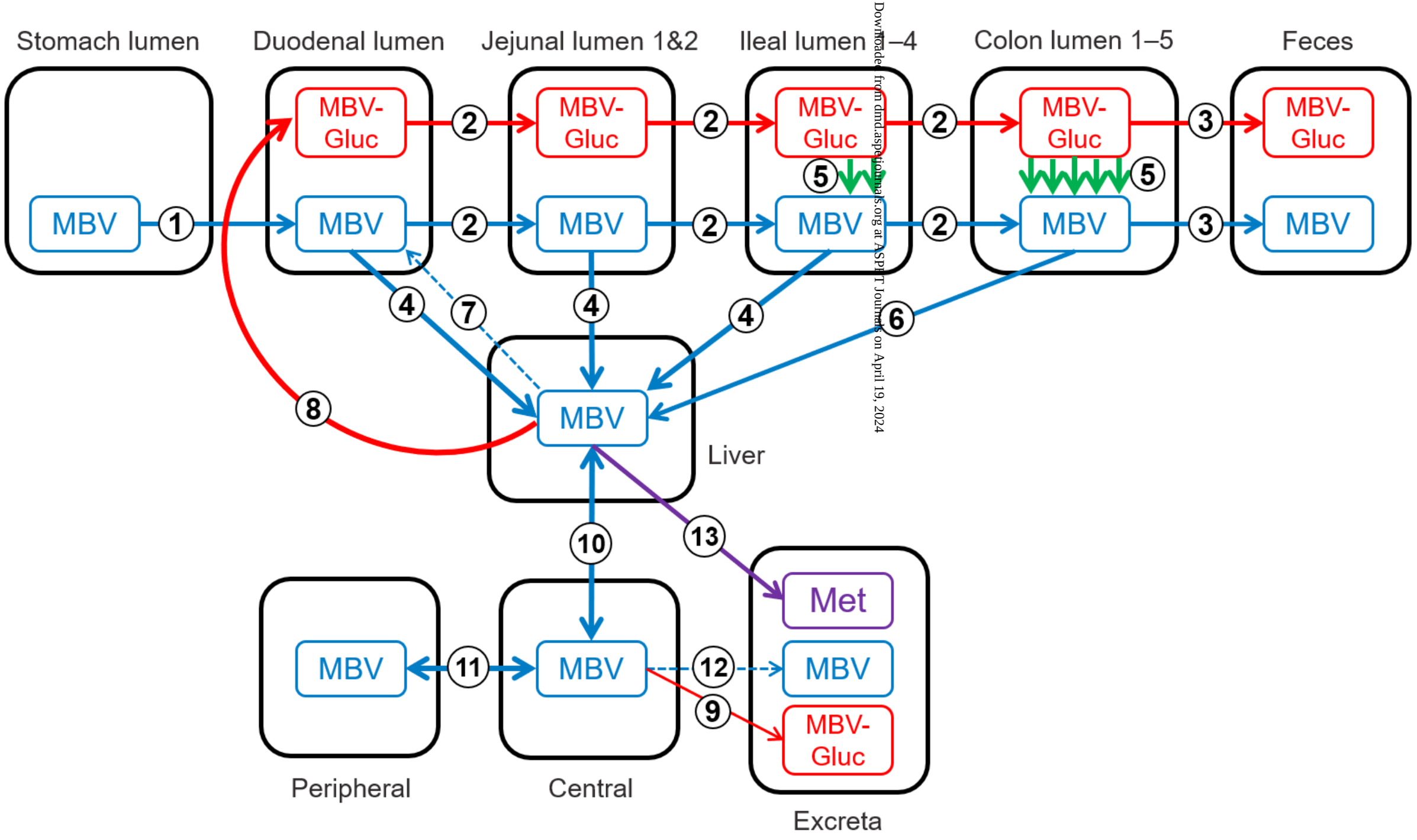

Figure 3A

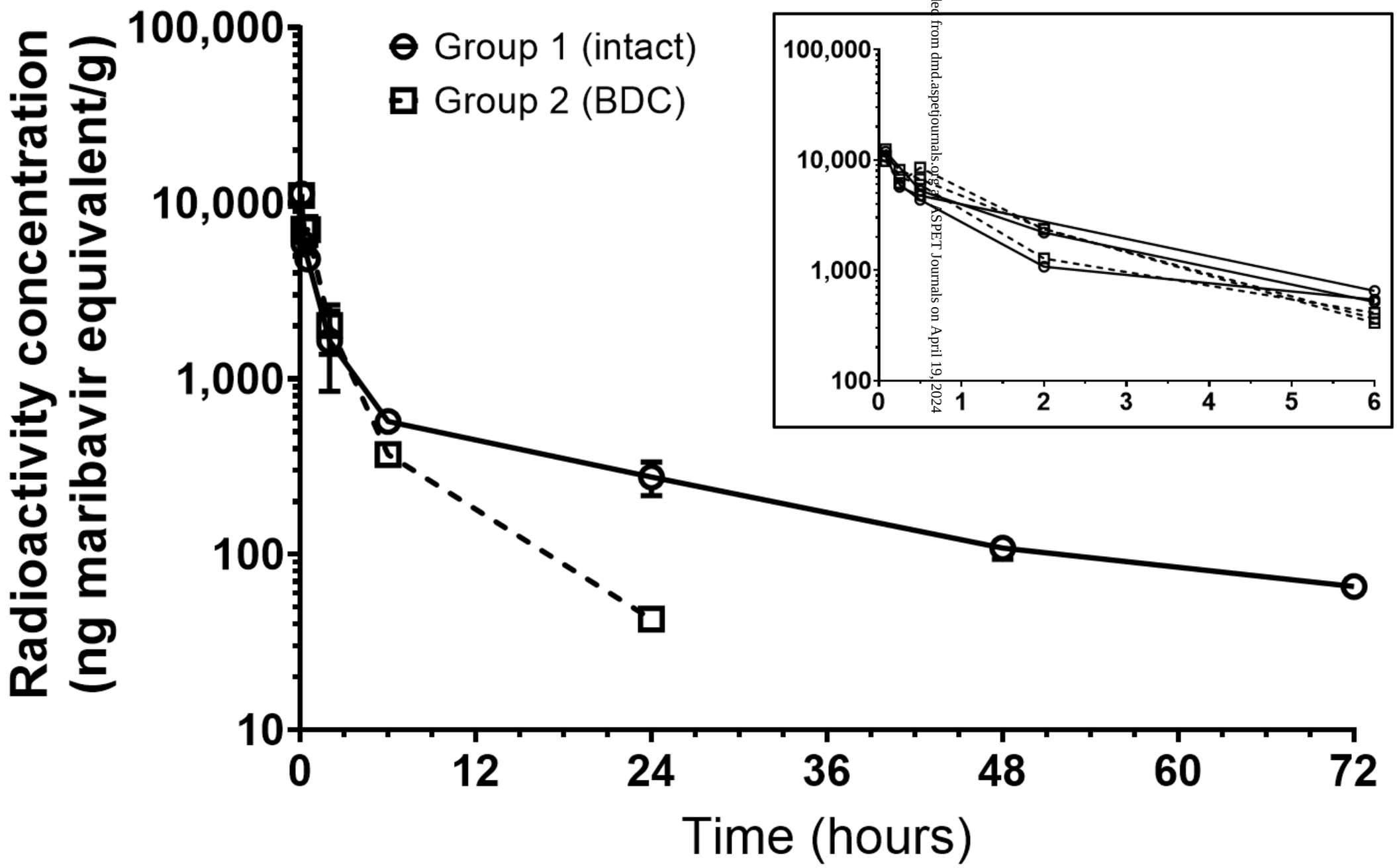

Figure 3B

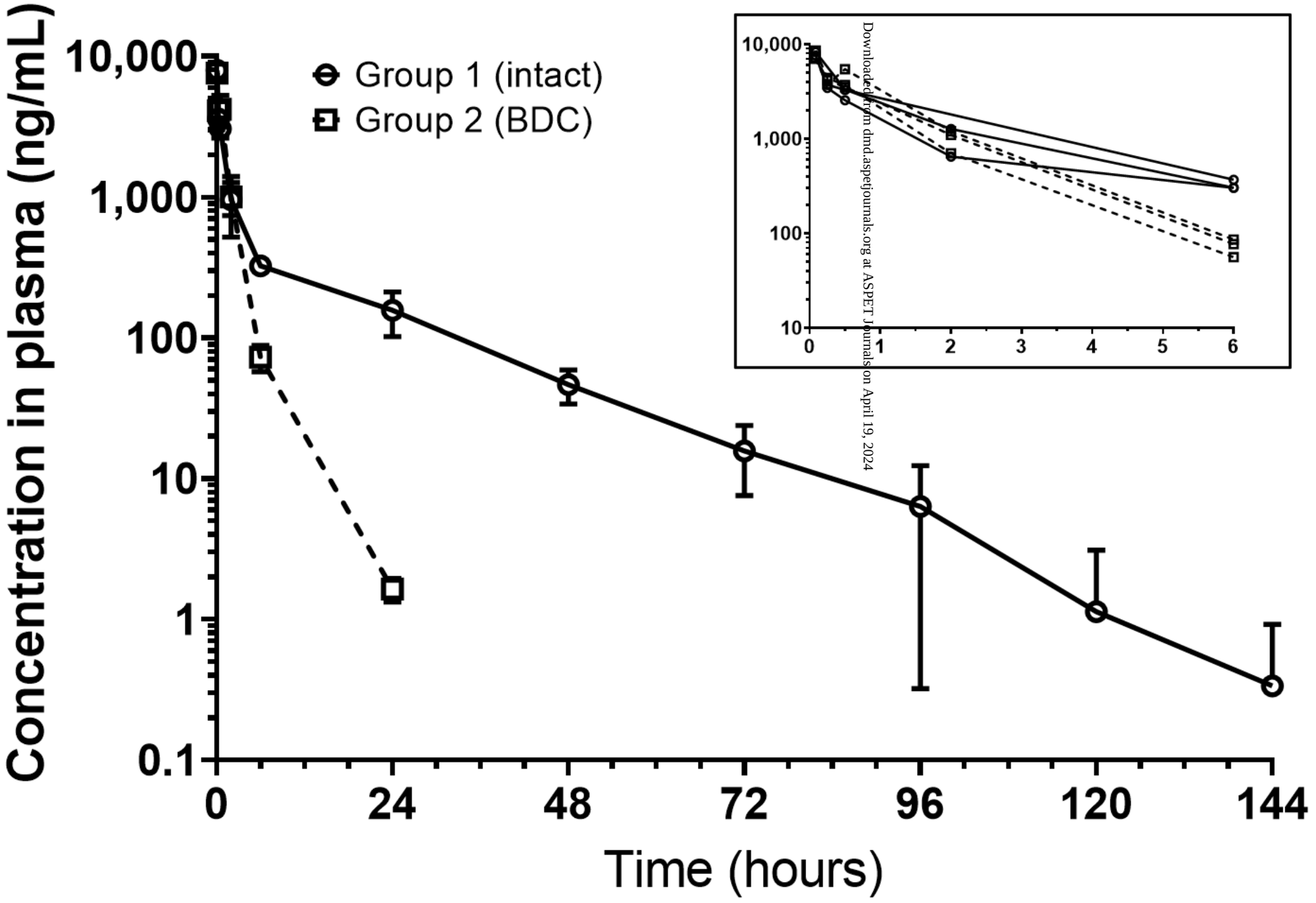

Figure 4A

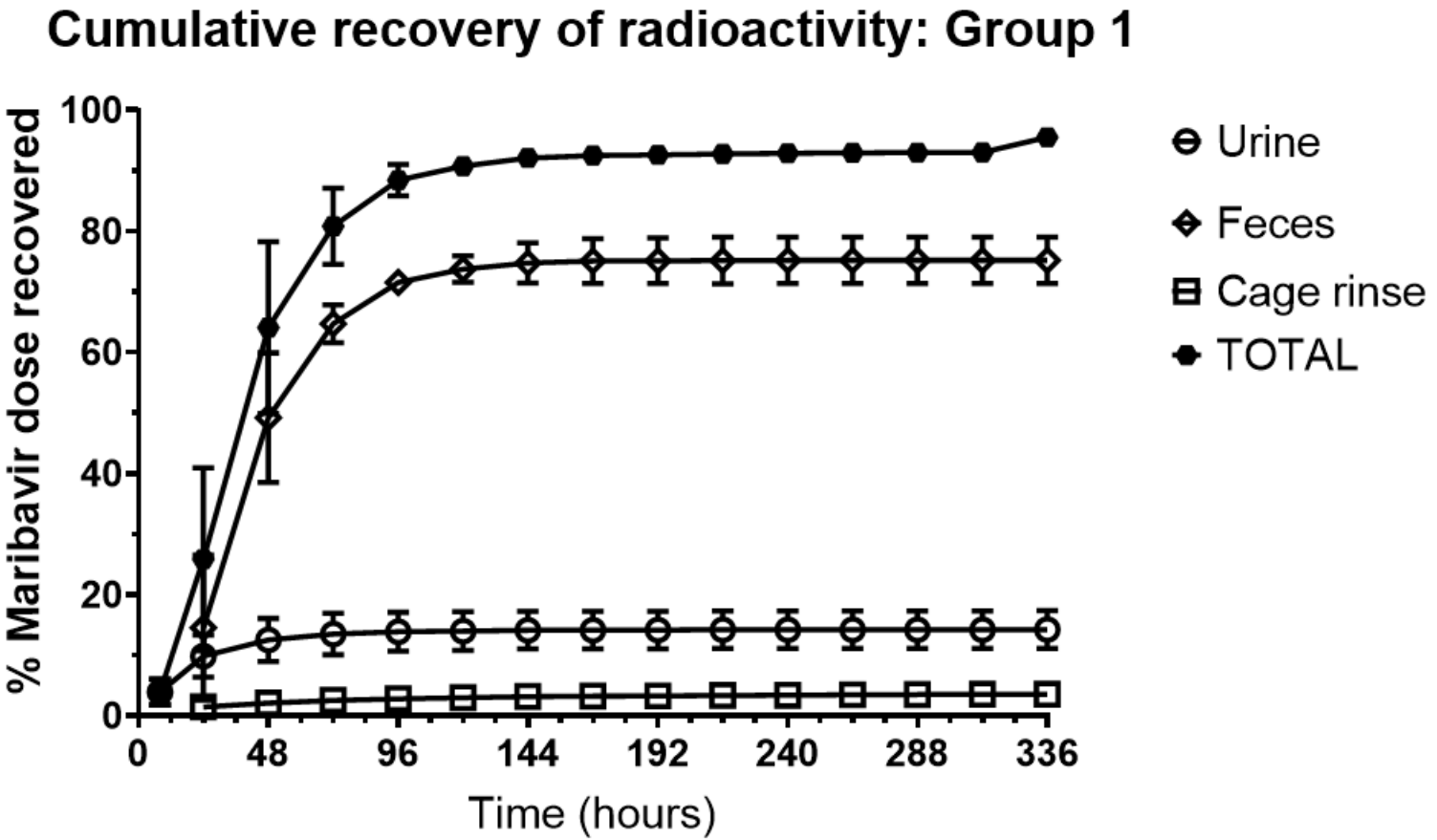
Cumulative recovery of radioactivity: Group 1
% Maribavir dose recovered
100
80
60
40
20
0
0
48
96
144
192
240
288
336
Time (hours)
Urine
Feces
Cage rinse
TOTAL

Figure 4B

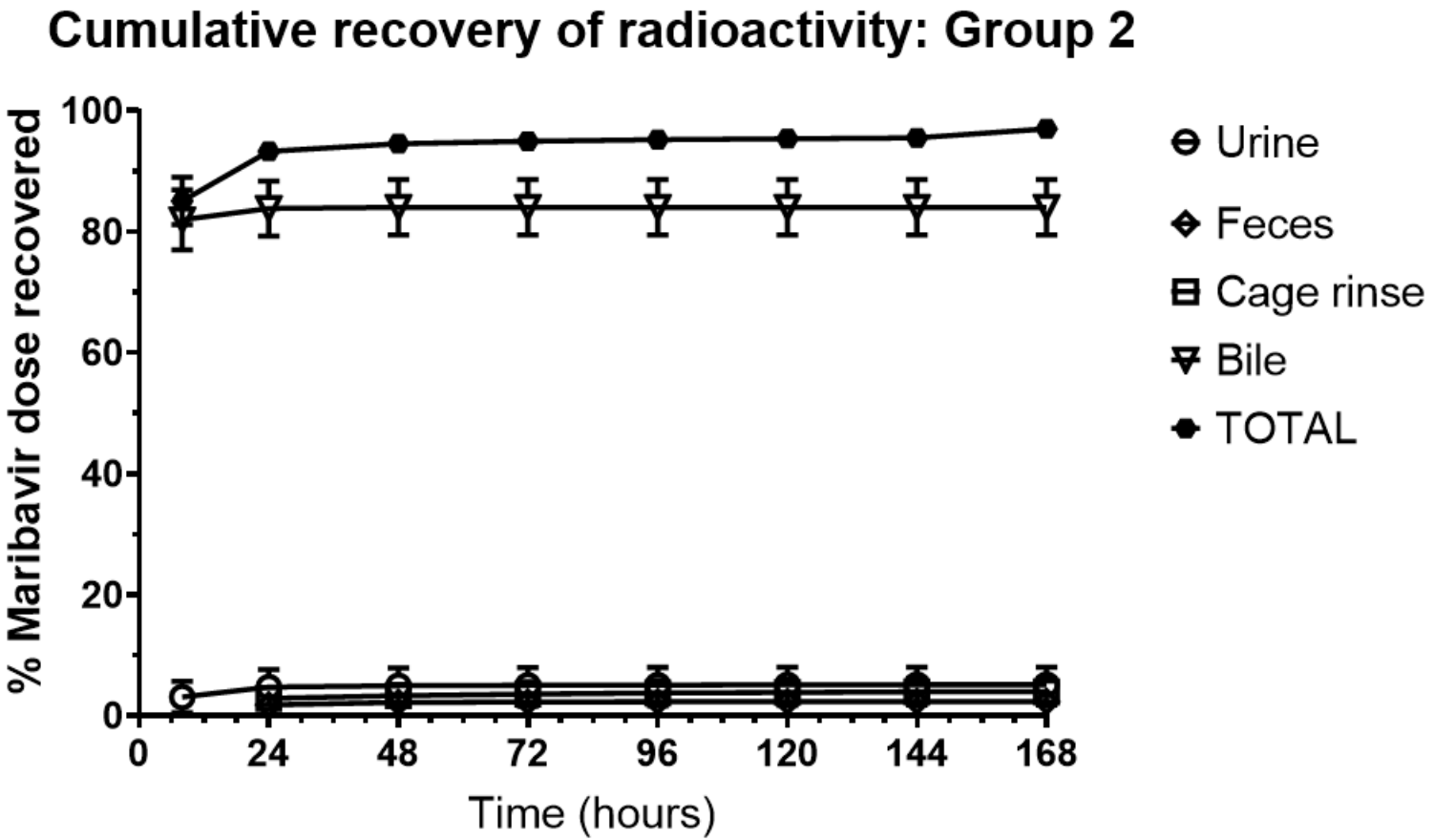
Cumulative recovery of radioactivity: Group 2
% Maribavir dose recovered
100
80
60
40
20
0
0
24
48
72
96
120
144
168
Time (hours)
Urine
Feces
Cage rinse
Bile
TOTAL

Figure 5

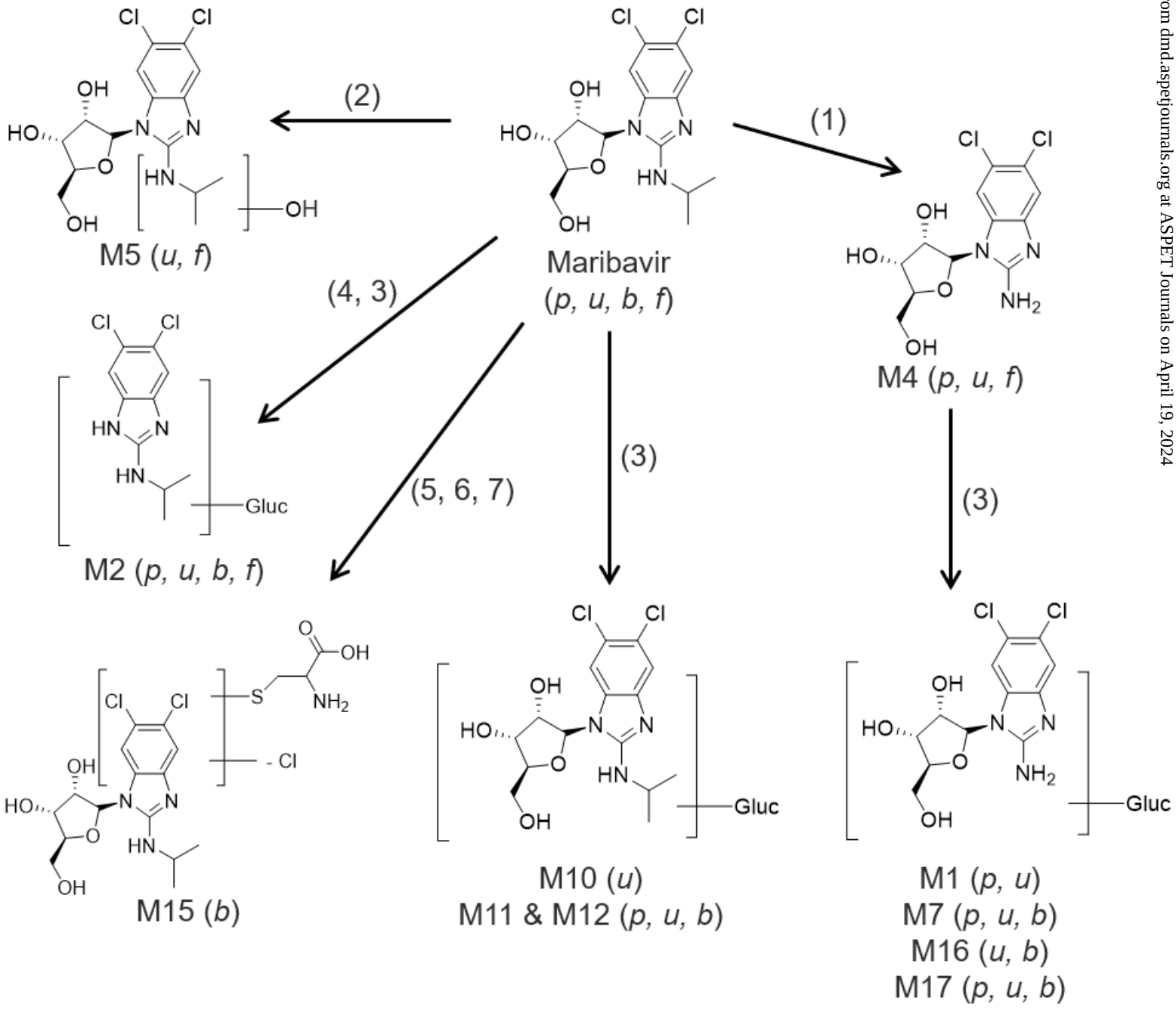

Figure 6A

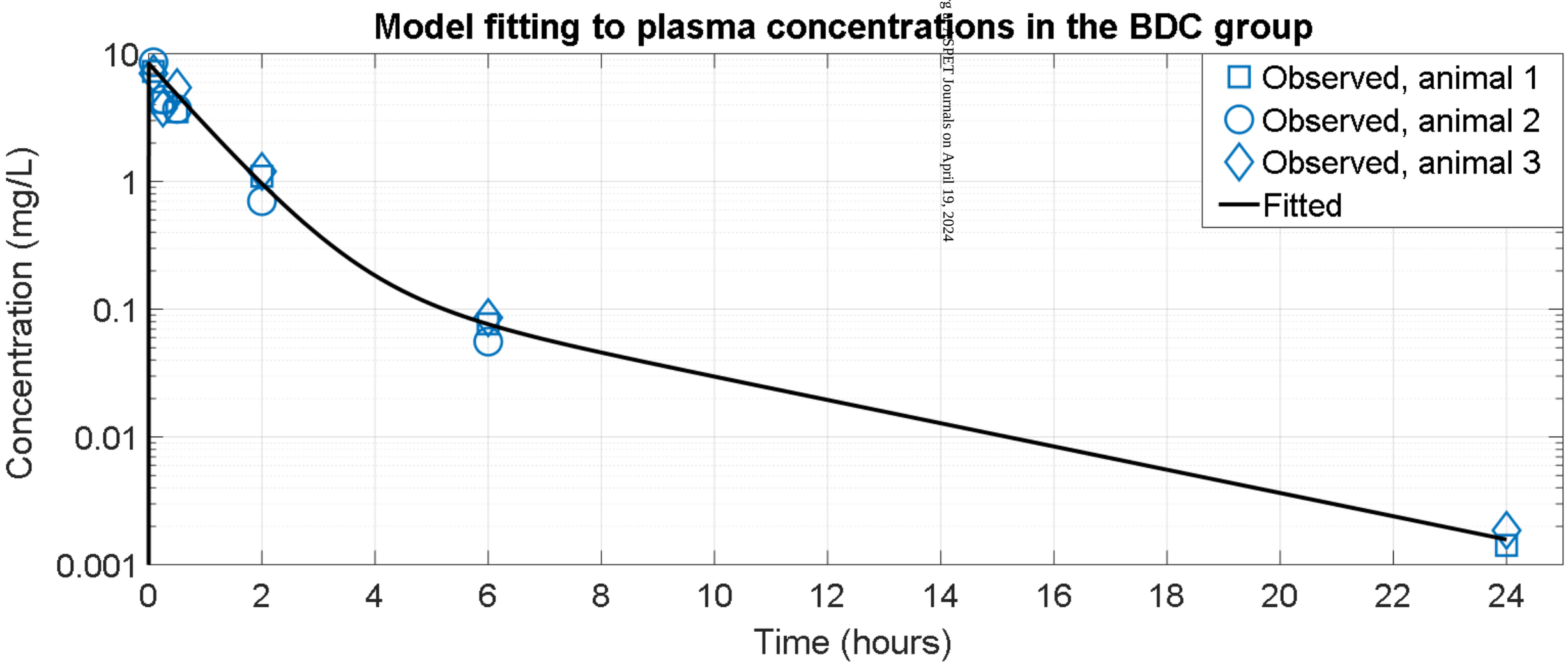

Figure 6B

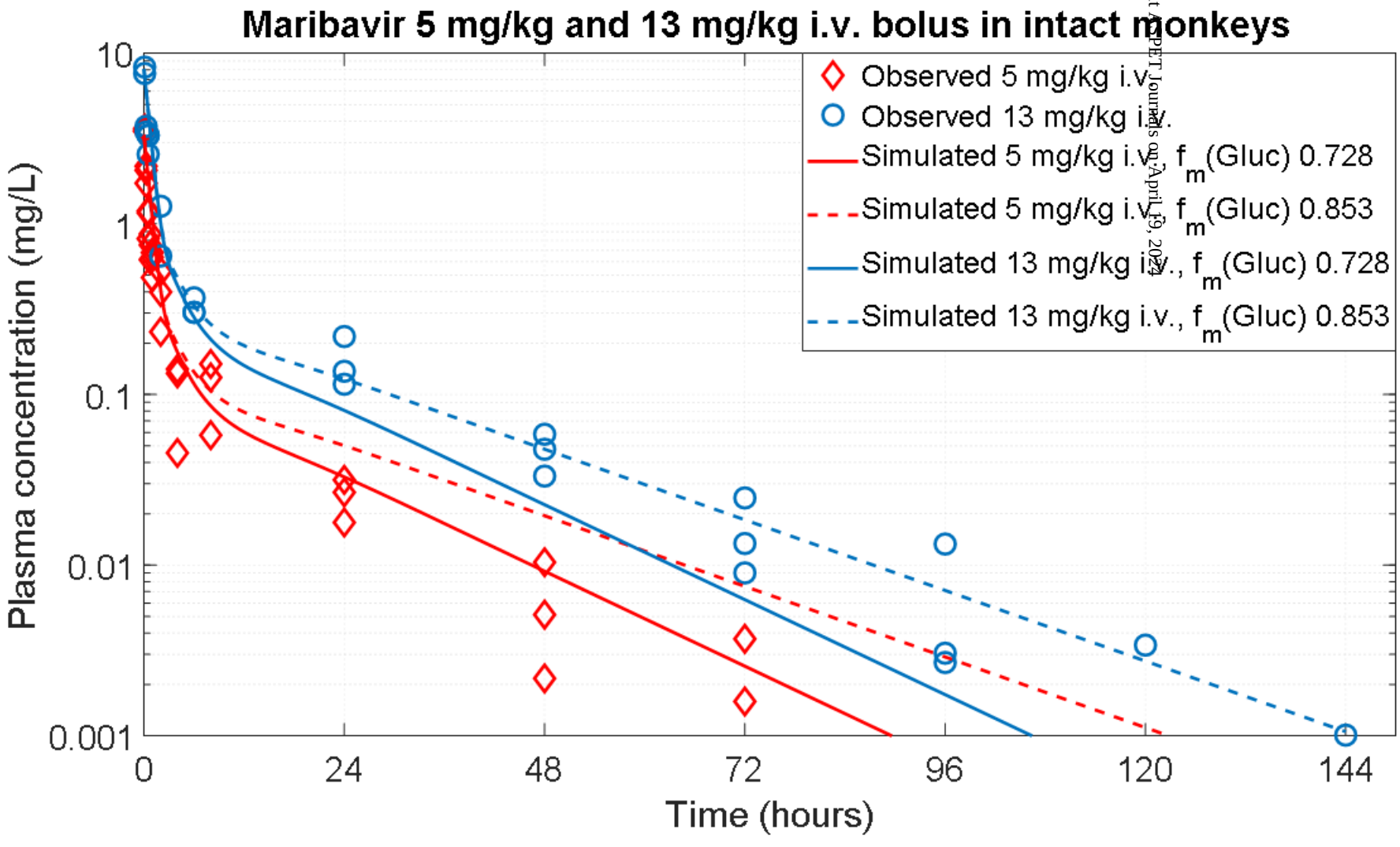

Figure 6C

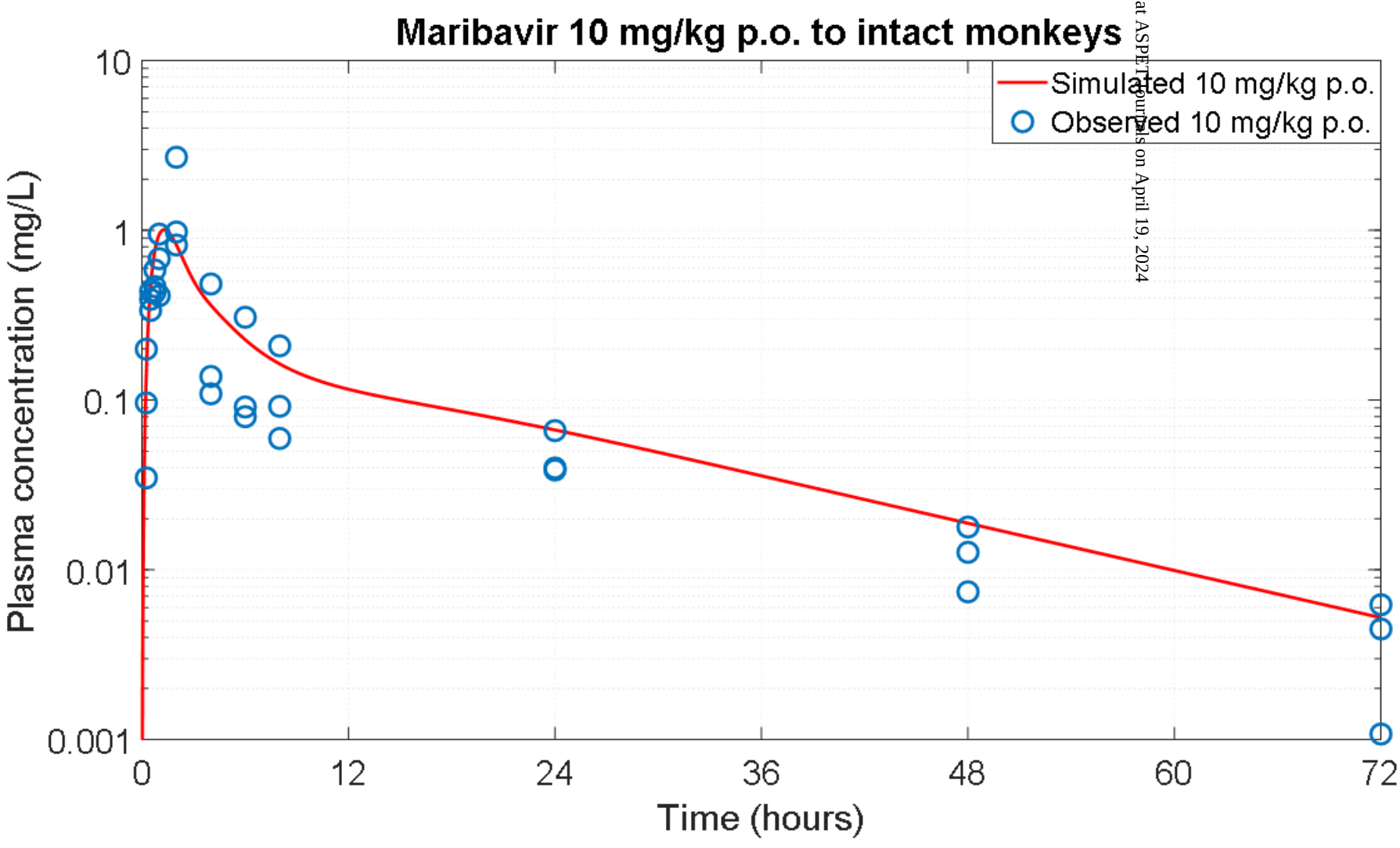

Figure 6D

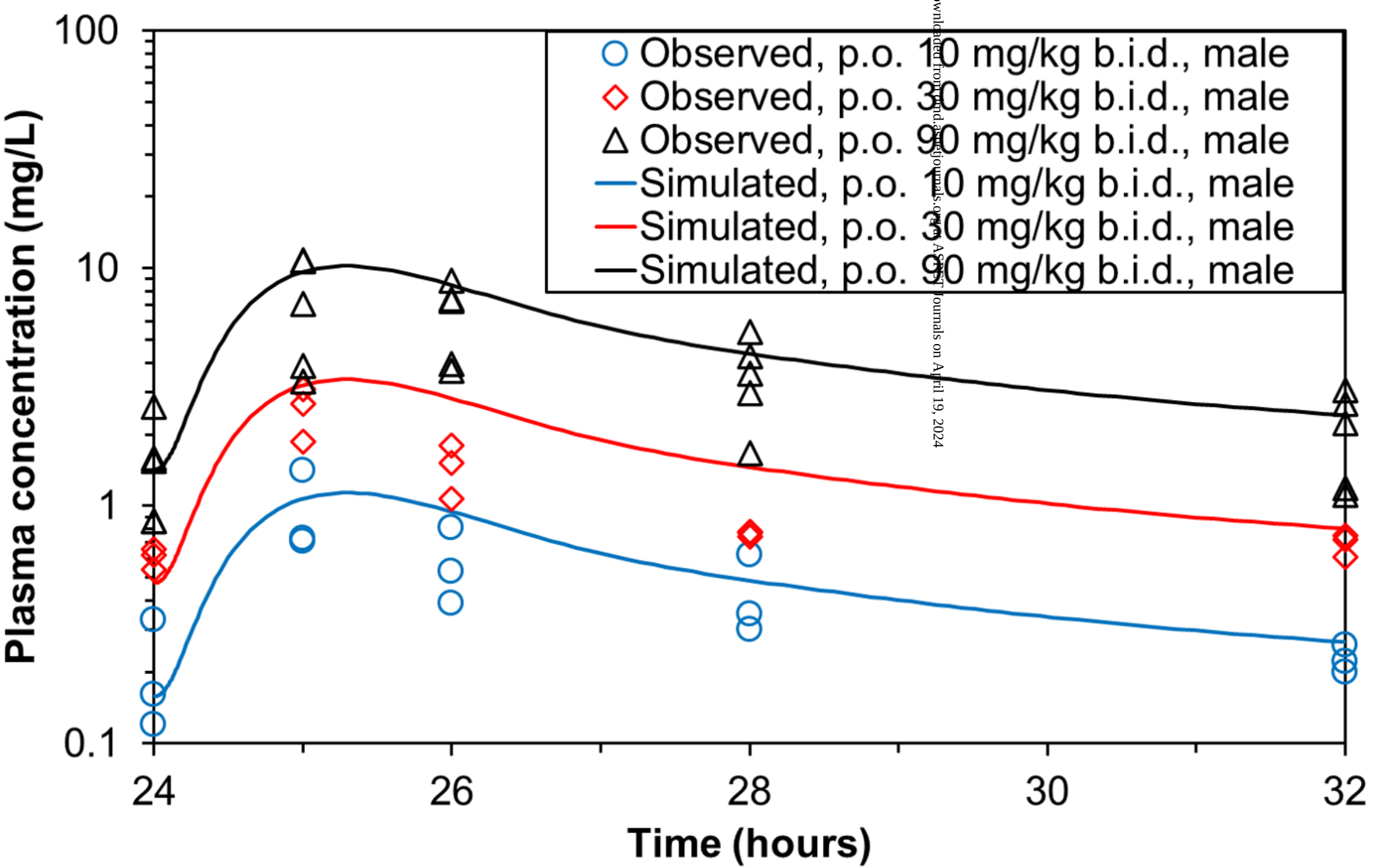

Figure 6E

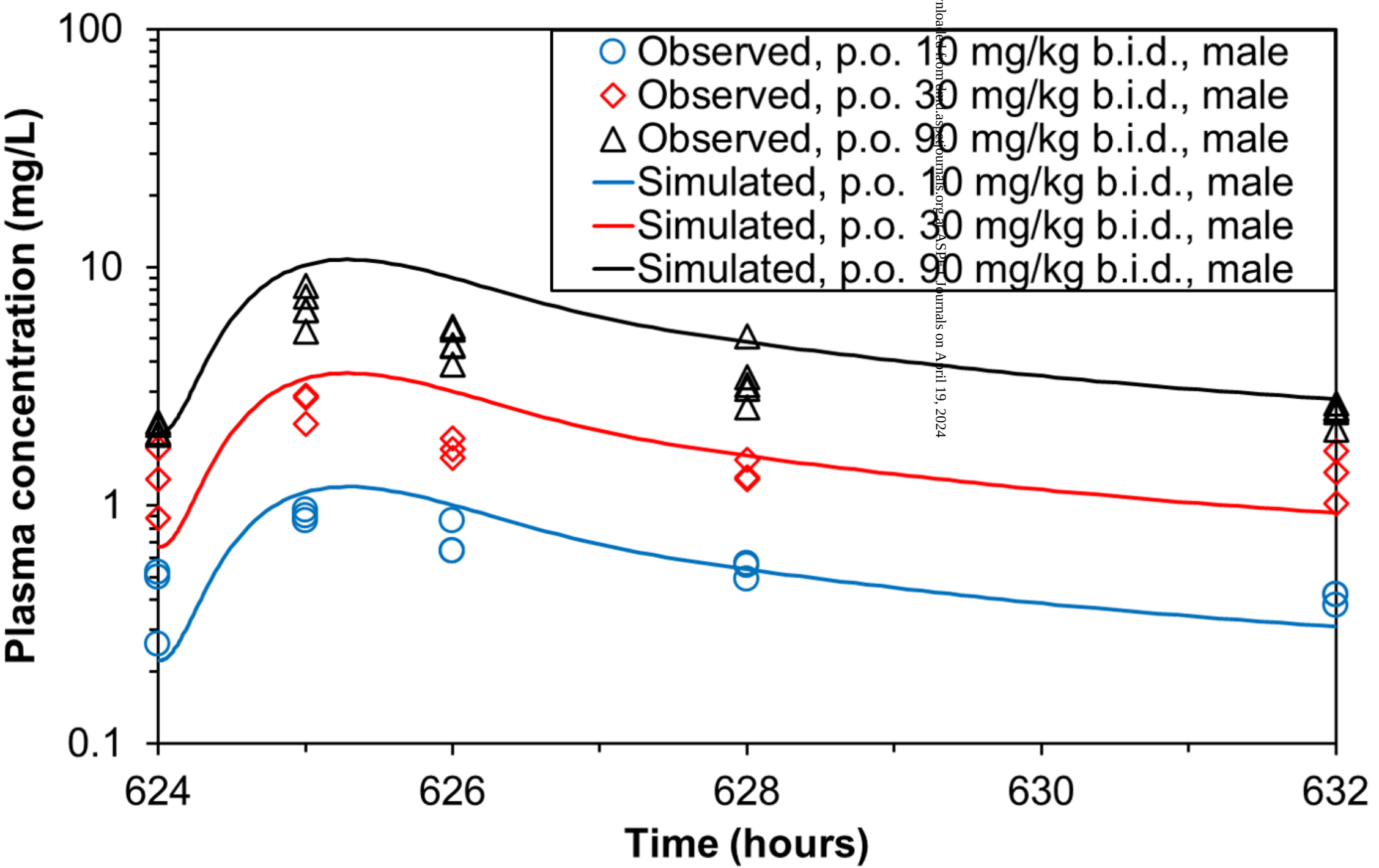

Figure 7A

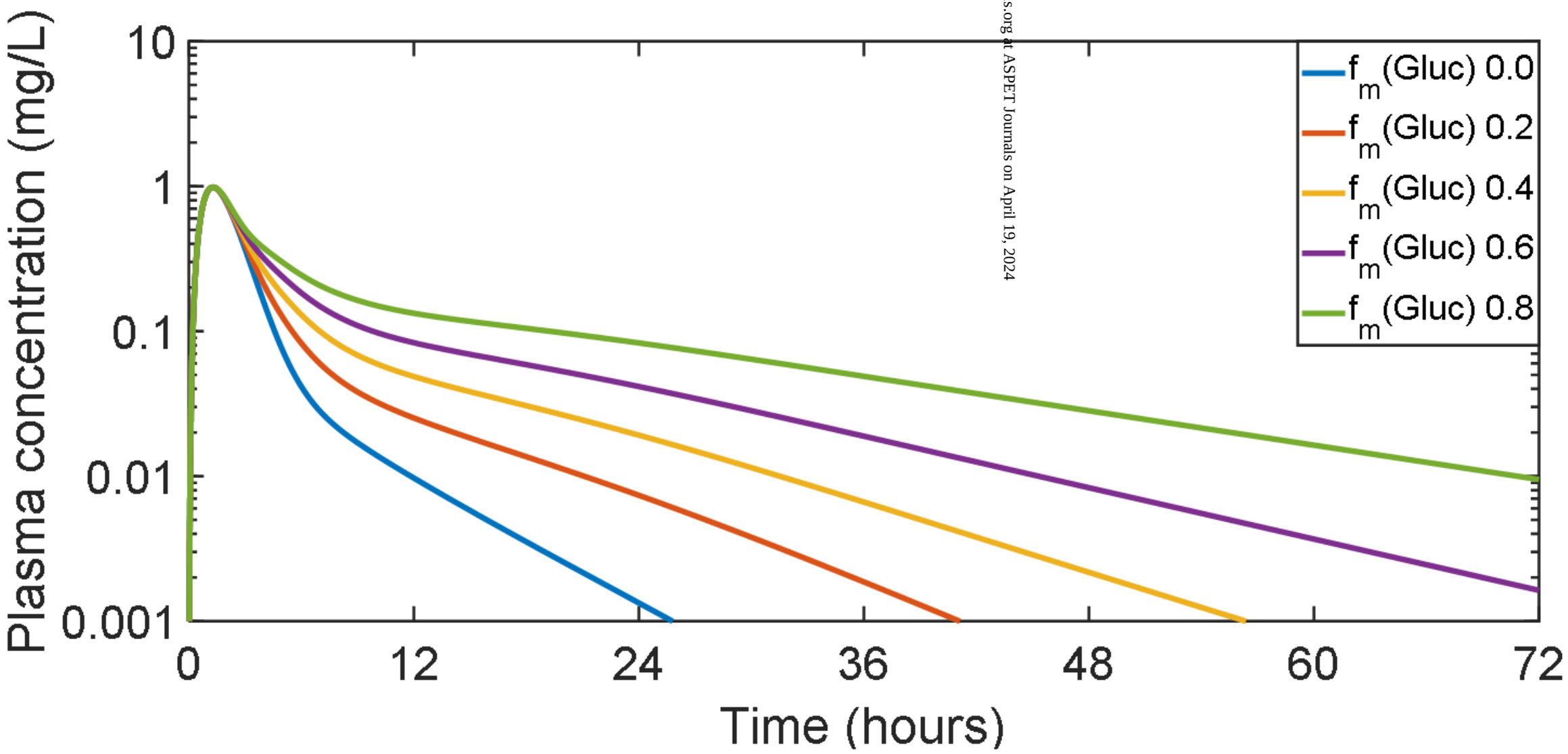

Figure 7B

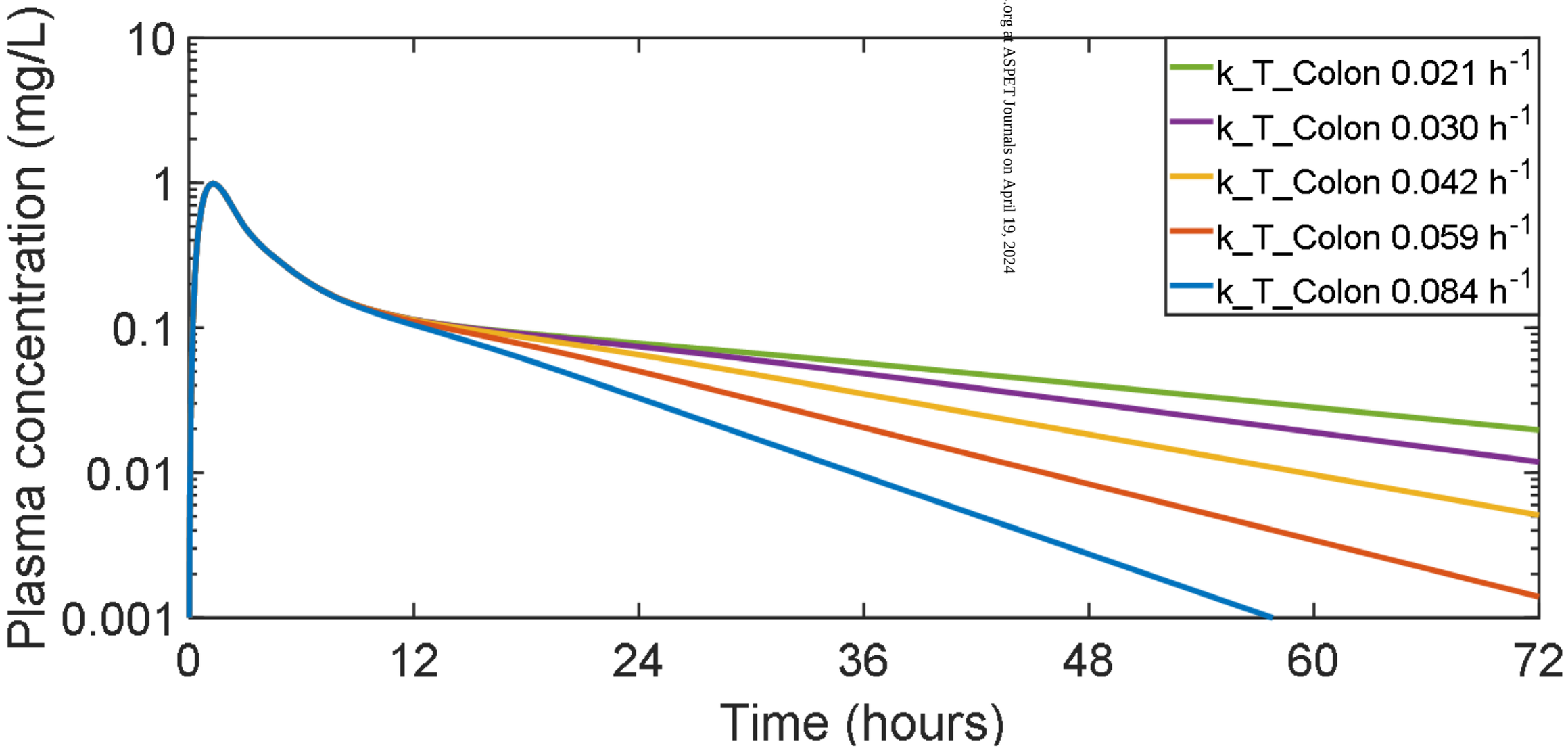

Supplemental Material

Title: Elucidation of Metabolic and Disposition Pathways for Maribavir in Non-human Primates Through Mass Balance and Semi-Physiologically Based Modeling Approaches

Authors: Kefeng Sun and Devin Welty

Journal: *Drug Metabolism and Disposition*

Manuscript number: DMD-AR-2021-000493

Methods

Animal Preparation, BDC Surgery and Dosing

Animal Preparation. Certified Primate Diet #5048 was provided to animals unless otherwise specified under surgical and clinical pathology procedures. Diets were supplemented with appropriate fruits and cereals. Water was provided fresh daily, ad libitum. During acclimation, animals were housed in stainless steel cages and provided with cage enrichment devices and treats. Enrichment devices and treats were withheld from the time of dose administration until at least 96 hours after dosing to ensure no radioactivity was ingested from contaminated sources.

The animal room was maintained at a temperature of 20–26 °C, relative humidity of 50 ± 20%, and with a 12-hour light/dark cycle. Dark cycles were interrupted to accommodate study procedures as necessary.

Prior to bile-duct cannulation (BDC) surgery, animals were acclimated to the jacket and tether system for bile collection. Immediately after surgery, a jacket was placed on each animal and the catheters were guided through a tether. Antibiotics, analgesics, and intravenous (i.v.) fluids were administered as deemed appropriate by a staff veterinarian.

Animals received 5% dextrose solution and Lactated Ringer’s solution via the duodenal cannula continuously through 0–3 days and 3–7 days post-surgery, respectively. Mixed bile salts replacements were administered to animals from 7 days post-surgery to sacrifice.

BDC Surgery. A pre-surgery physical examination was conducted on each animal by a veterinarian. Animals were fasted overnight before surgery. An anesthetic regimen of appropriate medications for sedation and inhaled anesthetic for maintenance was used. Using sterile surgical procedures, the bile duct was cannulated to allow collection of bile, and a second cannula was placed into the duodenum to allow infusion of a bile salts replacement solution or other fluids, as required. Immediately after surgery, a jacket was placed on each animal and the catheters were guided through a tether. Antibiotics, analgesics, and i.v. fluids were administered as deemed appropriate by a veterinarian. Animals were permitted to recover for 10–13 days after surgery.

Dosing. On the day of dosing, 432.2 mg of ^{14}C-maribavir was combined with 4.9 mL of ethanol and mixed. Then, 10.5 mL of propylene glycol was added and the formulation mixed. Finally, 54.6 mL of saline was added and the formulation was magnetically stirred for 15 minutes.

The volume of radiolabeled dose formulation administered to each animal was calculated based on the body weight (minus jacket weight as appropriate) taken on the day of dose administration. The actual amount administered was determined by weighing the dose syringe before and after dose administration. Stability of the radiolabeled maribavir under conditions of administration was demonstrated by analyzing pre-dose and post-dose aliquots by radio-HPLC. Confirmation of stability of the dose formulation under the conditions of administration (column recovery: 102% and 101% for pre- and post-dose aliquots, respectively) serves as confirmation of stability of the test article used to formulate the dose.

Pharmacokinetics and Excretion Balance

Sample Collection. Samples for peripheral blood mononuclear cell isolation were pooled into sodium nitrate cell preparation tubes. Tubes were inverted gently 3–4 times and stored upright at ambient temperature before being processed. Centrifugation was performed as soon as possible following collection.

Plasma. Blood collected for radioanalysis and metabolite profiling was collected into tubes containing K_2-ethylenediaminetetraacetic acid (K_2EDTA) and maintained in chilled cryoracks until aliquoted for radioanalysis. The remaining sample was stored at −70 °C for metabolite profiling. Blood samples obtained for plasma derivation were maintained in chilled cryoracks until

centrifuged to obtain plasma. A 200 µL aliquot was placed into a tube and retained for bioanalysis. The remaining plasma was retained for radioanalysis and metabolite profiling; cellular fractions were discarded. Samples were stored at −70 °C until radioanalysis.

Urine. Urine was collected in plastic containers surrounded by dry ice and the weight of each sample was recorded. Any urine excreted outside of the cage was collected with gauze and saved for radioanalysis.

Feces. Feces were collected at ambient temperature in plastic containers.

Bile collected from BDC animals was collected into plastic containers surrounded by dry ice. The weight of each sample was recorded.

Cage Wash/Cage Wipe. After each 24-hour excreta collection through to 312 hours post-dose, cages were rinsed with water. Cage rinse samples were collected into plastic containers, and the weight of each sample was recorded. Cage debris, consisting mainly of hair and food, was collected daily and pooled by animal. After the last excreta collections, cages were washed and wiped with a solution of 1% trisodium phosphate in water. The cage wash and cage wipe samples were collected into separate plastic containers, and the weight of each cage wash sample was recorded.

Radioactivity Measurement. Double aliquots of all samples were analyzed for radioactivity concentrations. Each sample was homogenized before analysis unless the entire sample was used. All samples were analyzed in duplicate if sample size allowed; if results from duplicates differed by more than 10% from the mean value, the sample was re-homogenized and reanalyzed.

Blood samples were digested with solubilizing agent before incubation with 0.1 M disodium salt of ethylenediaminetetraacetic acid (Na_2EDTA) and 30% hydrogen peroxide. Resultant samples were then left overnight and scintillation cocktail was added before analysis by liquid scintillation counters (LSC). Fecal samples were homogenized in solvent (reverse osmosis water:acetonitrile [ACN]; 60:40) and digested with sodium hydroxide before analysis by LSC.

Metabolite Profiling

Radioactivity Extraction Recovery. Extraction recoveries for each excreta was determined by combining samples with acetonitrile and the supernatant of sonicated, vortex-mixed, centrifuged samples removed. The extraction was repeated and the respective supernatants were combined. Duplicate aliquots were analyzed by LSC to determine the percentage of radioactivity extracted. The eluents for representative urine, feces, and bile samples were determined for the column recoveries, and ranged from 97.4 to 107%.

Plasma Samples. Plasma samples obtained from male monkeys in Groups 1 and 2 at 0.083, 0.25, 0.5, 2, 6, 24 (Group 1 only), and 48 (Group 1 only) hours post-dose were pooled by group and time point to generate seven (Group 1) and five (Group 2) pooled samples, including 0.06 to 0.15 g of each sample by weight. The radioactivity in each pooled sample was determined by LSC. Two additional plasma samples (Group 1, Animal #3, 72-hour and Group 2, Animal #3, 24-hour) were processed following the same procedures as the pooled samples. An aliquot of each plasma pool or individual sample was combined with acetonitrile, centrifuged, and the supernatant removed. The extraction was repeated and the respective supernatants combined. Combined supernatants were evaporated to dryness under nitrogen and reconstituted in reverse osmosis water (300 µL).

Urine samples. Thirteen pooled urine samples were generated for Group 1: a pooled 0–48-hour sample (from 0–8, 8–24, and 28–48 hours post-dose) and samples pooled by collection interval at 48–72, 72–96, 96–120, 120–144, 144–168, 168–192, 192–216, 216–240, 240–264, 264–288, 288–312, and 312–336 hours post-dose. Seven pooled urine samples were generated for Group 2: a pooled 0–24-hour sample (from 0–8 and 8–24 hours post-dose) and samples pooled by collection interval at 24–48, 48–72, 72–96, 96–120, 120–144, and 144–168 hours post-dose.

The Group 1 72–96, 96–120, and 120–144-hour samples and the Group 2 24–48-hour pooled samples were concentrated.

Feces Samples. Approximately 2 g of each sample was combined with acetonitrile, sonicated, vortex mixed, centrifuged, and the supernatant collected. The extraction was repeated and the respective supernatants combined. Combined supernatants were evaporated to dryness under

nitrogen and reconstituted in 300 µL of methanol (MeOH). Due to low recoveries, Group 2 24–48- and 48–72-hour samples were reconstituted in an additional 100 µL of MeOH.

LC-MS/MS Instrumentation and Conditions. Details of LC-MS/MS setup for metabolite profiling are listed below.

LC-MS instrumentation for metabolite profiling:

Controller:	Shimadzu/Prominence CBM-20A
Pumps:	Shimadzu/Nexera LC-30AD
Autoinjector:	Shimadzu/Nexera SIL-30ACMP (10 °C)
Column oven:	Shimadzu/Prominence CTO-20AC (45 °C)
Degasser:	Shimadzu/Prominence DGU-20A5R
Mass spectrometer:	Thermo Fisher Scientific Q Exactive
Fraction collector:	Leap Technologies PAL HTC-xt

LC-MS conditions for metabolite profiling:

Ionization interface:	Positive/negative heated electrospray interface (HESI)		
HPLC column:	Waters Atlantis T3, 4.6 x 250 mm, 5 µm		
Guard column:	Phenomenex C18, 3 x 4 mm		
Mobile phase A:	0.1% formic acid in water		
Mobile phase B:	acetonitrile		
Gradient:	Time (minutes)	%A	%B
	0.0	90	10
	2.0	90	10
	45.0	72	28
	50.0	5	95
	54.0	5	95
	54.5	90	10
	67	90	10
Flow rate:	1.00 mL/minute; split ratio 25:75 mass spectrometer:fraction collector		
Survey scan:	*m/z* 140−900 at 70,000 resolution		
Dependent scans:	MS^2 at 17,500 resolution		
Source voltage:	+4.0 kV, −2.4 kV		
S-Lens RF level:	40		

LC-MS/MS to Determine Maribavir Concentration

For calibration of liquid chromatography–tandem mass spectrometry (LC-MS/MS), nine non-zero calibration standards (1–1,000 ng/mL) and quality control samples (3, 32, 750, and 5,000 ng/mL) were prepared, using cynomolgus monkey plasma that was free of significant interference (BioIVT, Hicksville, NY, USA), and stored at −80 °C. All samples for a given subject were analyzed together in a single batch except when samples had to be re-assayed. A batch, at a minimum, consisted of ≥2 control blanks (control matrix with no internal standard) equal to at least 2% of the unknown samples, 2 standard zero samples (control matrix with internal standard only), and 1 replicate of at least 6 different calibration standards (non-zero standards); replicate low, medium, and high concentration QC samples were also included to reflect at least 5% of the number of unknown samples (minimum *n* = 2 QC samples per concentration level). Calibration curves and standard curves were created based on linear regression. The batch acceptance criteria were: (1) standards were rejected if they were greater than ±15% (all standards but the LLOQ) or ±20% (LLOQ only) of the nominal concentration; (2) at least 75% of the non-zero standards were within the respective acceptance criterion; and (3) at least two-thirds of the low, medium, and high QCs, including at least 50% at each concentration, were valid data points and were within ±15% of the nominal concentration. In terms of between-batch precision and accuracy, the percent coefficient of variation (%CV) for the 3, 32, 750, and 5,000 ng/mL QC samples were 3.3%, 1.1%, 2.6%, and 1.6%, and the percent bias was −7.7%, −8.4%, −10.8%, and −12.4% for the QC samples at the 4 respective concentrations. The percent bias for the standard curve samples ranged from −4.5% to 6.6%.

Metabolism of ^{14}C-maribavir in Hepatocytes

Cryopreserved cynomolgus monkey or human hepatocytes were thawed in a 37 °C water bath with gentle shaking and suspensions were immediately transferred to a centrifuge tube containing pre-warmed media. The suspension was centrifuged at 50 G for 5 minutes. After centrifugation, the supernatant was removed, pre-warmed incubation media added, and the hepatocytes re-suspended. Cell viability was >70%, determined by Trypan Blue staining. ^{14}C-maribavir (10 µM) was incubated in 10^6 cells/mL at 37 °C for 4 hours and ACN then added. After centrifugation, the

supernatant was transferred, dried, and reconstituted in 25% ACN in water. Aliquots were analyzed by LC/UV/MS and LC/UV/radioactivity, using an Agilent 1100 high-performance liquid chromatography (quaternary pumps, autosampler, and diode array UV detector), a Linear Trap Quadropole (LTQ) Orbitrap mass spectrometer (Thermo Scientific, San Jose, CA, USA), and a PerkinElmer 625TR radioactivity flow detector. The radioactivity flow detector equipped with a 200 µL flow cell was operated using scintillation cocktail (Ultima Flo M) at flow rate of 1.2 mL/min. Separation was achieved on a Phenomenex Luna C18 (2) column (2.0 × 250 mm, 5 µm) (Torrance, CA, USA). The mass spectrometer was operated in electrospray positive (ES+) ionization mode. Mass spectra were acquired in full scan (m/z 150 to 1,500) and data-dependent scan (MS^2 and MS^3) modes. The radioactivity in extracts of hepatocyte incubations was determined by liquid scintillation analysis of aliquots of the extracts.

Permeability of Maribavir Across Caco-2 Cell Monolayer

The permeability assay buffer was Hank's Balanced Salt solution containing 10 mM HEPES (4-(2-hydroxyethyl)-1-piperazineethanesulfonic acid) and 15 mM glucose at a pH of 7.0–7.2; the receiver side contained 1% bovine serum albumin. The dosing solution concentration contained 10 µM compounds in assay buffer. Compounds tested were maribavir, atenolol (as low permeability control), and propranolol (as high permeability control). Cells were dosed, in duplicates, on the apical side (apical-to-basolateral) or basolateral side (basolateral-to-apical) and incubated at 37 °C with 5% carbon dioxide in a humidified incubator. At 1 and 2 hours, a 200 µL aliquot was taken from the receiver chamber and replaced with fresh assay buffer. Lucifer Yellow permeation was also measured for each monolayer after being subjected to the test article to confirm monolayer integrity. Concentrations of test article were determined by LC/MS in ES+ mode. The apparent permeability (P_{app}) for each compound was calculated using Supplemental Equation 1:

$$P_{\mathrm{app}} = \frac{dC_{\mathrm{R}}}{dt} \cdot \frac{V_{\mathrm{R}}}{A \cdot C_0}$$ Supplemental Equation 1

where dC_R/dt is the slope for concentrations in the receiving chamber over time, V_R is the volume of the receiving chamber, A is the area for the monolayer, and C_0 is the initial concentration in the donor chamber.

Calculation of Intestinal Effective Permeability from Apparent Permeability. Linear regression analyses were first performed with natural logs (Ln) of human effective permeability (P_{eff}) to Ln(Caco-2 P_{app}) on reference compounds using one set of human P_{eff} data (Larregieu and Benet, 2013) and two sets of Caco-2 P_{app} data (Alsenz et al., 2003; Li et al., 2007; Supplemental Table 4). The regression graphs are shown in Supplemental Fig. 2. The equation for linear regression is:

$$y = a \cdot x + b \qquad \text{Supplemental Equation 2}$$

where y is Ln(human $P_{eff} \times 10^{-4}$ cm/s) and x is Ln(Caco-2 $P_{app} \times 10^{-6}$ cm/s); a is the coefficient on x and b is the intercept of the regression line when $x = 0$.

After averaging the two a and b values from both datasets (Supplemental Fig. 2), the linear relationship becomes:

$$y = 0.645 \cdot x - 1.642 \qquad \text{Supplemental Equation 3}$$

Before plugging in Ln(Caco-2 $P_{app} \times 10^{-6}$ cm/s) of maribavir into x to project y, it has to be adjusted based on differences in the measured P_{app} data for propranolol and atenolol (Supplemental Table 4, rightmost column):

$$\text{Adjusted Ln}(P_{app}) = \text{Original Ln}(P_{app}) + \text{Average(Difference in Ln}(P_{app})\text{ for reference compounds)} \qquad \text{Supplemental Equation 4}$$

The Ln(Caco-2 $P_{app} \times 10^{-6}$ cm/s) for maribavir changed to 3.00 from 1.775 after adjustment with P_{app} data of propranolol and atenolol to previous studies. With $x = 3.00$ in Supplemental Eq. 2, y is calculated to be 0.264; the projected P_{eff} ($\times 10^{-4}$ cm/s) is, therefore, $e^{0.264} = 1.30$. The P_{eff} in monkey is assumed to be the same as in human at 1.30×10^{-4} cm/s.

Calculation of Segmental Permeability in the Gastrointestinal Tract. The first-order absorption rate (k_a) in the jejunum was calculated at 2.34 h^{-1} with:

$$Drug\_ka\_Jejunum = 2 \cdot P_{eff} / Radius \qquad \text{Supplemental Equation 5}$$

where the radius for cynomolgus monkey jejunum is 0.4 cm (Sugano et al., 2012).

According to Supplemental Eq. 5, the k_a at different segments of the gastrointestinal (GI) tract will be determined by the regional P_{eff} as well as the radius. The regional permeability in duodenum, ileum, and colon could be adjusted from the jejunal permeability using a surface area expansion factor (SAEF; Supplemental Table 3, from Olivares-Morales et al., 2015):

$$Drug\_ka\_GI\_region = Drug\_ka\_jejunum \cdot \frac{SAEF(GI\ region)}{SAEF(Jejunum)} \qquad \text{Supplemental Equation 6}$$

As no information on radii of different regions of the cynomolgus monkey GI tract is readily available, the ratios of radii in duodenum, ileum, and colon to that of the jejunum in monkeys were assumed to be the same as those in humans. The information on SAEF and radii are listed in Supplemental Table 3. The order of the calculated k_a in the four regions of the GI tract is Drug_ka_jejunum > Drug_ka_Ileum > Drug_ka_Duodenum >> Drug_ka_Colon.

Calculation of Hydrolysis Rate of Typical *O*-glucuronide by Bacteria Expressing β-glucuronidases. The activity of β-glucuronidase (GUS) from healthy human fecal samples with 1 mM substrate incubation has been reported to be approximately 2.6 μmol/min/(g dry weight of bacteria) (Kim et al., 2001). The intrinsic clearance is, therefore, 2.6 μmol/min/g / 1 mM = 2.6 mL/min/(g dry weight of bacteria). The total dry weight of bacteria in humans has been reported to be around 50 g from a healthy 70 kg human (Sender et al., 2016). Assuming similarity between cynomolgus monkey and human for bacterial activity on a per-kg basis, the activity of bacterial GUS in a 4 kg monkey was calculated at 2.6 mL/min/(g dry weight of bacteria) × 50 (g dry weight bacteria) / 70 kg × 4 kg = 7.4 mL/min. If these bacteria are evenly distributed within the luminal space of the colon, given the colonic luminal volume of 146 mL in monkey (Peters et al., 2012), the degradation rate for typical *O*-glucuronides is thus 7.4 mL/min / 146 mL = 0.051 min^{-1} or 3.1 h^{-1}.

Semi-Physiologically Based Pharmacokinetic Model for Disposition of Maribavir in Monkeys

The semi-physiologically based pharmacokinetic (semi-PBPK) model comprises a modified compartmental absorption and transit (CAT) module for the GI tract (Yu and Amidon, 1999) with five colon luminal compartments plus three systemic compartments (peripheral, central, and liver). The observed plasma concentrations were assumed to resemble those of the central

compartment. The CAT GI model consists of 13 total luminal compartments: one for the stomach, one for the duodenum, two for the jejunum, four for the ileum, and five for the colon. The transit of maribavir or maribavir glucuronides through the GI tract is modeled by small intestine and colon transit rates. The intact versus BDC mode in i.v. dosing was controlled by enabling (BDC_On = 0) or disabling (BDC_On = 1) transit from the duodenum to jejunum. Within each GI luminal segment, maribavir is absorbed with first-order kinetics, with the rate (k_a) determined by P_{eff}.

The liver compartment was necessary to model the first-pass metabolism of maribavir after absorption from the gut, as well as the metabolic and biliary elimination of maribavir as glucuronides or others. The Drug_Liver_CL parameter is used to describe the clearance of the drug from the liver compartment. The formation of maribavir glucuronides in the duodenal lumen through hepatic glucuronidation and biliary secretion was assumed to be a first-order process and driven primarily by the formation rate of glucuronides; another module that incorporated the periodic waves of bile flow was initially developed and evaluated, but was found to not improve the predictability of the systemic concentration profile and was ultimately not included in the final model. Luminal conversion of maribavir glucuronides to maribavir was assumed to occur in the distal small intestine and throughout the colon, and that the entirety of regenerated maribavir is available for (re-)absorption. The minor renal excretion pathway was modeled as a first-order elimination process from the central compartment. The fraction absorbed (F_a) for maribavir after oral dosing is calculated with:

$$F_{\mathrm{a}} = 1 - \frac{Drug\_Fecal}{Dose}$$ Supplemental Equation 7

Where Drug_Fecal is the simulated amount of maribavir in the feces after a substantial amount of time (≥10 days) post-oral dosing.

To simulate the fraction absorbed from each GI segment, the absorption fluxes (Supplemental Table 1 and Supplemental Fig. 1) were turned off in a stepwise fashion from the last segment of the colon to the duodenum, and the incremental AUC change for each GI segment was recorded. The F_a from each GI segment is calculated by dividing the incremental AUC change from each segment with the total AUC (when all absorption fluxes were enabled).

The volume of distribution at steady state (V_{ss}) for intravenous bolus dosing in intact animals is calculated with:

$$V_{\mathrm{SS}} = \frac{Dose \cdot AUMC}{AUC^2} = \frac{Dose \cdot \int_0^\infty (C_\mathrm{p} \cdot t)\, dt}{\left(\int_0^\infty C_\mathrm{p} dt\right)^2} \qquad \text{Supplemental Equation 8}$$

Where C_p denotes plasma concentration of maribavir and AUMC is the area under the plasma concentration first moment versus time curve.

Results and Discussion

Parameter Estimation in the Semi-PBPK Model

Drug clearance from the liver compartment (Drug_Liver_CL). The Drug_Liver_CL parameter, estimated at 16 L/h, denotes the clearance of maribavir from the liver compartment. This is different from the conventional drug clearance concept in the plasma compartment (CL_{plasma}). An approximate conversion between Drug_Liver_CL and CL_{plasma} can be performed using the well-stirred model (Supplemental Equation 9; assuming negligible non-hepatic clearance pathways):

$$CL_{\mathrm{Plasma}} = \frac{Q_\mathrm{h} \cdot Drug\_Liver\_CL}{Q_\mathrm{h} + Drug\_Liver\_CL} \qquad \text{Supplemental Equation 9}$$

Where Q_h is the hepatic blood flow at 2.6 L/h/kg or 9.2 L/h (from 2.6 L/h/kg × 4 kg body weight) in the mass balance study of maribavir in cynomolgus monkeys (Supplemental Table 5).

When using the Q_h and Drug_Liver_CL values of 9.6 L/h and 16 L/h, respectively, in Supplemental Equation 9, the drug clearance from the plasma compartment was calculated as 6.0 L/h; this was similar to the plasma clearance of maribavir calculated separately from non-compartmental analysis (NCA) of the plasma PK time course (5.72 L/h) for BDC animals.

Additional Sensitivity Analyses on Important Parameters in the Semi-PBPK Model

Intestinal permeability (P_{eff}). For rapidly absorbed drugs that do not undergo enterohepatic recirculation, changes to P_{eff} only affect the absorption phase after oral dosing (C_{max}, T_{max}) and the

AUC; it typically does not impact the terminal slope of the PK time course. For a drug that displays prominent EHR behavior (eg, maribavir in monkeys), the terminal PK slope is shallower for a parent drug with high P_{eff}, and steeper if the parent drug has a lower P_{eff} (Supplemental Fig. 29A).

Drug clearance from the liver (Drug_Liver_CL). For a rapidly absorbed drug that does not undergo enterohepatic recirculation, the terminal elimination phase of the PK time course is in part driven by the systemic clearance of the drug; changing the plasma clearance while fixing other PK parameters would result in changes to the terminal slope of the PK curve. However, for a drug that displays prominent EHR behavior (eg, maribavir in monkeys), altering the drug clearance in the liver (affecting the nominal drug clearance in plasma; Supplemental Equation 9) would not result in a change to the terminal phase of the plasma PK time course (Supplemental Fig. 29B). Nonetheless, overall exposure (AUC) is still impacted by Drug_Liver_CL.

Small intestine transit time (SITT). A change to SITT had no impact on the C_{max} of maribavir in monkeys after oral dosing and did not significantly impact the AUC of the parent drug, although faster small intestinal transit was simulated to result in a slightly lower AUC (Supplemental Fig. 29C).

Rate of hydrolysis of maribavir glucuronides (Gluc_k_hydrolysis). Variation of Gluc_k_hydrolysis across a wide range of values had no significant effect on the exposure to maribavir after oral dosing (Supplemental Fig. 29D).

Intercompartmental drug clearance between the central and peripheral compartments (Drug_Q12). Variation of the Drug_Q12 also had little effect on the exposure to maribavir after oral dosing (Supplemental Fig. 29E).

Supplemental Tables

SUPPLEMENTAL TABLE 1

All fluxes used in the semi-physiologically based pharmacokinetic model for maribavir in cynomolgus monkeys.

Flux in SimBiology®	**Expression in SimBiology®**	**Description**
Absorption_1	Drug_ka_Duodenum*Drug_SI1*(1-BDC_On)	Flux of parent from duodenal lumen to liver
Absorption_2	Drug_ka_Jejunum*Drug_SI2	Flux of parent from jejunal lumen 1 to liver
Absorption_3	Drug_ka_Jejunum*Drug_SI3	Flux of parent from jejunal lumen 2 to liver
Absorption_4	Drug_ka_Ileum*Drug_SI4	Flux of parent from ileal lumen 1 to liver
Absorption_5	Drug_ka_Ileum*Drug_SI5	Flux of parent from ileal lumen 2 to liver
Absorption_6	Drug_ka_Ileum*Drug_SI6	Flux of parent from ileal lumen 3 to liver
Absorption_7	Drug_ka_Ileum*Drug_SI7	Flux of parent from ileal lumen 4 to liver
Absorption_Colon1	Drug_ka_Colon*Drug_Colon1	Flux of parent from colon lumen 1 to liver
Absorption_Colon2	Drug_ka_Colon*Drug_Colon2	Flux of parent from colon lumen 2 to liver
Absorption_Colon3	Drug_ka_Colon*Drug_Colon3	Flux of parent from colon lumen 3 to liver
Absorption_Colon4	Drug_ka_Colon*Drug_Colon4	Flux of parent from colon lumen 4 to liver
Absorption_Colon5	Drug_ka_Colon*Drug_Colon5	Flux of parent from colon lumen 5 to liver
Biliary_secretion_liver	(Drug_Liver_ke_Biliary*Drug_Liver)*Liver	Flux of parent from liver to gastrointestinal lumen through biliary excretion
CL_R	(Drug_ke_renal*Drug_Central)*Central	Flux of parent from central to excreta through renal excretion
Drug_ka_IV	k_IV_infuse*Dose_IV	Flux of parent during intravenous injection
Drug_Liver_Met1	(Drug_Liver_ke_met1*Drug_Liver)*Liver	Flux of parent from liver to excreta through non-glucuronidation metabolism to metabolites
Drug_Stomach_Transit	k_T_Stomach*Dose_PO	Flux of parent from stomach lumen to duodenum
Drug_Tran_Colon1	k_T_Colon_5Cpt*Drug_Colon1	Flux of parent from colon lumen 1 to colon lumen 2

Drug_Tran_Colon2	k_T_Colon_5Cpt*Drug_Colon2	Flux of parent from colon lumen 2 to colon lumen 3
Drug_Tran_Colon3	k_T_Colon_5Cpt*Drug_Colon3	Flux of parent from colon lumen 3 to colon lumen 4
Drug_Tran_Colon4	k_T_Colon_5Cpt*Drug_Colon4	Flux of parent from colon lumen 4 to colon lumen 5
Drug_Tran_Colon5	k_T_Colon_5Cpt*Drug_Colon5	Flux of parent from colon lumen 5 to feces
Drug_Transit_SI_1	k_T_Duod*Drug_SI1*(1-BDC_On)	Flux of parent from duodenal lumen to jejunal lumen 1
Drug_Transit_SI_2	k_T_Jej_2Cpt*Drug_SI2	Flux of parent from jejunal lumen 1 to jejunal lumen 2
Drug_Transit_SI_3	k_T_Jej_2Cpt*Drug_SI3	Flux of parent from jejunal lumen 2 to ileal lumen 1
Drug_Transit_SI_4	k_T_Ile_4Cpt*Drug_SI4	Flux of parent from ileal lumen 1 to ileal lumen 2
Drug_Transit_SI_5	k_T_Ile_4Cpt*Drug_SI5	Flux of parent from ileal lumen 2 to ileal lumen 3
Drug_Transit_SI_6	k_T_Ile_4Cpt*Drug_SI6	Flux of parent from ileal lumen 3 to ileal lumen 4
Drug_transit_SI_7	k_T_Ile_4Cpt*Drug_SI7	Flux of parent from ileal lumen 4 to colon lumen 1
Gluc_from_Liver	(Drug_Liver_ke_gluc*Drug_Liver) *Liver	Flux of parent from liver to duodenum through glucuronidation to glucuronides
Gluc_exc	(Drug_ke_gluc_exc*Drug_Central) *Central	Flux of parent from central to excreta through glucuronidation to glucuronides
Gluc_SI_Transit_1	k_T_Duod*Gluc_SI1*(1-BDC_On)	Flux of glucuronides from duodenal lumen to jejunal lumen 1
Gluc_SI_Transit_2	k_T_Jej_2Cpt*Gluc_SI2	Flux of glucuronides from jejunal lumen 1 to jejunal lumen 2
Gluc_SI_Transit_3	k_T_Jej_2Cpt*Gluc_SI3	Flux of glucuronides from jejunal lumen 2 to ileal lumen 1
Gluc_SI_Transit_4	k_T_Ile_4Cpt*Gluc_SI4	Flux of glucuronides from ileal lumen 1 to ileal lumen 2
Gluc_SI_Transit_5	k_T_Ile_4Cpt*Gluc_SI5	Flux of glucuronides from ileal lumen 2 to ileal lumen 3
Gluc_SI_Transit_6	k_T_Ile_4Cpt*Gluc_SI6	Flux of glucuronides from ileal lumen 3 to ileal lumen 4
Gluc_SI_transit_7	k_T_Ile_4Cpt*Gluc_SI7	Flux of glucuronides from ileal lumen 4 to colon lumen 1
Gluc_Tran_Colon1	k_T_Colon_5Cpt*Gluc_Colon1	Flux of glucuronides from colon lumen 1 to colon lumen 2
Gluc_Tran_Colon2	k_T_Colon_5Cpt*Gluc_Colon2	Flux of glucuronides from colon lumen 2 to colon lumen 3
Gluc_Tran_Colon3	k_T_Colon_5Cpt*Gluc_Colon3	Flux of glucuronides from colon lumen 3 to colon lumen 4
Gluc_Tran_Colon4	k_T_Colon_5Cpt*Gluc_Colon4	Flux of glucuronides from colon lumen 4 to colon lumen 5
Gluc_Tran_Colon5	k_T_Colon_5Cpt*Gluc_Colon5	Flux of glucuronides from colon lumen 5 to feces

Hydrolysis_Colon_1	Gluc_k_hydrolysis*Gluc_Colon1	Flux of glucuronides to parent within colon lumen 1
Hydrolysis_Colon_2	Gluc_k_hydrolysis*Gluc_Colon2	Flux of glucuronides to parent within colon lumen 2
Hydrolysis_Colon_3	Gluc_k_hydrolysis*Gluc_Colon3	Flux of glucuronides to parent within colon lumen 3
Hydrolysis_Colon_4	Gluc_k_hydrolysis*Gluc_Colon4	Flux of glucuronides to parent within colon lumen 4
Hydrolysis_Colon_5	Gluc_k_hydrolysis*Gluc_Colon5	Flux of glucuronides to parent within colon lumen 5
Hydrolysis_Ileum3	Gluc_k_hydrolysis*Gluc_SI6	Flux of glucuronides to parent within ileal lumen 3
Hydrolysis_Ileum4	Gluc_k_hydrolysis*Gluc_SI7	Flux of glucuronides to parent within ileal lumen 4
QCHep	(k_h2C*Drug_Liver)*Liver-(k_C2h*Drug_Central)*Central	Flux of parent between liver and central compartments
QCP	(Drug_k12*Drug_Central)*Central-(Drug_k21*Drug_Peripheral) *Peripheral	Flux of parent between central and peripheral compartments

SUPPLEMENTAL TABLE 2

All differential equations used in the semi-physiologically based pharmacokinetic model for maribavir in cynomolgus monkeys. The fluxes on the right side of the differential equations are specified in Supplemental Table 1.

d(Dose_IV)/dt = -Drug_ka_IV
d(Dose_PO)/dt = -Drug_Stomach_Transit
d(Drug_Central)/dt = 1/Central*(-QCP - CL_R + QCHep - Gluc_liver_exc + Drug_ka_IV)
d(Drug_Peripheral)/dt = 1/Peripheral*(QCP)
d(Drug_Liver)/dt = 1/Liver*(Absorption_1 + Absorption_Colon1 + Absorption_2 + Absorption_3 + Absorption_4 + Absorption_5 - Biliary_secretion_liver - QCHep - Gluc_from_Liver - Drug_Liver_Met1 + Absorption_Colon2 + Absorption_Colon3 + Absorption_Colon4 + Absorption_Colon5 + Absorption_6 + Absorption_7)
d(Drug_SI1)/dt = -Absorption_1 + Drug_Stomach_Transit - Drug_Transit_SI_1 + Biliary_secretion_liver
d(Drug_SI2)/dt = Drug_Transit_SI_1 - Drug_Transit_SI_2 - Absorption_2
d(Drug_SI3)/dt = Drug_Transit_SI_2 - Absorption_3 - Drug_Transit_SI_3
d(Drug_SI4)/dt = Drug_Transit_SI_3 - Absorption_4 - Drug_Transit_SI_4
d(Drug_SI5)/dt = Drug_Transit_SI_4 - Absorption_5 - Drug_Transit_SI_5
d(Drug_SI6)/dt = Drug_Transit_SI_5 - Drug_Transit_SI_6 - Absorption_6 + Hydrolysis_Ileum3
d(Drug_SI7)/dt = Drug_Transit_SI_6 + Hydrolysis_Ileum4 - Absorption_7 - Drug_transit_SI_7
d(Drug_Colon1)/dt = Hydrolysis_Colon_1 - Absorption_Colon1 - Drug_Tran_Colon1 + Drug_transit_SI_7
d(Drug_Colon2)/dt = Drug_Tran_Colon1 + Hydrolysis_Colon_2 - Drug_Tran_Colon2 - Absorption_Colon2
d(Drug_Colon3)/dt = Drug_Tran_Colon2 + Hydrolysis_Colon_3 - Absorption_Colon3 - Drug_Tran_Colon3
d(Drug_Colon4)/dt = Hydrolysis_Colon_4 + Drug_Tran_Colon3 - Absorption_Colon4 - Drug_Tran_Colon4
d(Drug_Colon5)/dt = Hydrolysis_Colon_5 + Drug_Tran_Colon4 - Absorption_Colon5 - Drug_Tran_Colon5
d(Drug_Fecal)/dt = Drug_Tran_Colon5
d(Gluc_SI1)/dt = -Gluc_SI_Transit_1 + Gluc_from_Liver
d(Gluc_SI2)/dt = Gluc_SI_Transit_1 - Gluc_SI_Transit_2

d(Gluc_SI3)/dt = Gluc_SI_Transit_2 - Gluc_SI_Transit_3
d(Gluc_SI4)/dt = Gluc_SI_Transit_3 - Gluc_SI_Transit_4
d(Gluc_SI5)/dt = -Gluc_SI_Transit_5 + Gluc_SI_Transit_4
d(Gluc_SI6)/dt = Gluc_SI_Transit_5 - Gluc_SI_Transit_6 - Hydrolysis_Ileum3
d(Gluc_SI7)/dt = Gluc_SI_Transit_6 - Hydrolysis_Ileum4 - Gluc_SI_transit_7
d(Gluc_Colon1)/dt = -Hydrolysis_Colon_1 - Gluc_Tran_Colon1 + Gluc_SI_transit_7
d(Gluc_Colon2)/dt = Gluc_Tran_Colon1 - Hydrolysis_Colon_2 - Gluc_Tran_Colon2
d(Gluc_Colon3)/dt = Gluc_Tran_Colon2 - Hydrolysis_Colon_3 - Gluc_Tran_Colon3
d(Gluc_Colon4)/dt = -Hydrolysis_Colon_4 + Gluc_Tran_Colon3 - Gluc_Tran_Colon4
d(Gluc_Colon5)/dt = -Hydrolysis_Colon_5 + Gluc_Tran_Colon4 - Gluc_Tran_Colon5
d(Gluc_Fecal)/dt = Gluc_Tran_Colon5
d(Amt_Drug_exc)/dt = CL_R
d(Amt_Drug_met1)/dt = Drug_Liver_Met1
d(Amt_Gluc_exc)/dt = Gluc_liver_exc

SUPPLEMENTAL TABLE 3

Calculations of first-order absorption rate (k_a) in different segments of the intestine based on the surface area expansion factor (SAEF) and radii (Olivares-Morales et al., 2015).

Intestinal segment	**Radius (cm)**	**SAEF**	**Calculated first-order absorption rate (k_a) in monkey (h^{-1})**
Jejunum	1.75 in human, 0.4 in cynomolgus monkey	1	2.34
Duodenum	2.37 in human	0.49	0.847
Ileum	1.50 in human	0.58	1.58
Colon	2.42 in human	0.033	0.0558

SUPPLEMENTAL TABLE 4

Human intestinal effective permeability (P_{eff}) and apparent permeability (P_{app}) across the Caco-2 cell monolayer for reference drugs in historic studies and for maribavir. The rightmost column shows the difference of Ln(P_{app}) of propranolol and atenolol in previous studies to those measured in the current study with maribavir.

Ln, natural log.

Drug	**Human intestinal P_{eff} (Larregieu and Benet, 2013)**		**Caco-2 P_{app} (Alsenz et al., 2003)**		**Caco-2 P_{app} (Li et al., 2007)**		**Caco-2 P_{app} in study with maribavir**		
	Measured value ($\times 10^{-4}$ cm/s)	Ln (value)	Measured value ($\times 10^{-6}$ cm/s)	Ln (value)	Measured value ($\times 10^{-6}$ cm/s)	Ln (value)	Measured value ($\times 10^{-6}$ cm/s)	Ln (value)	Difference of Ln(value) to previous data
Propranolol	2.91	1.07	47.2	3.85	39.4	3.67	17.1	2.84	0.925
Metoprolol	1.34	0.293	31.8	3.46	33.2	3.50			
Atenolol	0.20	−1.61	1.73	0.548	1.6	0.470	0.36	−1.02	1.53
Cimetidine	0.26	−1.35	0.59	−0.528	2.7	0.993			
Ranitidine	0.27	−1.31	0.67	−0.400	2.1	0.742			
Maribavir							5.90	1.78	

SUPPLEMENTAL TABLE 5

All compartments, species, and parameters and their values used in the semi-physiologically based pharmacokinetic model for maribavir in cynomolgus monkeys. " └" denotes that the species were contained in the corresponding compartment above it. The SimBiology® diagram is depicted in Supplemental Fig. 1.

BDC, bile duct cannulated; CL, clearance.

Compartment and species	Description	Value or unit	Notes
Stomach	Stomach lumen	0.1 L	From Peters et al., 2012
└ Dose_PO	Oral dose	in mg	
Duodenum	Duodenal lumen	0.015 L	From Peters et al., 2012
└ Drug_SI1	Amount of parent in duodenal lumen	in mg	
└ Gluc_SI1	Amount of maribavir glucuronides in duodenal lumen	in mg	
Jejunum_1	Jejunal lumen compartment 1	0.016 L	From Peters et al., 2012
└ Drug_SI2	Amount of parent in jejunal lumen 1	in mg	
└ Gluc_SI2	Amount of maribavir glucuronides in jejunal lumen 1	in mg	
Jejunum_2	Jejunal lumen compartment 2	0.016 L	From Peters et al., 2012
└ Drug_SI3	Amount of parent in jejunal lumen 2	in mg	
└ Gluc_SI3	Amount of maribavir glucuronides in jejunal lumen 2	in mg	
Ileum_1	Ileal lumen compartment 1	0.010 L	From Peters et al., 2012
└ Drug_SI4	Amount of parent in ileal lumen 1	in mg	
└ Gluc_SI4	Amount of maribavir glucuronides in ileal lumen 1	in mg	
Ileum_2	Ileal lumen compartment 2	0.010 L	From Peters et al., 2012
└ Drug_SI5	Amount of parent in ileal lumen 2	in mg	
└ Gluc_SI5	Amount of maribavir glucuronides in ileal lumen 2	in mg	
Ileum_3	Ileal lumen compartment 3	0.010 L	From Peters et al., 2012
└ Drug_SI6	Amount of parent in ileal lumen 3	in mg	

└ Gluc_SI6	Amount of maribavir glucuronides in ileal lumen 3	in mg	
Ileum_4	Ileal lumen compartment 4	0.010 L	From Peters et al., 2012
└ Drug_SI7	Amount of parent in ileal lumen 4	in mg	
└ Gluc_SI7	Amount of maribavir glucuronides in ileal lumen 4	in mg	
Colon_1	Colon lumen compartment 1	0.0292 L	From Peters et al., 2012
└ Drug_Colon1	Amount of parent in ileal lumen 1	in mg	
└ Gluc_Colon1	Amount of maribavir glucuronides in ileal lumen 1	in mg	
Colon_2	Colon lumen compartment 2	0.0292 L	From Peters et al., 2012
└ Drug_Colon2	Amount of parent in ileal lumen 2	in mg	
└ Gluc_Colon2	Amount of maribavir glucuronides in ileal lumen 2	in mg	
Colon_3	Colon lumen compartment 3	0.0292 L	From Peters et al., 2012
└ Drug_Colon3	Amount of parent in ileal lumen 3	in mg	
└ Gluc_Colon3	Amount of maribavir glucuronides in ileal lumen 3	in mg	
Colon_4	Colon lumen compartment 4	0.0292 L	From Peters et al., 2012
└ Drug_Colon4	Amount of parent in ileal lumen 4	in mg	
└ Gluc_Colon4	Amount of maribavir glucuronides in ileal lumen 4	in mg	
Colon_5	Colon lumen compartment 5	0.0292 L	From Peters et al., 2012
└ Drug_Colon5	Amount of parent in ileal lumen 5	in mg	
└ Gluc_Colon5	Amount of maribavir glucuronides in ileal lumen 5	in mg	
Feces	A generic fecal compartment	0.05 L	
└ Drug_Fecal	Amount of parent in feces	in mg	
└ Gluc_Fecal	Amount of maribavir glucuronides in feces	in mg	
Liver	Liver compartment	0.027 L/kg	From Peters et al., 2012
└ Drug_Liver	Drug concentration in the liver	in mg/L	Initial value set at 1E-9 mg/L
Central	Central compartment	in L	Value from fitting the BDC group data
└ Drug_Central	Drug concentration in the central compartment	in mg/L	Initial value set at 1E-9 mg/L
└ Dose_IV	Intravenous bolus dose	in mg	

Peripheral	Peripheral compartment	in L	Value from fitting the BDC group data
└ Drug_Peripheral	Drug concentration in the peripheral compartment	in mg/L	Initial value set at 1E-9 mg/L
Excreta	A generic excreta compartment	1 L	
└ Amt_Drug_exc	Amount of parent renally excreted	in mg	
└ Amt_Gluc_exc	Amount of maribavir glucuronides that were renally excreted	in mg	
└ Amt_Drug_met1	Amount of maribavir metabolites that are not direct glucuronides	in mg	
Parameter in SimBiology®	**Description**	**Value**	**Notes**
BW_Ref	Reference body weight	4.0 kg	Average body weight in the mass balance study
k_T_Stomach	Rate of transit from stomach to duodenum	2 h^{-1}	From fasted state, gastric emptying time of 30 min
SIRadius	Radius of the small intestine in cynomolgus monkey	0.4 cm	From Sugano et al., 2012
SITT	Small intestine transit time	2.7 h	From Ikegami et al., 2003
k_T_Duod	Duodenal lumen transit rate; defined as 1/(0.08*SITT), where 0.08 is the fractional length of duodenum within the small intestine	4.63 h^{-1}	Fractional length from Olivares-Morales et al., 2015
k_T_Jej_2Cpt	Jejunal lumen transit rate (two segments); defined as 2/(0.37*SITT), where 0.37 is the fractional length of jejunum within the small intestine	2.00 h^{-1}	Fractional length from Olivares-Morales et al., 2015
k_T_Ile_4Cpt	Ileal lumen transit rate (four segments); defined as 4/(0.55*SITT), where 0.55 is the fractional length of ileum within the small intestine	2.69 h^{-1}	Fractional length from Olivares-Morales et al., 2015
k_T_Colon	Colon transit rate	0.0422 h^{-1}	From Peters et al., 2012
k_T_Colon_5Cpt	Colon transit rate between its five compartments	0.211 h^{-1}	From 5 * k_T_Colon
Qh	Hepatic blood flow in cynomolgus monkey	2.60 L/h/kg	From Peters et al., 2012
k_C2h and k_h2C	Transfer rates between central and liver compartments; defined as: k_C2h = Qh / Central; k_h2C = Qh / Liver	in h^{-1}	
Drug_Peff	Effective permeability in jejunum	1.30 × 10^{-4} cm/s	Calculated from Caco-2 cell data; see Supplemental Methods

Drug_ka_Duodenum	First-order absorption rate in duodenum	0.847 h^{-1}	Calculations in Supplemental Methods
Drug_ka_Jejunum	First-order absorption rate in jejunum compartments 1 and 2	2.34 h^{-1}	Calculations in Supplemental Methods
Drug_ka_Ileum	First-order absorption rate in ileum compartments 1 through 4	1.58 h^{-1}	Calculations in Supplemental Methods
Drug_ka_Colon	First-order absorption rate in colon compartments 1 through 5	0.0558 h^{-1}	Calculations in Supplemental Methods
Drug_fm_gluc	Fraction metabolized by direct glucuronidation pathway	0.728 or 0.853	0.728 from in vivo data in BDC group (main text Table 5); 0.853 from in vitro hepatocyte data
Gluc_k_hydrolysis	Rate of hydrolysis of maribavir glucuronides	3.1 h^{-1}	See Supplemental Methods
Drug_CL_Renal	Renal clearance of parent from central compartment	0.0128 L/h	From BDC mean systemic CL × %dose in urine: 5.72 L/h × 0.224% (main text Tables 3 and 4)
Drug_ke_renal	Renal elimination rate of parent; defined as: Drug_CL_Renal / Central	in h^{-1}	
Drug_CL_Biliary	Biliary clearance of parent from central compartment	0.0719 L/h	From BDC mean systemic CL × %dose in bile: 5.72 L/h × 1.26% (main text Tables 3 and 4)
Drug_Liver_CL_met	Metabolic clearance from the liver compartment; defined as: Drug_Liver_CL-Qh*Drug_CL_Biliary / (Qh-Drug_CL_Biliary)	in L/h	Drug_CL_Biliary was derived from central concentrations. A reverse well-stirred model was necessary to empirically convert it to a liver-based clearance
Drug_Liver_ke_gluc	Rate of maribavir glucuronidation and excretion to duodenum; defined as: Drug_Liver_CL_met * Drug_fm_gluc / Liver	in h^{-1}	
Drug_Liver_ke_met1	Rate of non-glucuronidation metabolic elimination of parent; defined as: Drug_Liver_CL_met * (1-Drug_fm_gluc) / Liver	in h^{-1}	
Drug_k12 and Drug_k21	Rate of transfer between central and peripheral compartments; defined as: Drug_k12 = Drug_Q12 / Central	in h^{-1}	

	Drug_k21 = Drug_Q12 / Peripheral		
Drug-specific parameters from fitting the model to observed data in BDC animals			
Parameter in SimBiology®	**Description**	**Value**	**Notes**
Drug_Q12	Central to peripheral transfer	0.660 L/h	
Drug_Liver_CL	Drug clearance from the liver compartment	15.7 L/h	
Drug_Vc_Ref	Volume of the central compartment	6.32 L	
Drug_Vp_Ref	Volume of peripheral compartment	2.79 L	

SUPPLEMENTAL TABLE 6

Tentative structures, characteristics, and matrices in which metabolites of maribavir were identified after a single intravenous bolus administration to male cynomolgus monkeys. Note that there is no sufficient information on differentiating the N- from the O-glucuronides among M1/7/16/17, nor to clearly locate the *O*-glucuronidation site among M10/11/12.

$[M+H]^+$, molecular weight of protonated compound with ^{35}Cl isotope; Gluc, glucuronide; m/z, mass over net charge.

Metabolite designation	**$[M+H]^+$**	**Characteristic product ions (m/z)**	**Proposed metabolite structure**	**Matrix**
M15	461	329, 240, 198, 85	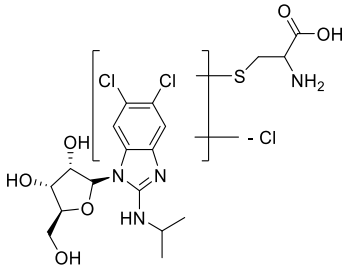	Bile
M1	510	202, 167, 115, 85	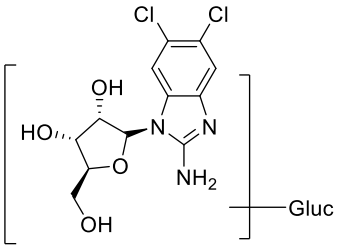	Plasma Urine
M7	510	202, 167, 115, 85	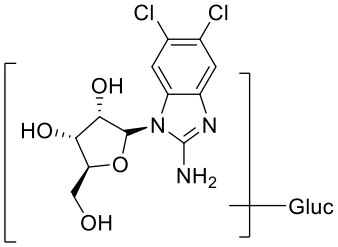	Plasma Urine Bile
M16	510	202, 167, 85	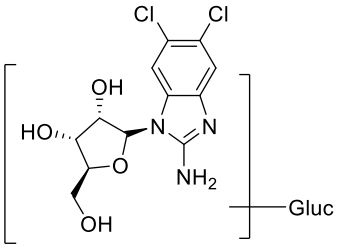	Urine Bile
M17	510	202, 167, 115, 85	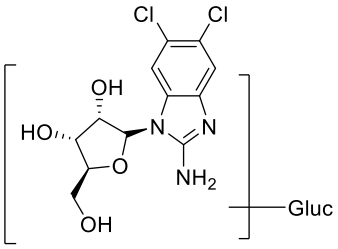	Plasma Urine Bile

M2	420	244, 202, 167	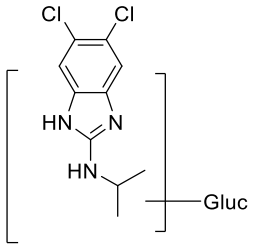	Plasma Urine Bile Feces
M10	552	244, 202, 167, 115, 85	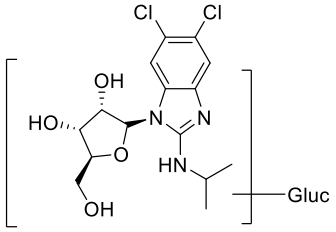	Urine
M4	334	202, 167, 133, 115, 85	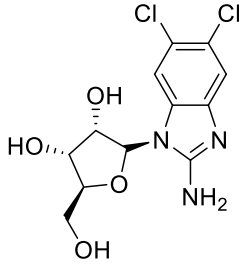	Plasma Urine Feces
M5	392	260, 202	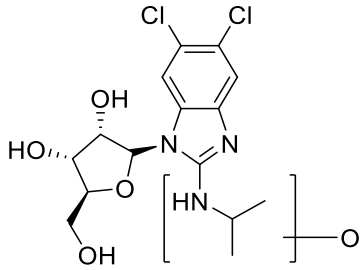	Urine Feces
M11	552	244, 202, 167, 115, 85	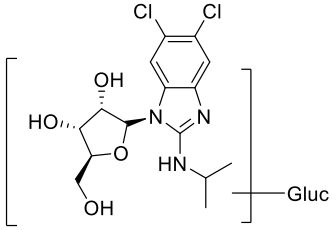	Plasma Urine Bile
M12	552	244, 202, 167, 115, 85	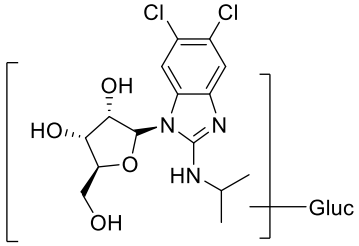	Plasma Urine Bile
Maribavir (SHP620)	376	244, 202, 167, 133, 115, 85	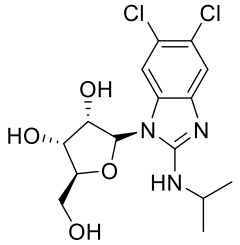	Plasma Urine Bile Feces

SUPPLEMENTAL TABLE 7

(A) Percentage of sample radioactivity as ^{14}C-maribavir or metabolites of ^{14}C-maribavir in pooled plasma samples after a single intravenous dose of ^{14}C-maribavir to male intact monkeys (Group 1 [*n* = 3], 13 mg/kg). (B) Percentage of sample radioactivity as ^{14}C-maribavir or metabolites of ^{14}C-maribavir in pooled plasma samples after a single intravenous dose of ^{14}C-maribavir to male bile duct-cannulated monkeys (Group 2 [*n* = 3], 13 mg/kg). ND, peak not detected or below the established limit of quantitation (1% of run and 10 cpm peak height). Note that the samples were not pooled based on the Hamilton method (Hamilton et al., 1981) and that individuals may exhibit slightly different circulating parent and metabolite profiles.

A

Metabolite designation	Collection time (Hours)					
	0.083	**0.25**	**0.5**	**2**	**6**	**24**
	Percent of radioactivity injected (% of run)					
M1	ND	ND	ND	ND	ND	ND
M7	ND	1.40	2.11	ND	ND	ND
M17/M2	ND	2.79	2.98	ND	ND	ND
M4	2.60	3.10	1.99	ND	ND	ND
M11	1.78	4.96	2.98	ND	ND	ND
M12	4.79	6.36	7.94	8.76	ND	ND
Parent	90.4	80.3	82.0	82.5	86.4	93.3
TOTAL	99.6	98.9	100	91.3	86.4	93.3

B

Metabolite designation	Collection time (Hours)				
	0.083	**0.25**	**0.5**	**2**	**6**
	Percent of radioactivity injected (% of run)				
M1	ND	ND	ND	2.51	ND
M7	1.20	2.90	4.07	4.27	ND
M17/M2	ND	2.90	ND	ND	ND
M4	3.07	4.45	4.55	3.52	ND
M11	3.07	3.87	2.15	ND	25.8
M12	2.40	4.45	2.87	2.76	14.5
Parent	88.9	81.0	83.0	83.9	46.8
TOTAL	98.7	99.6	96.7	97.0	87.1

SUPPLEMENTAL TABLE 8

Segmental absorption percentages of maribavir in the cynomolgus monkey gastrointestinal tract, followed by intravenous bolus or oral dosing (Table 5, main text), as predicted by the semi-PBPK model. For i.v. dosing, the reabsorption does not occur in duodenum, jejunum, or upper ileum due to a lack of GUS-expressing bacteria under normal conditions (grayed out cells). For oral dosing, the overall fraction absorbed (F_a) is 67% at f_m(Gluc) = 0.728.

	5 mg/kg intravenous bolus		**10 mg/kg oral**	
GI segment in the model	AUC (h*mg/L) contributed from segment	Percent contribution to the reabsorbed amount	AUC (h*mg/L) contributed from segment	Percent contribution to overall fraction absorbed
Duodenum			0.40	4.3%
Jejunum 1			1.18	12.5%
Jejunum 2			0.55	5.8%
Ileum 1			0.17	1.8%
Ileum 2			0.11	1.2%
Ileum 3	0.21	11%	0.48	5.1%
Ileum 4	0.34	18%	0.71	7.6%
Colon 1	0.26	14%	0.53	5.6%
Colon 2	0.27	14%	0.56	6.0%
Colon 3	0.28	15%	0.56	6.0%
Colon 4	0.26	14%	0.55	5.8%
Colon 5	0.25	13%	0.51	5.4%

Supplemental Figures

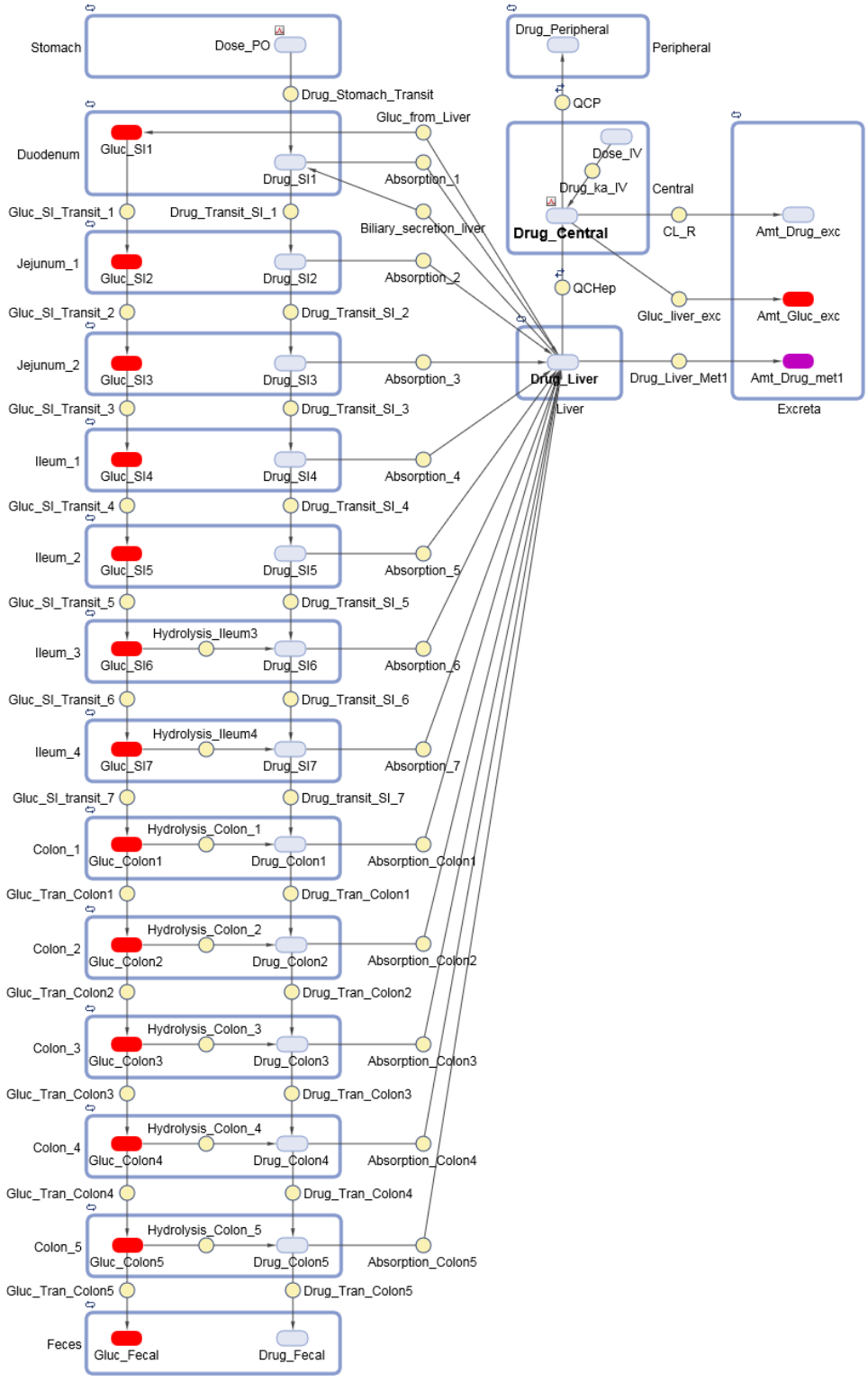

Supplemental Fig. 1. SimBiology® diagram for the semi-physiologically based pharmacokinetic model for maribavir in monkeys. Circles, empty large rectangles, and filled small rectangles denote mass transfers, compartments, and species, respectively, and are detailed in Supplemental Table 1.

A

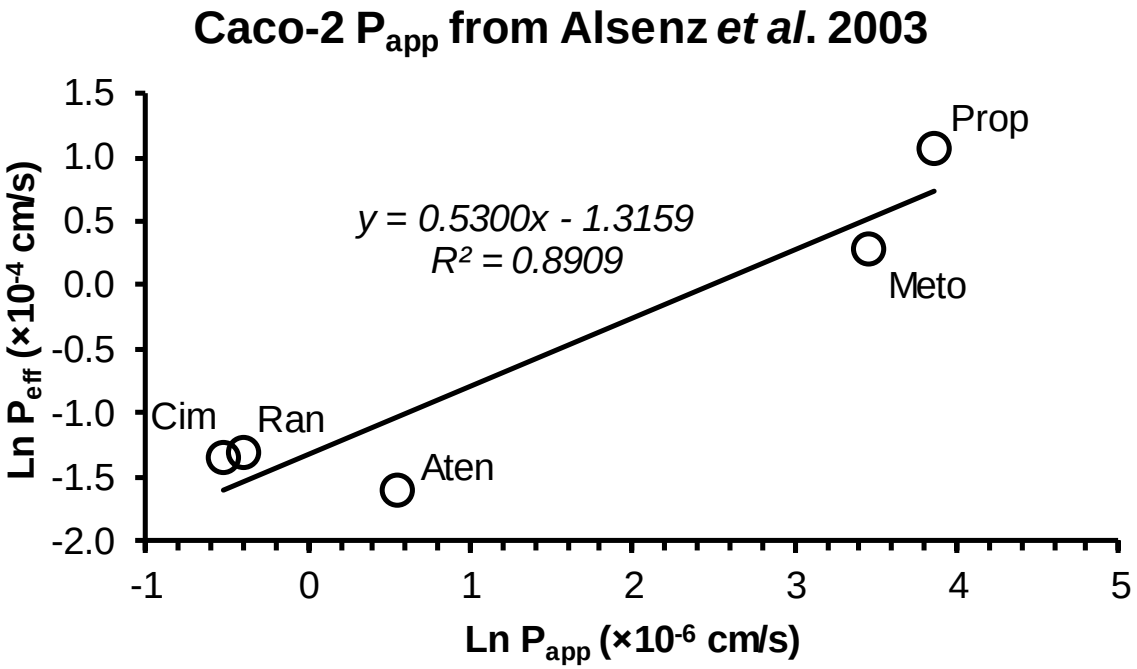

B

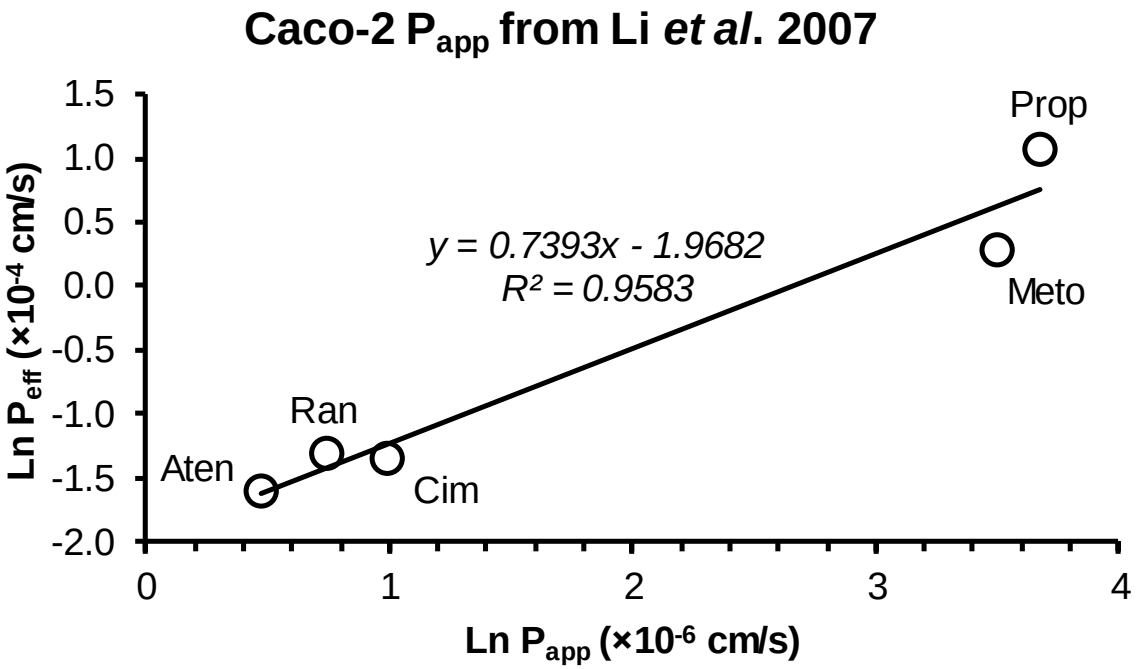

Supplemental Fig. 2. Linear regressions of natural logs (Ln) of human intestinal permeability (P_{eff}, in 10^{-4} cm/s; data in Supplemental Table 4 and from Larregieu and Benet, 2013) versus Ln of apparent permeability (P_{app}, in 10^{-6} cm/s) across cultured Caco-2 cell monolayers. (A) Caco-2 P_{app} data from Alsenz et al., 2003; (B) Caco-2 P_{app} data from Li et al., 2007. Equations show the results from linear regression.

Aten, atenolol; Cim, cimetidine; Meto, metoprolol; P_{app}, apparent permeability; P_{eff}, effective permeability; Prop, propranolol; Ran, ranitidine.

A

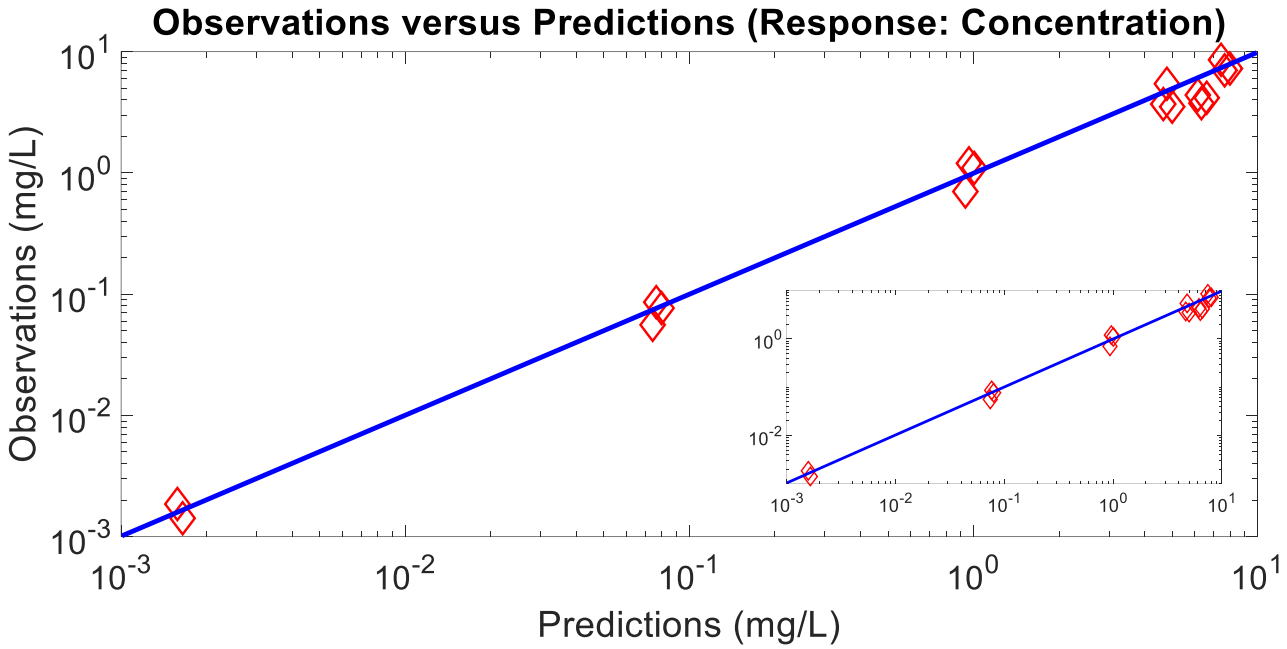

B

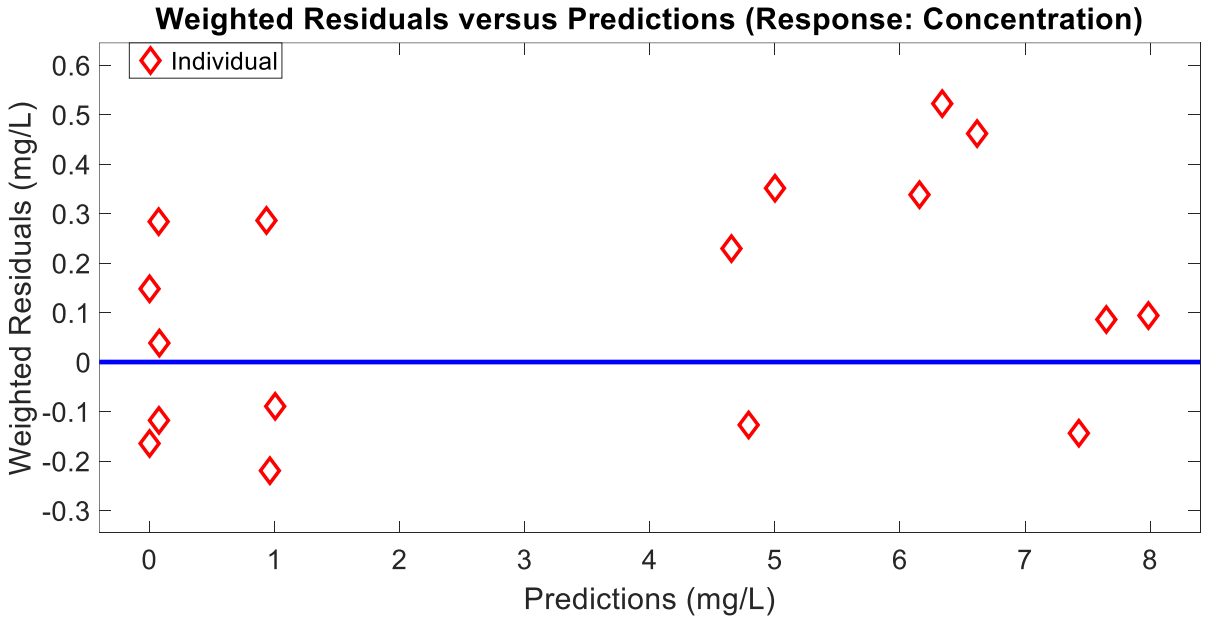

Supplemental Fig. 3. Diagnostic graphs after fitting the semi-physiologically based pharmacokinetic model to observed plasma concentration versus time data in the bile duct-cannulated group of cynomolgus monkeys. (A) Observation (mg/L, y axis) versus predictions (mg/L, x axis). Blue line denotes unity; inset shows the same graph with x and y axes in log scale. (B) Weighted residuals (mg/L, y axis) versus predictions (mg/L, x axis). Blue line denotes y = 0.

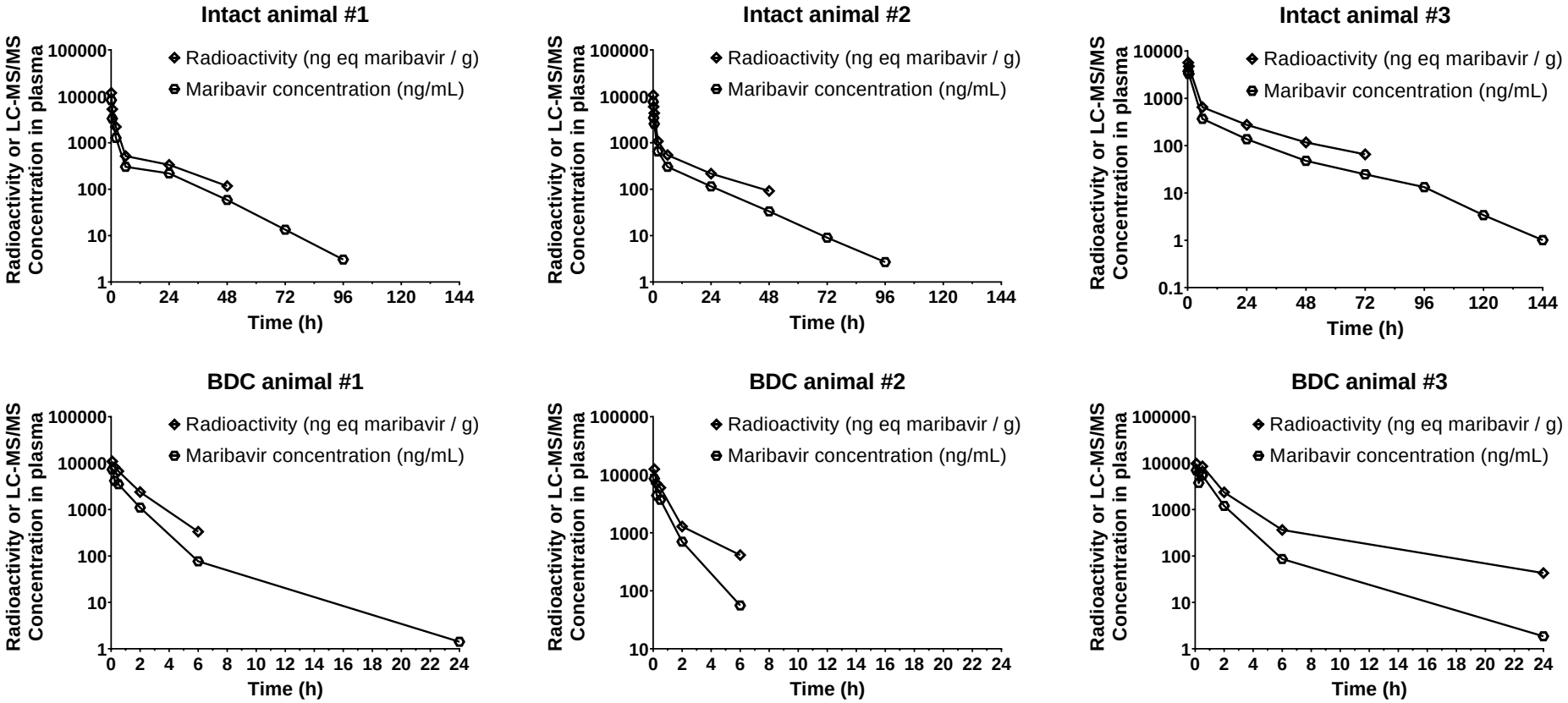

Supplemental Fig. 4. Total radioactivity in plasma as determined by LSC (diamonds) and concentration of maribavir in plasma determined by LC-MS/MS (hexagons) versus time profile after a single i.v. bolus administration of 13 mg/kg ^{14}C-maribavir to intact or BDC animals. Note that the time scale (x axis) for intact and BDC animals are different. Missing samples and BLQ data are not plotted.

BDC, bile duct-cannulated; BLQ, below the limit of quantitation; i.v., intravenous; LC-MS/MS, liquid chromatography–tandem mass spectrometry; LSC, liquid scintillation counters.

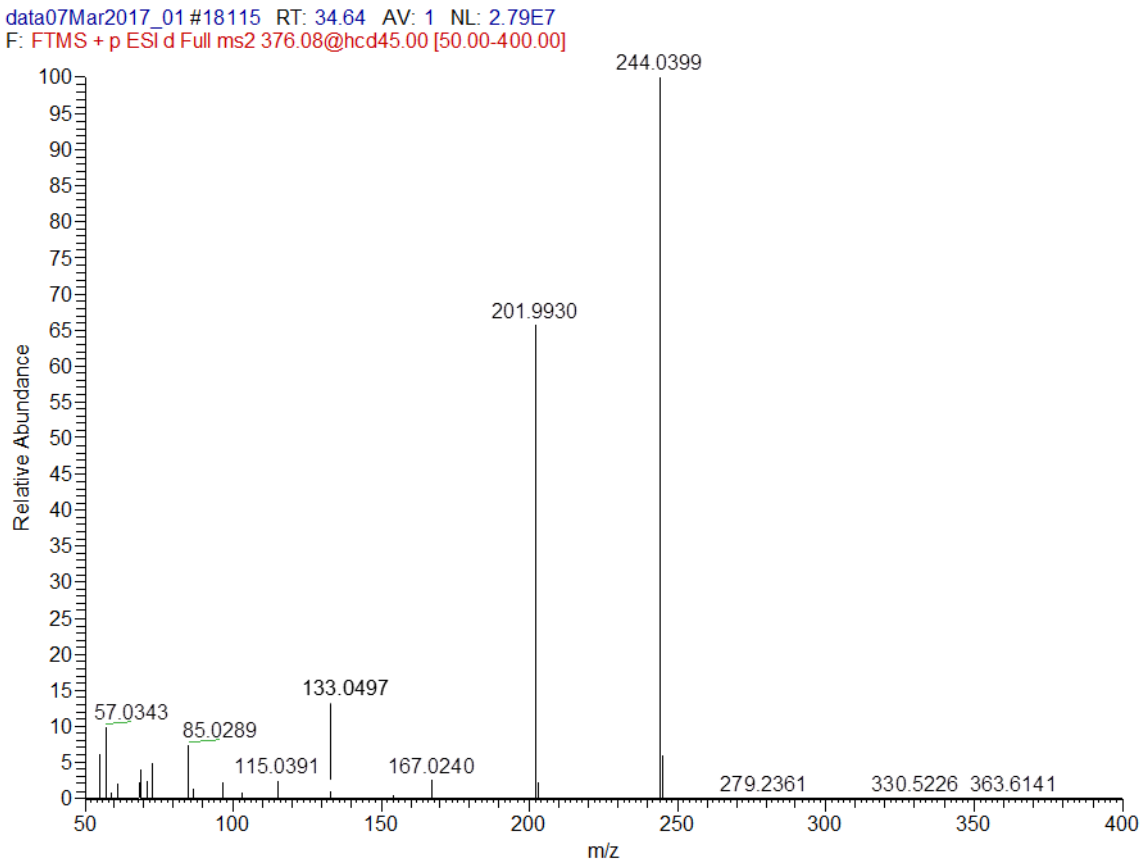

Structure and proposed fragmentation pattern

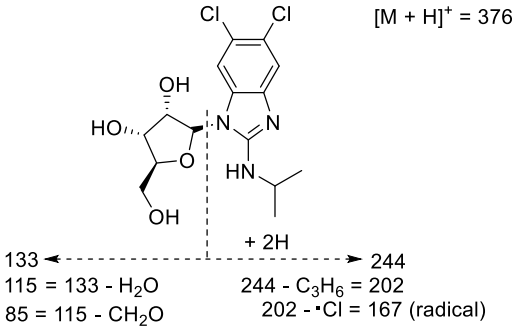

Supplemental Fig. 5. Product ion (*m/z* 376) mass spectrum of maribavir from analysis of a standard solution of maribavir.

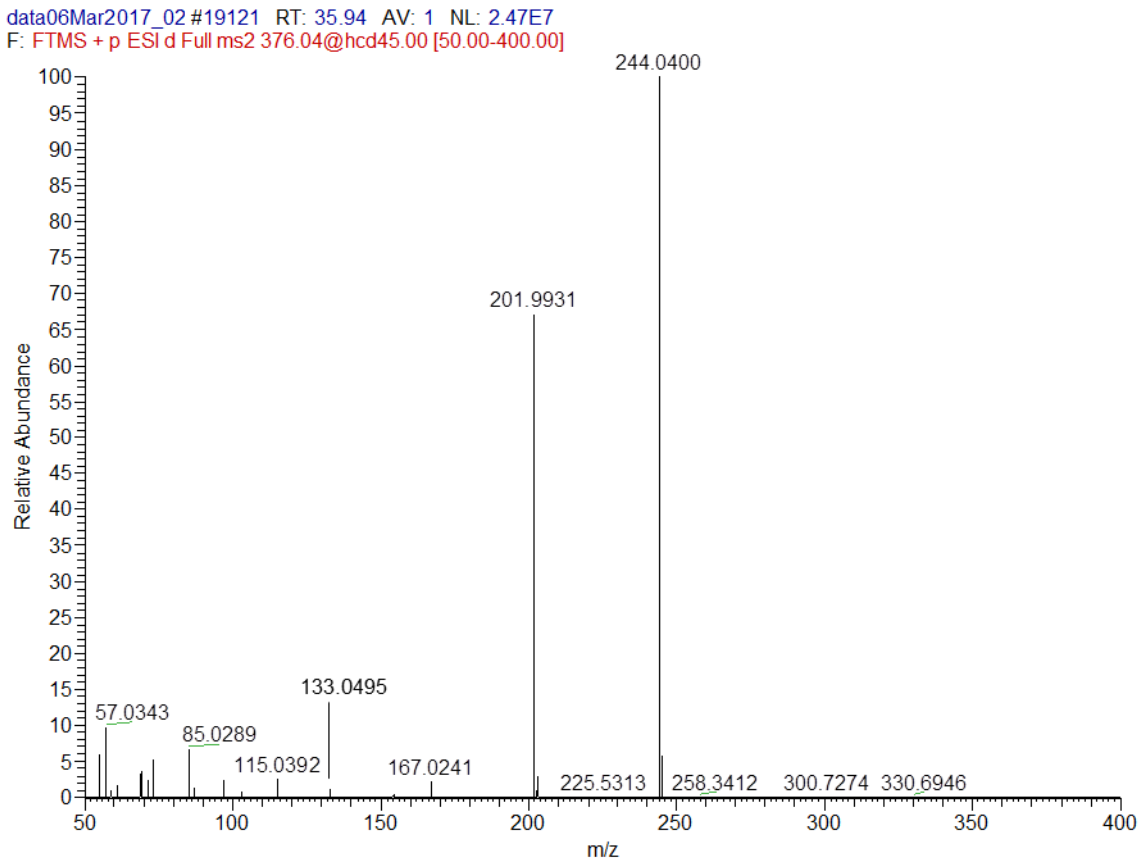

Structure and proposed fragmentation pattern

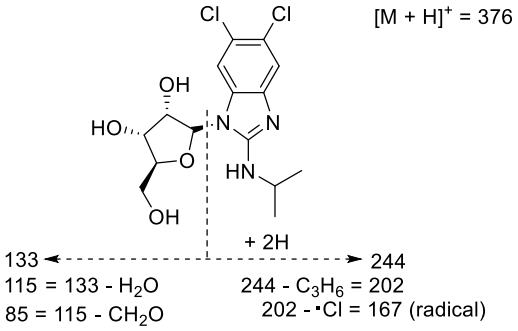

Supplemental Fig. 6. Product ion (*m/z* 376) mass spectrum of maribavir from analysis of a 0- to 48-hour pooled urine sample after a single intravenous dose of ^{14}C-maribavir to male monkeys (Group 1, 13 mg/kg)

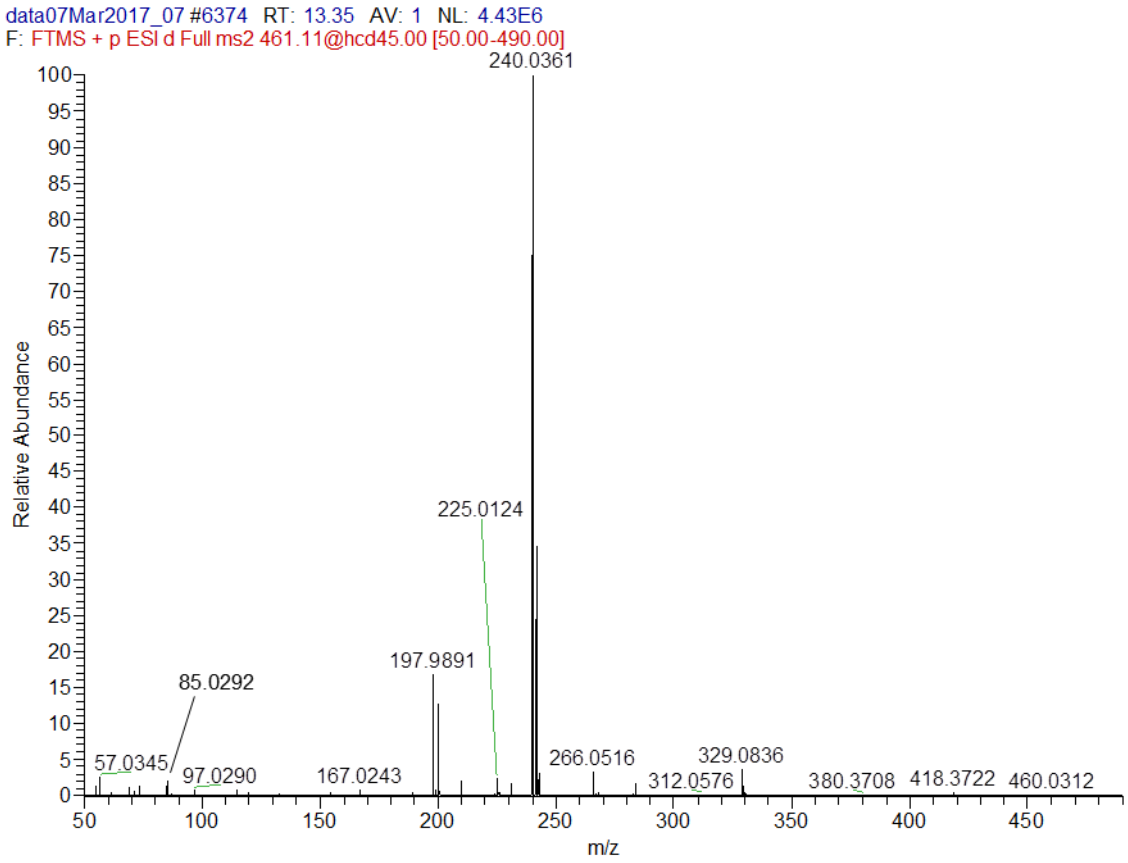

Proposed structure and fragmentation pattern

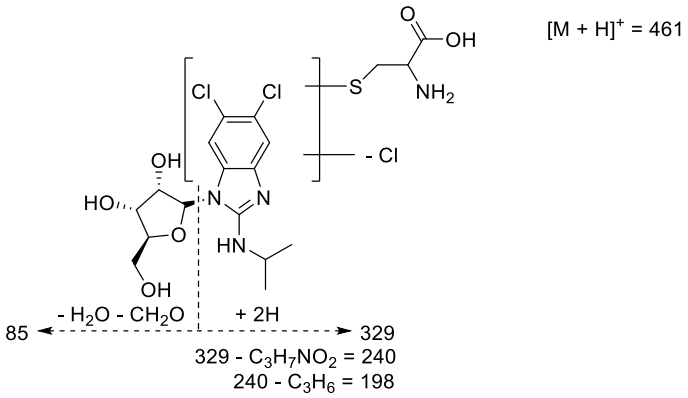

Supplemental Fig. 7. Product ion (*m/z* 461) mass spectrum of metabolite M15 from analysis of a 0- to 8-hour pooled bile sample after a single intravenous dose of ^{14}C-maribavir to male bile-duct cannulated monkeys (Group 2, 13 mg/kg).

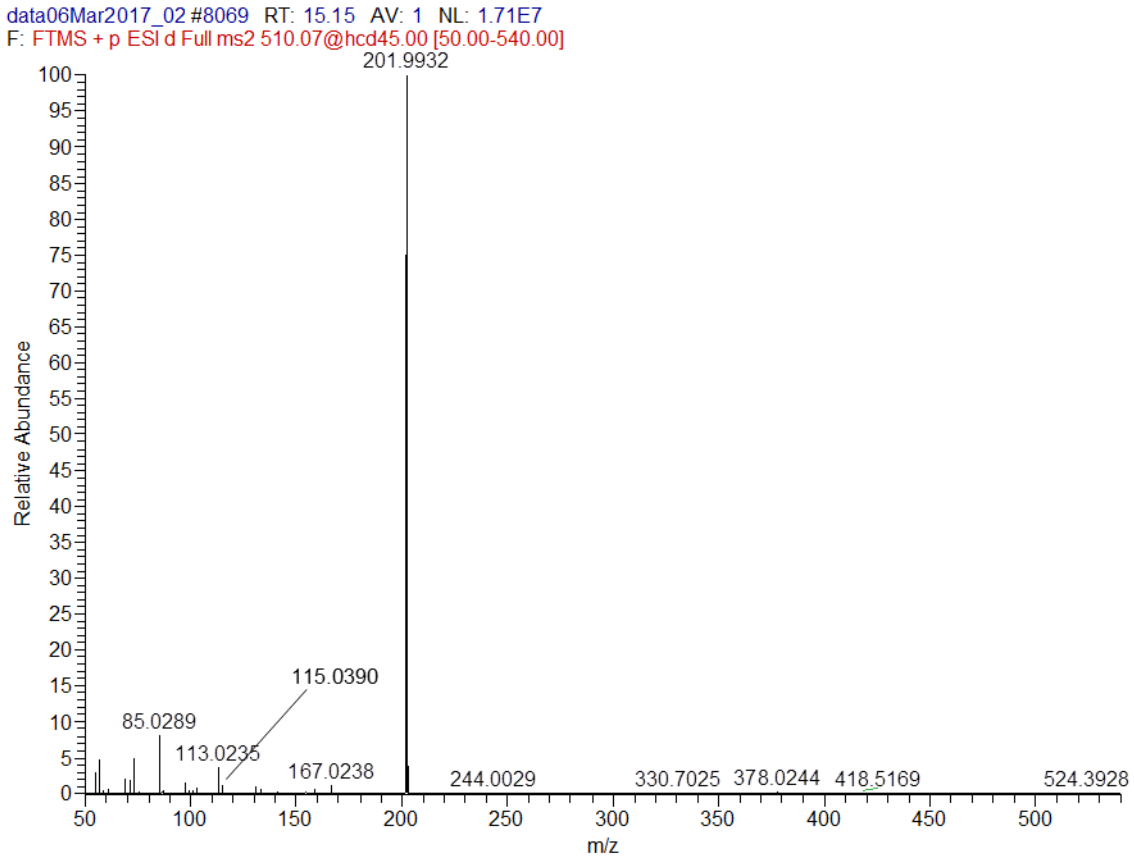

Proposed structure and fragmentation pattern

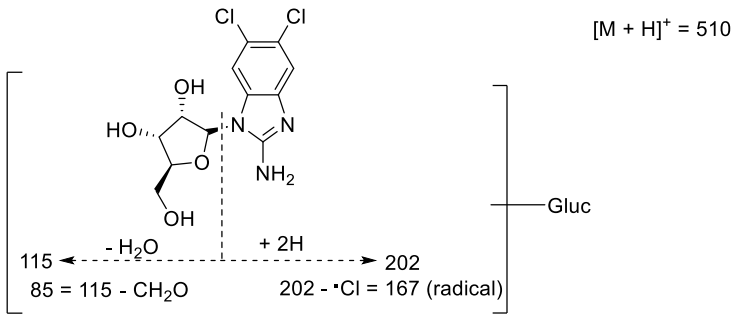

Supplemental Fig. 8. Product ion (*m/z* 510) mass spectrum of metabolite M1 from analysis of a 0- to 48-hour pooled urine sample after a single intravenous dose of ^{14}C-maribavir to male monkeys (Group 1, 13 mg/kg).

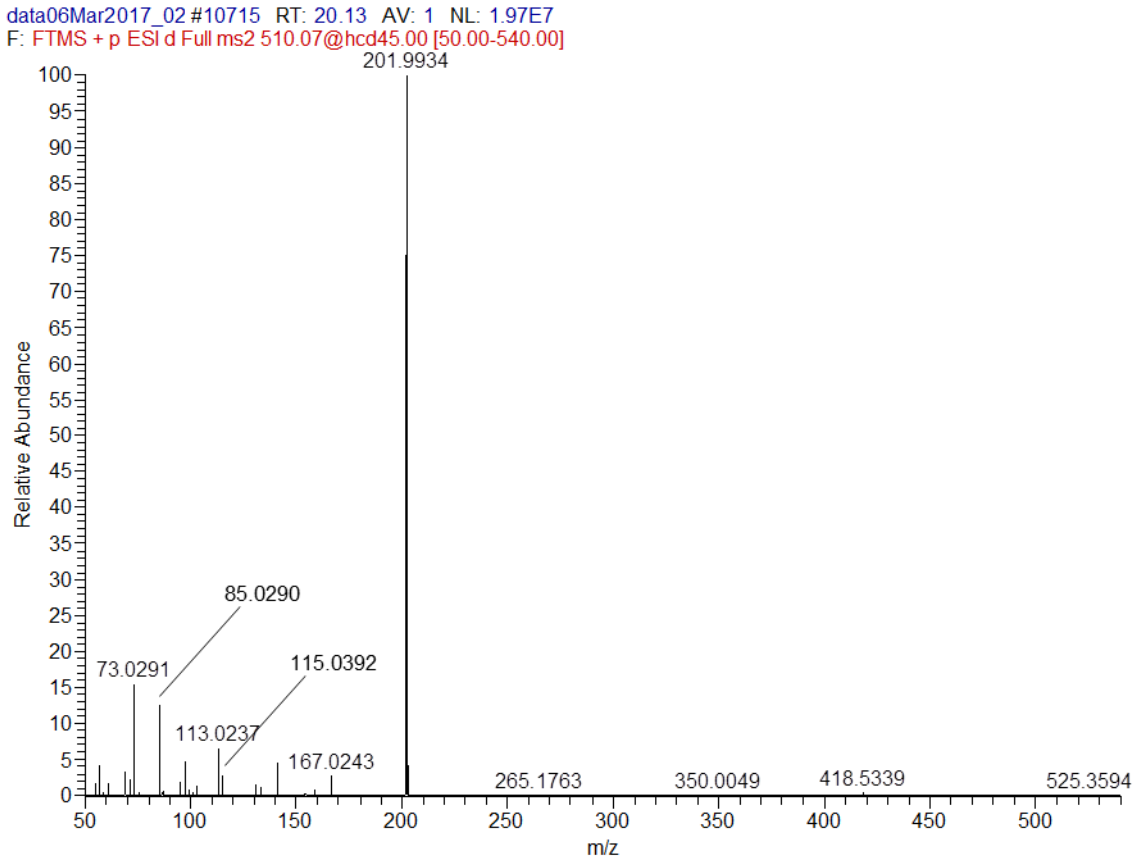

Proposed structure and fragmentation pattern

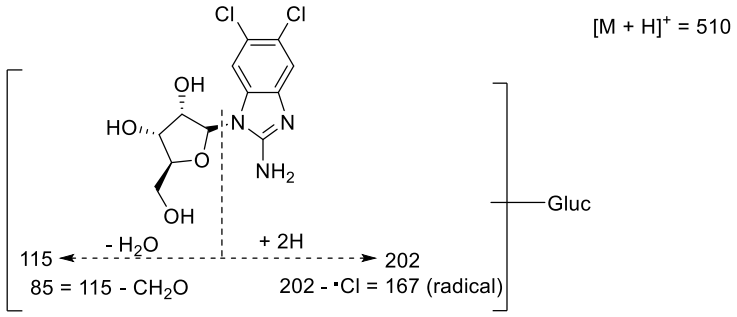

Supplemental Fig. 9. Product ion (*m/z* 510) mass spectrum of metabolite M7 from analysis of a 0- to 48-hour pooled urine sample after a single intravenous dose of ^{14}C-maribavir to male monkeys (Group 1, 13 mg/kg).

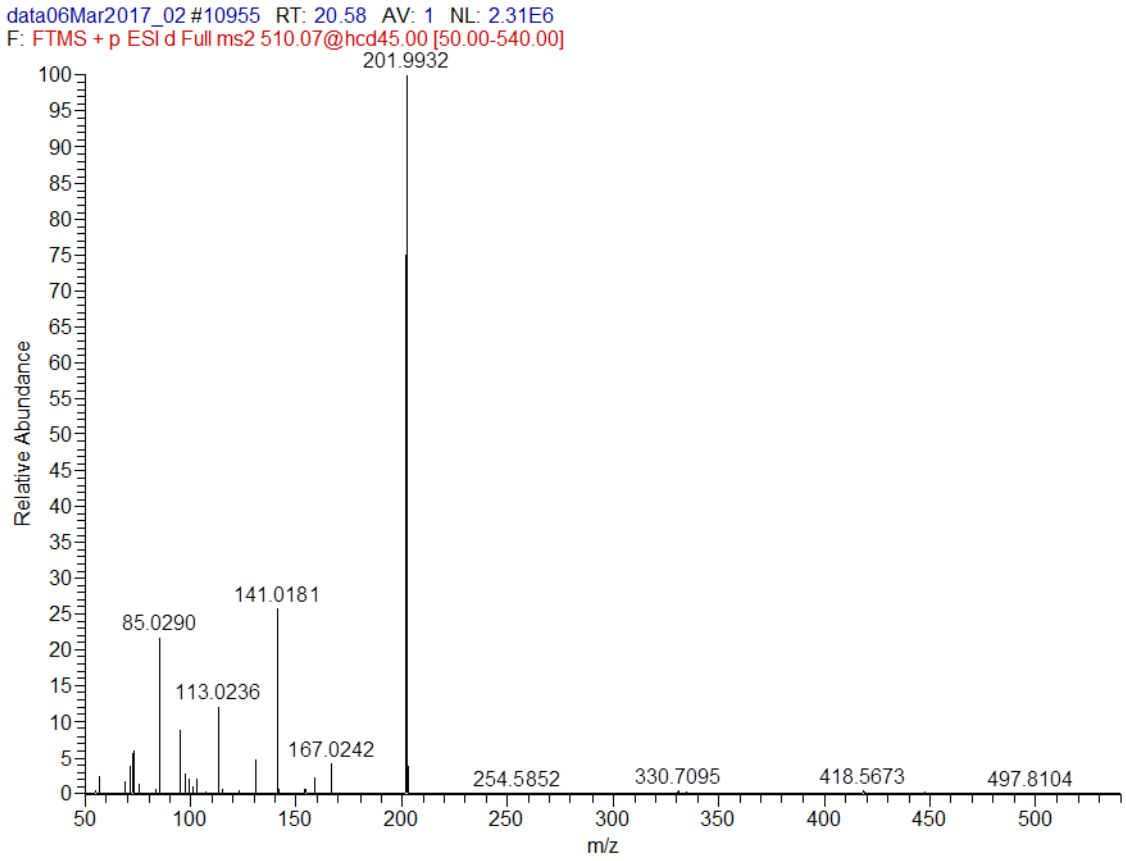

Proposed structure and fragmentation pattern

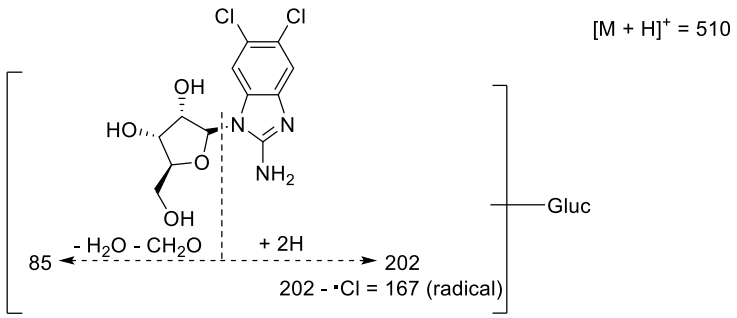

Supplemental Fig. 10. Product ion (*m/z* 510) mass spectrum of metabolite M16 from analysis of a 0- to 48-hour pooled urine sample after a single intravenous dose of ^{14}C-maribavir to male monkeys (Group 1, 13 mg/kg).

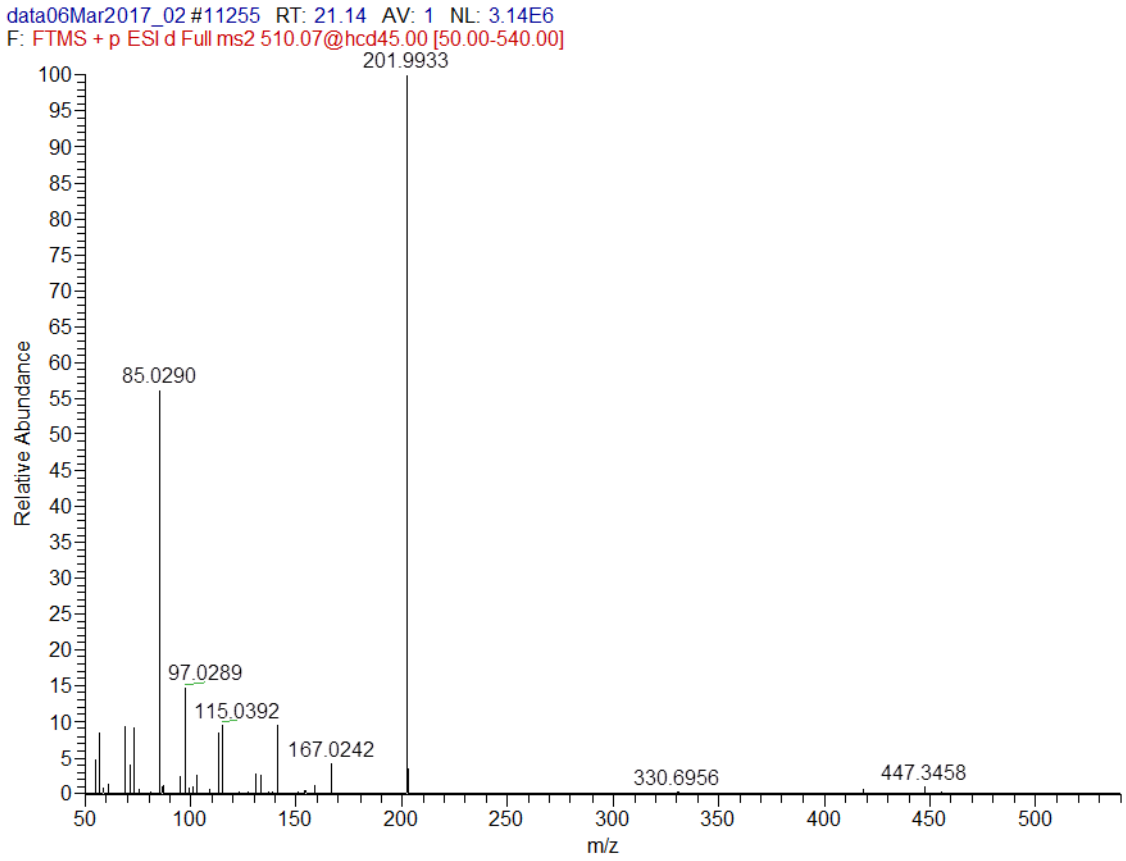

Proposed structure and fragmentation pattern

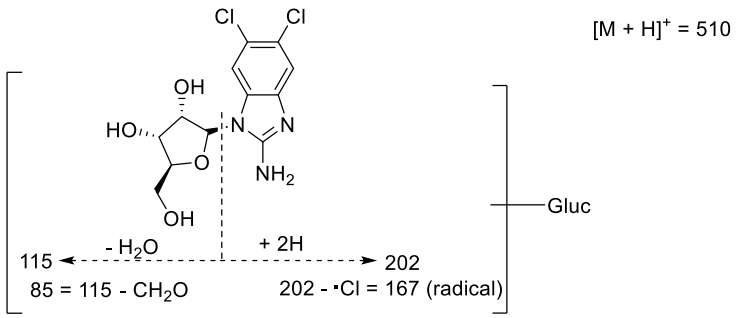

Supplemental Fig. 11. Product ion (*m/z* 510) mass spectrum of metabolite M17 from analysis of a 0- to 48-hour pooled urine sample after a single intravenous dose of ^{14}C-maribavir to male monkeys (Group 1, 13 mg/kg).

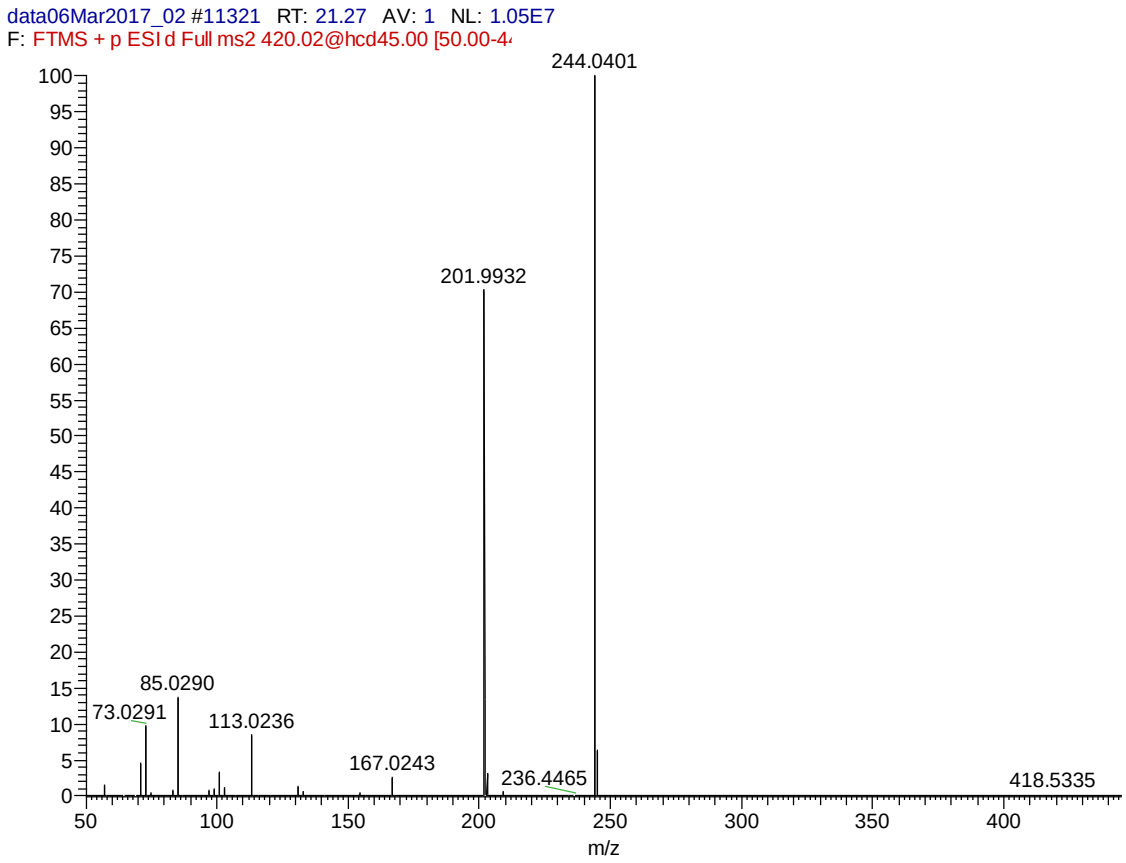

Proposed structure and fragmentation pattern

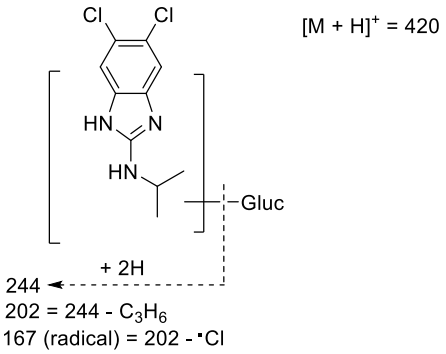

Supplemental Fig. 12. Product ion (*m/z* 420) mass spectrum of metabolite M2 from analysis of a 0- to 48-hour pooled urine sample after a single intravenous dose of ^{14}C-maribavir to male monkeys (Group 1, 13 mg/kg).

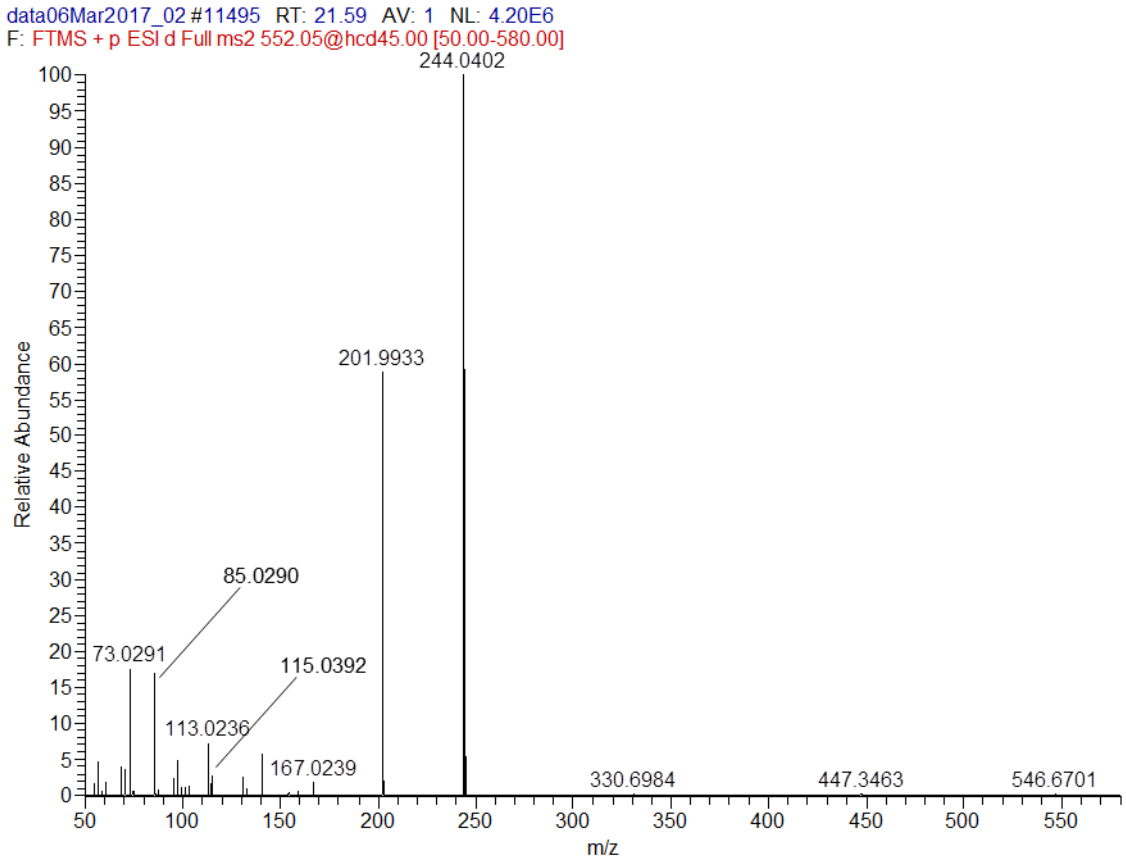

Proposed structure and fragmentation pattern

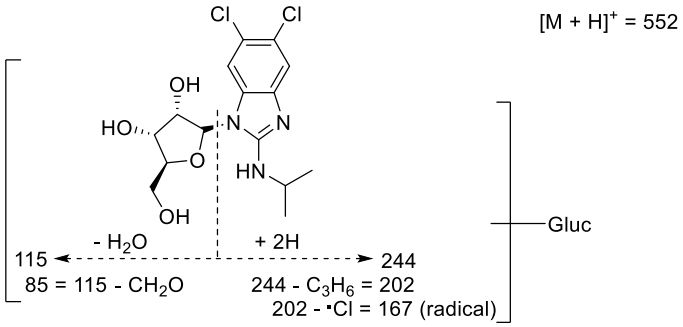

Supplemental Fig. 13. Product ion (*m/z* 552) mass spectrum of metabolite M10 from analysis of a 0- to 48-hour pooled urine sample after a single intravenous dose of ^{14}C-maribavir to male monkeys (Group 1, 13 mg/kg).

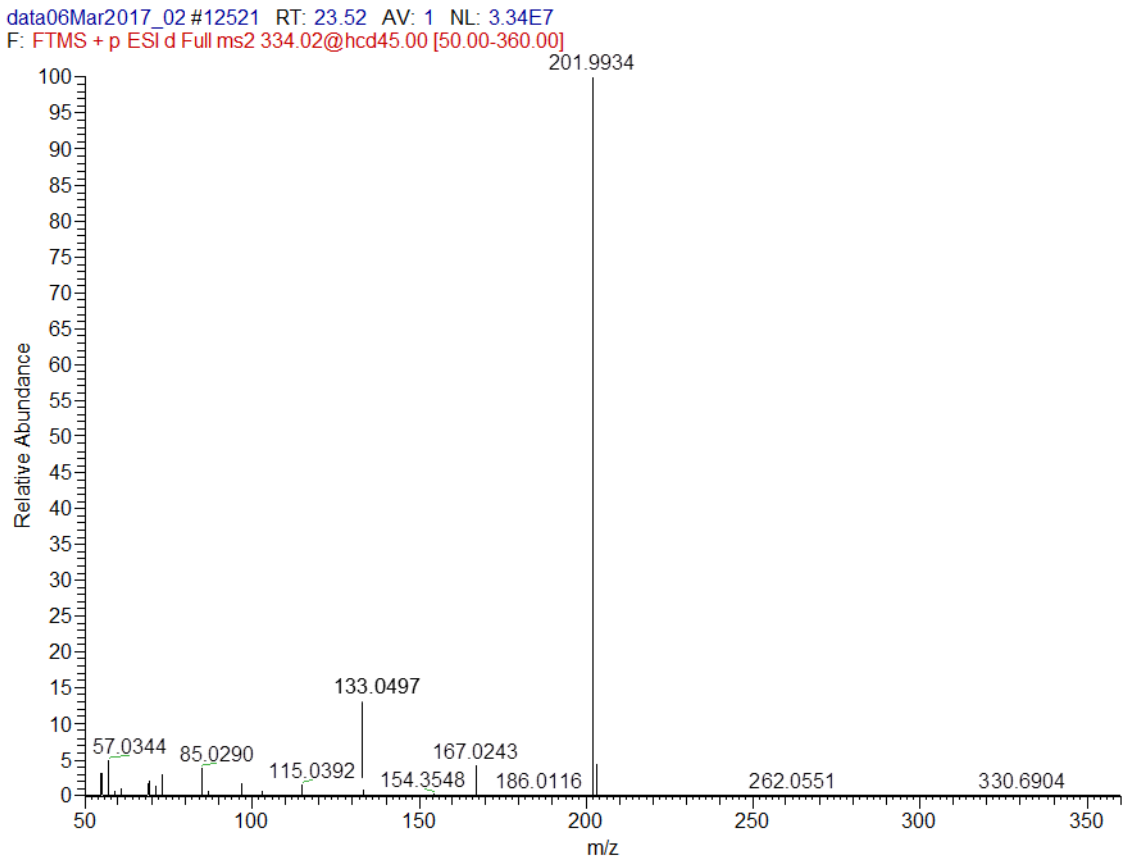

Proposed structure and fragmentation pattern

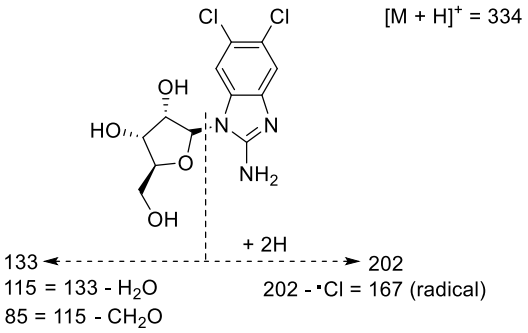

Supplemental Fig. 14. Product ion (*m/z* 334) mass spectrum of metabolite M4 from analysis of a 0- to 48-hour pooled urine sample after a single intravenous dose of ^{14}C-maribavir to male monkeys (Group 1, 13 mg/kg).

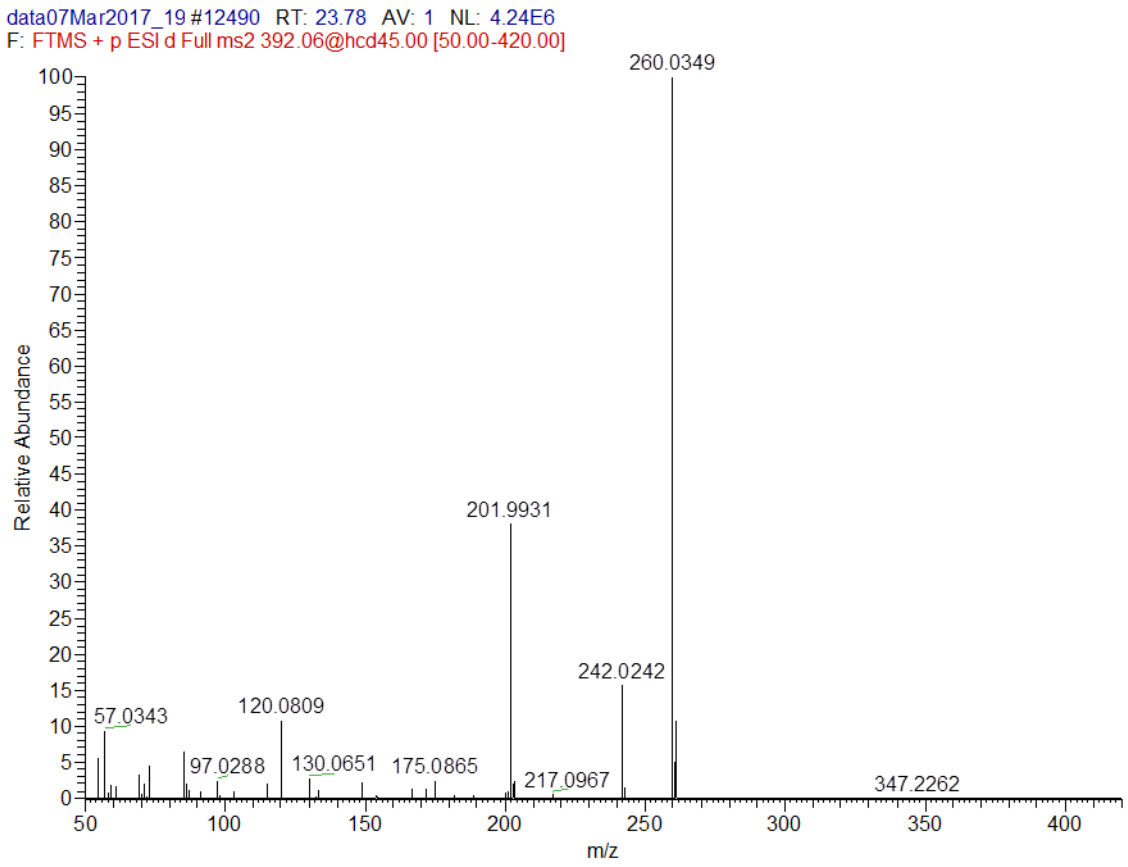

Proposed structure and fragmentation pattern

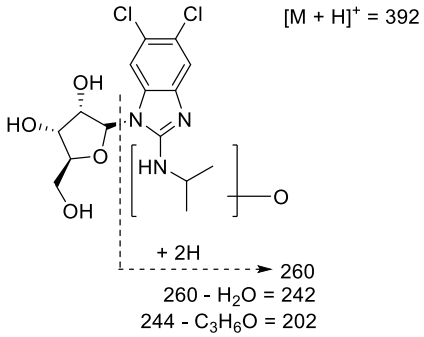

Supplemental Fig. 15. Product ion (*m/z* 392) mass spectrum of metabolite M5 from analysis of a 0- to 120-hour pooled feces sample after a single intravenous dose of ^{14}C-maribavir to male monkeys (Group 1, 13 mg/kg)

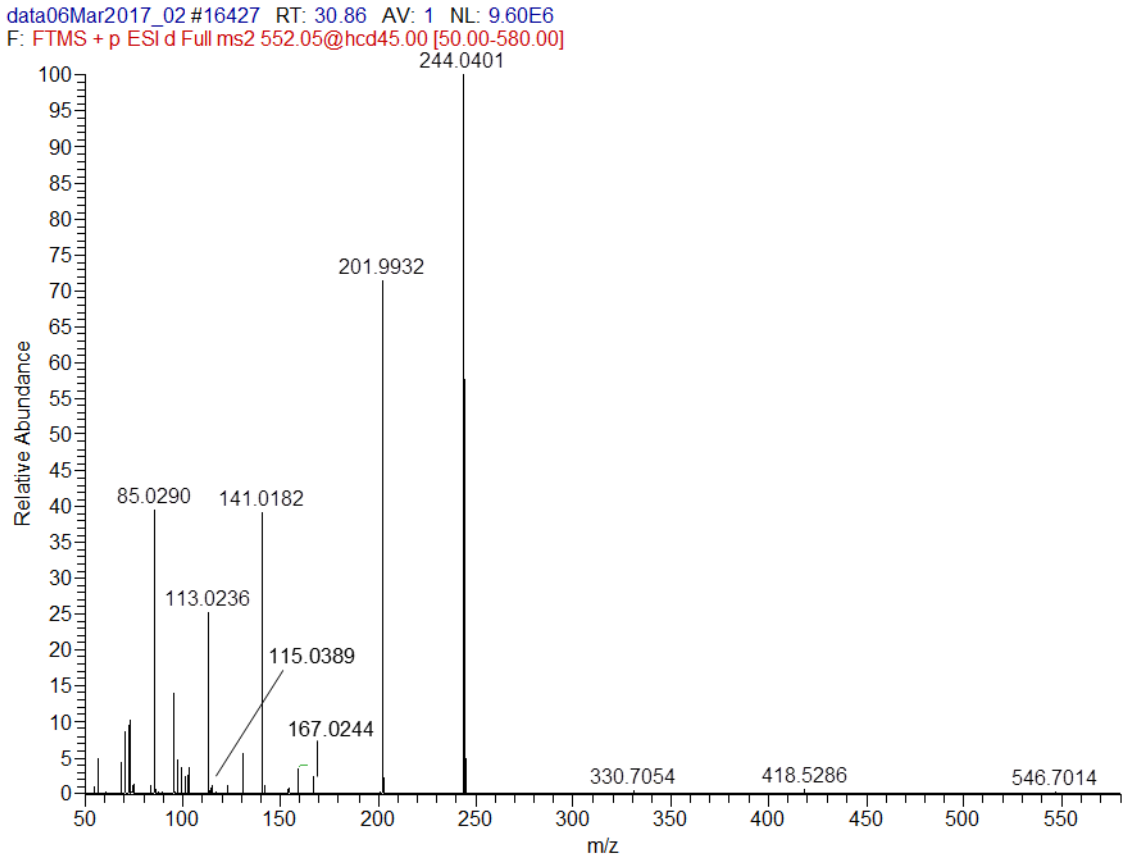

Proposed structure and fragmentation pattern

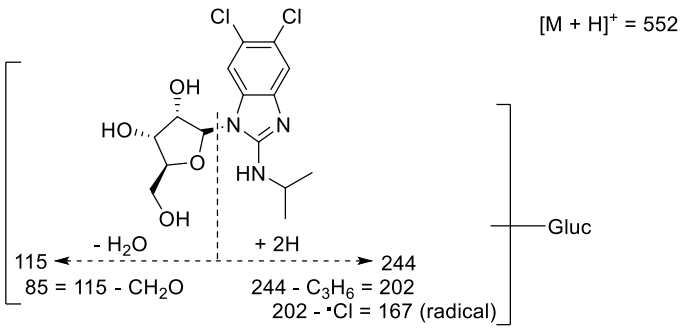

Supplemental Fig. 16. Product ion (*m/z* 552) mass spectrum of metabolite M11 from analysis of a 0- to 48-hour pooled urine sample after a single intravenous dose of ^{14}C-maribavir to male monkeys (Group 1, 13 mg/kg).

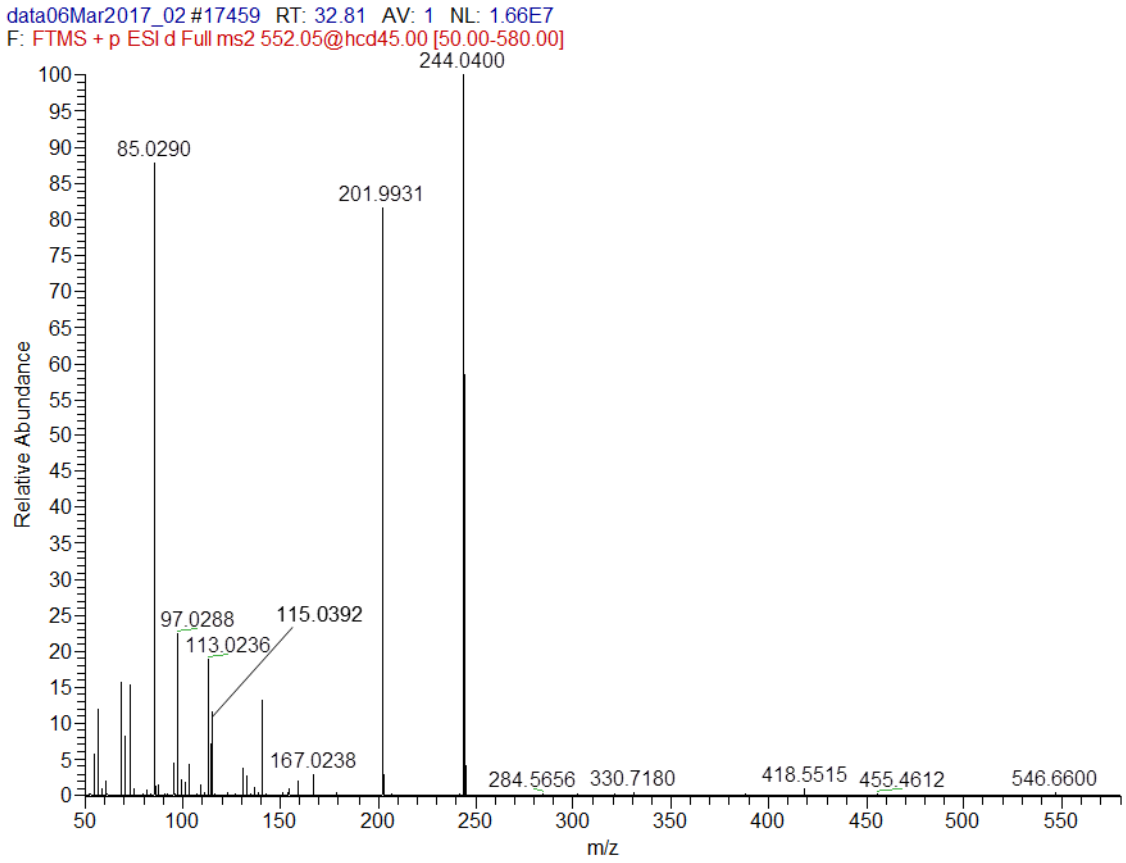

Proposed structure and fragmentation pattern

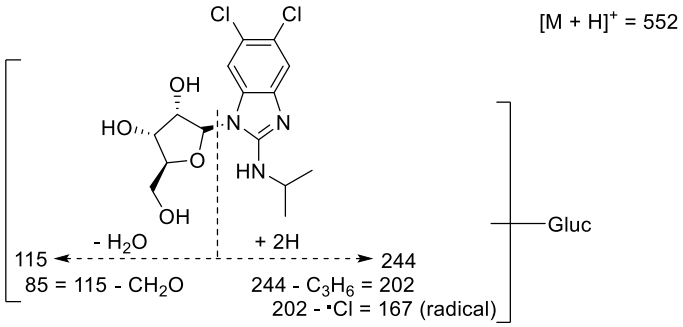

Supplemental Fig. 17. Product ion (*m/z* 552) mass spectrum of metabolite M12 from analysis of a 0- to 48-hour pooled urine sample after a single intravenous dose of ^{14}C-maribavir to male monkeys (Group 1, 13 mg/kg).

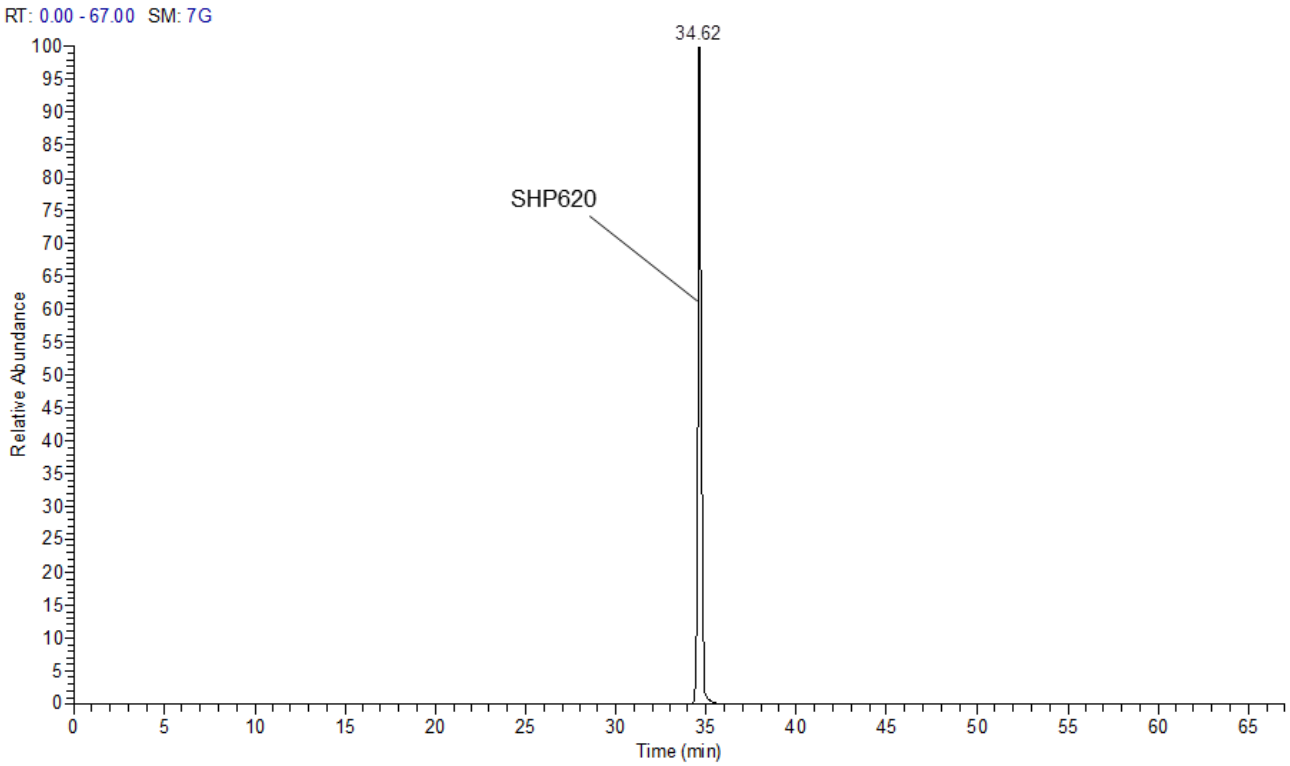

Supplemental Fig. 18. Extracted ion chromatogram from analysis of a standard solution of maribavir (SHP620).

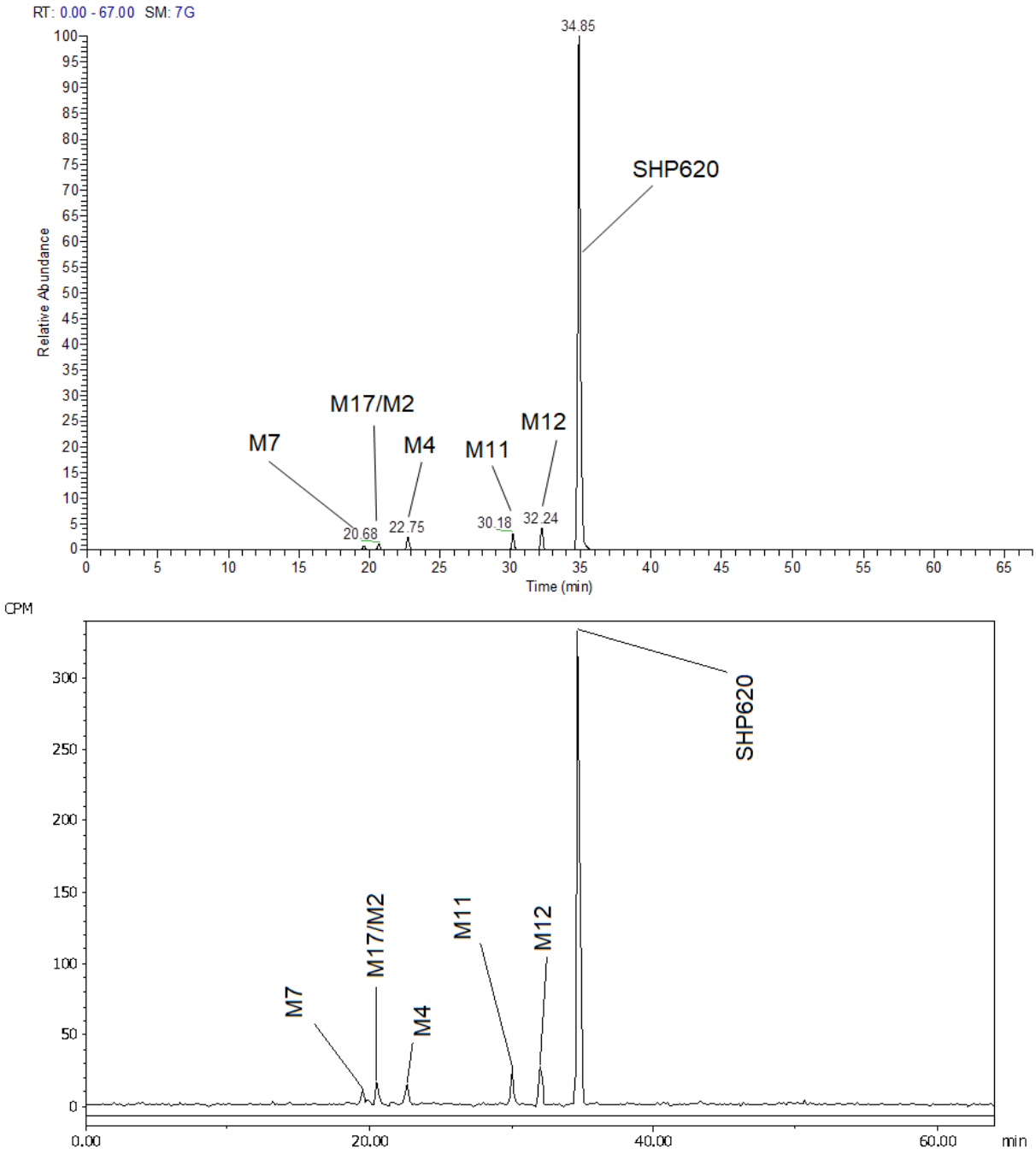

Supplemental Fig. 19. Reconstructed ion chromatogram and radiochromatogram from analysis of a 0.25-hour pooled plasma sample after a single intravenous dose of ^{14}C-maribavir to intact male monkeys (Group 1, 13 mg/kg)

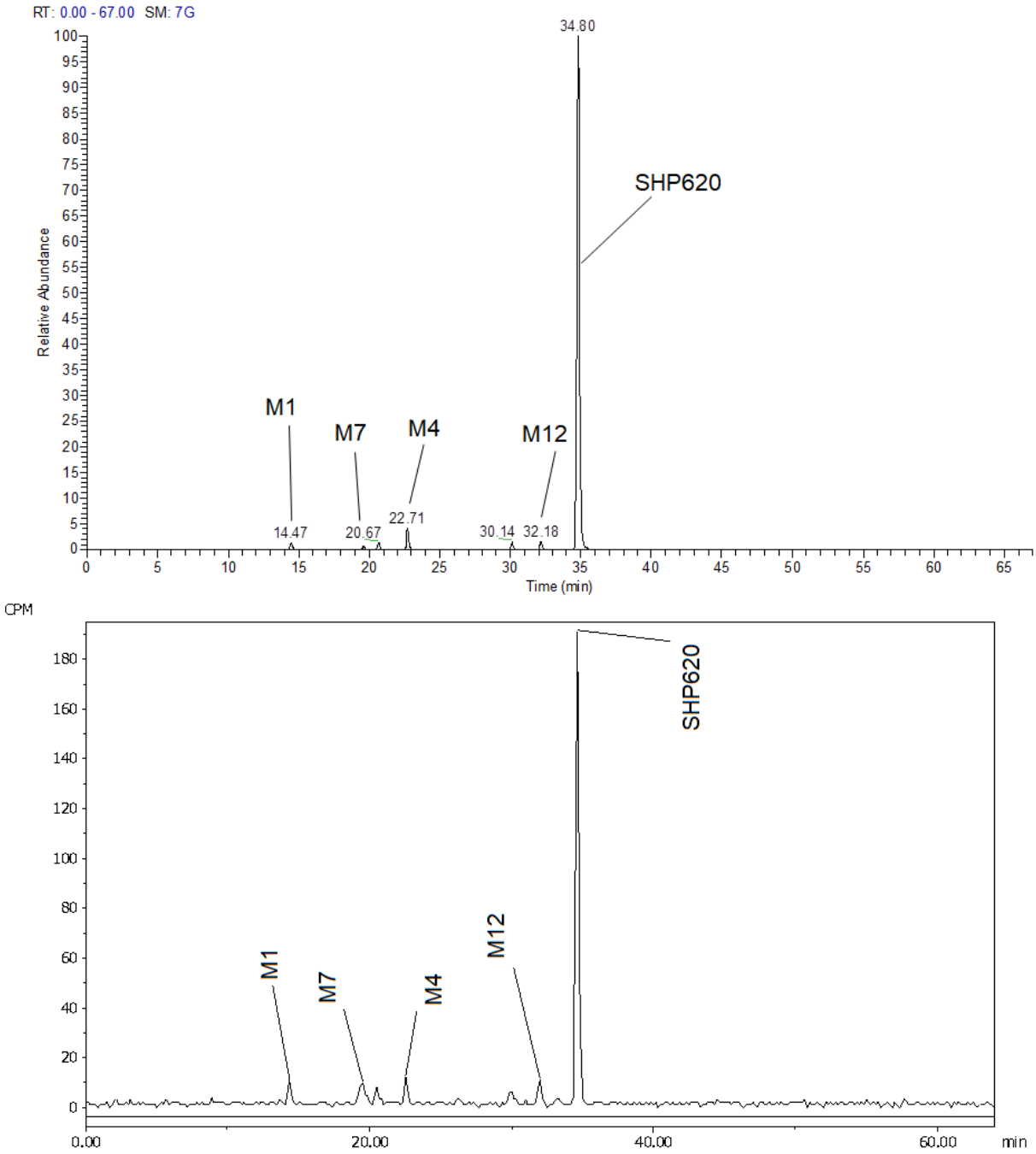

Supplemental Fig. 20. Reconstructed ion chromatogram and radiochromatogram from analysis of a 2-hour pooled plasma sample after a single intravenous dose of ^{14}C-maribavir to male bile-duct cannulated monkeys (Group 2, 13 mg/kg).

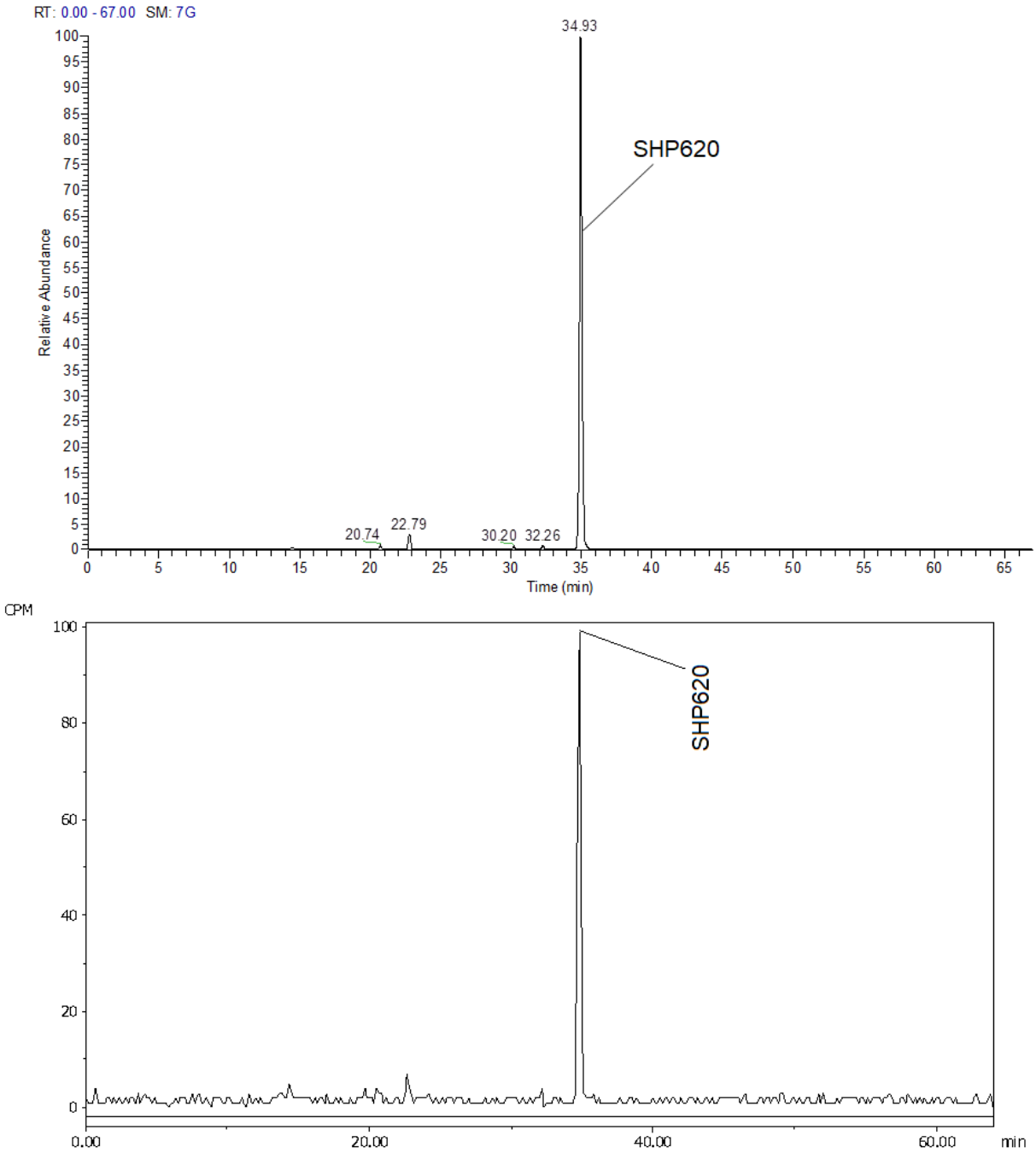

Supplemental Fig. 21. Reconstructed ion chromatogram and radiochromatogram from analysis of a 24-hour pooled plasma sample after a single intravenous dose of ^{14}C-maribavir to intact male monkeys (Group 1, 13 mg/kg).

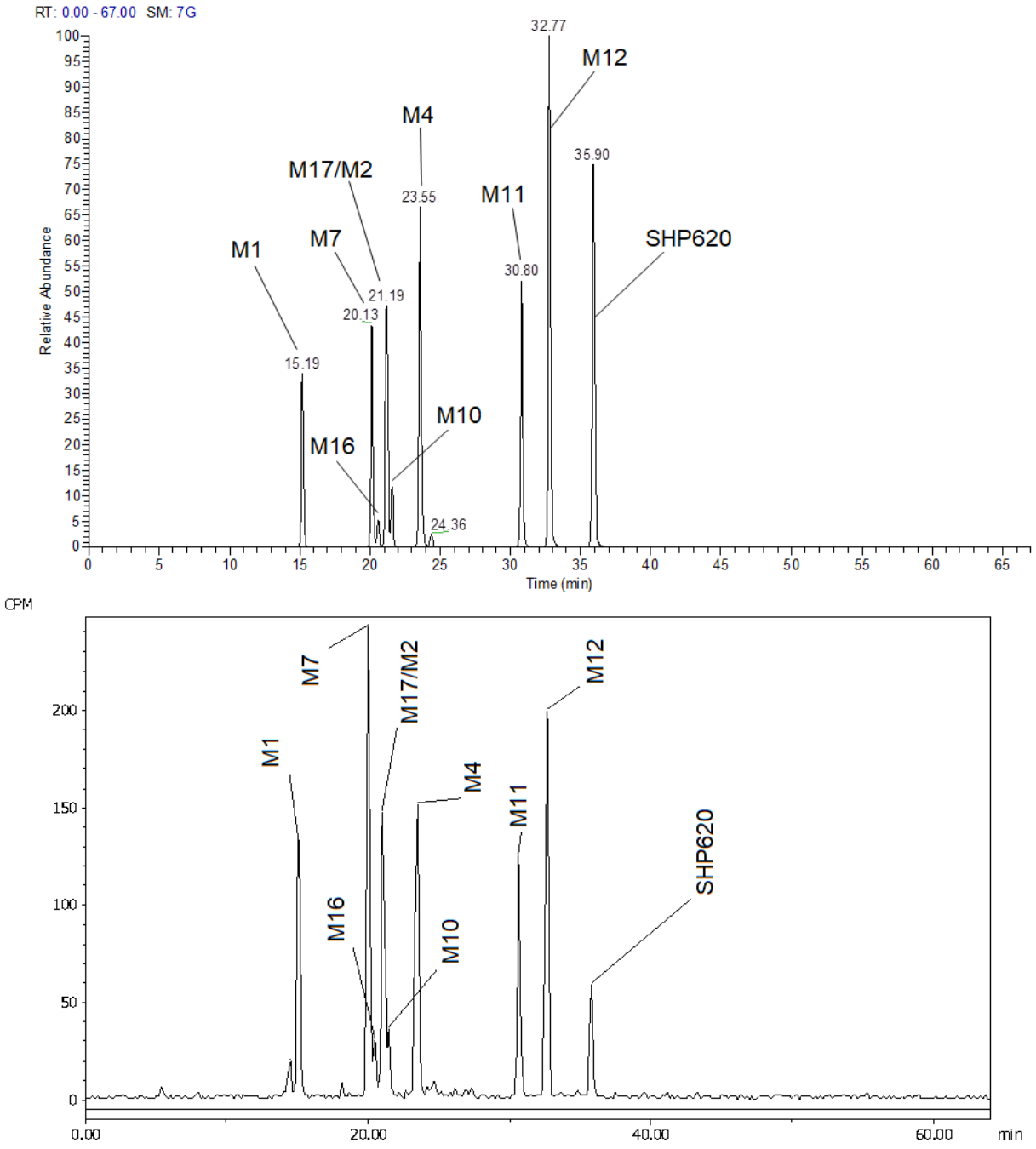

Supplemental Fig. 22. Reconstructed ion chromatogram and radiochromatogram from analysis of a 0- to 48-hour pooled urine sample after a single intravenous dose of ^{14}C-maribavir to intact male monkeys (Group 1, 13 mg/kg).

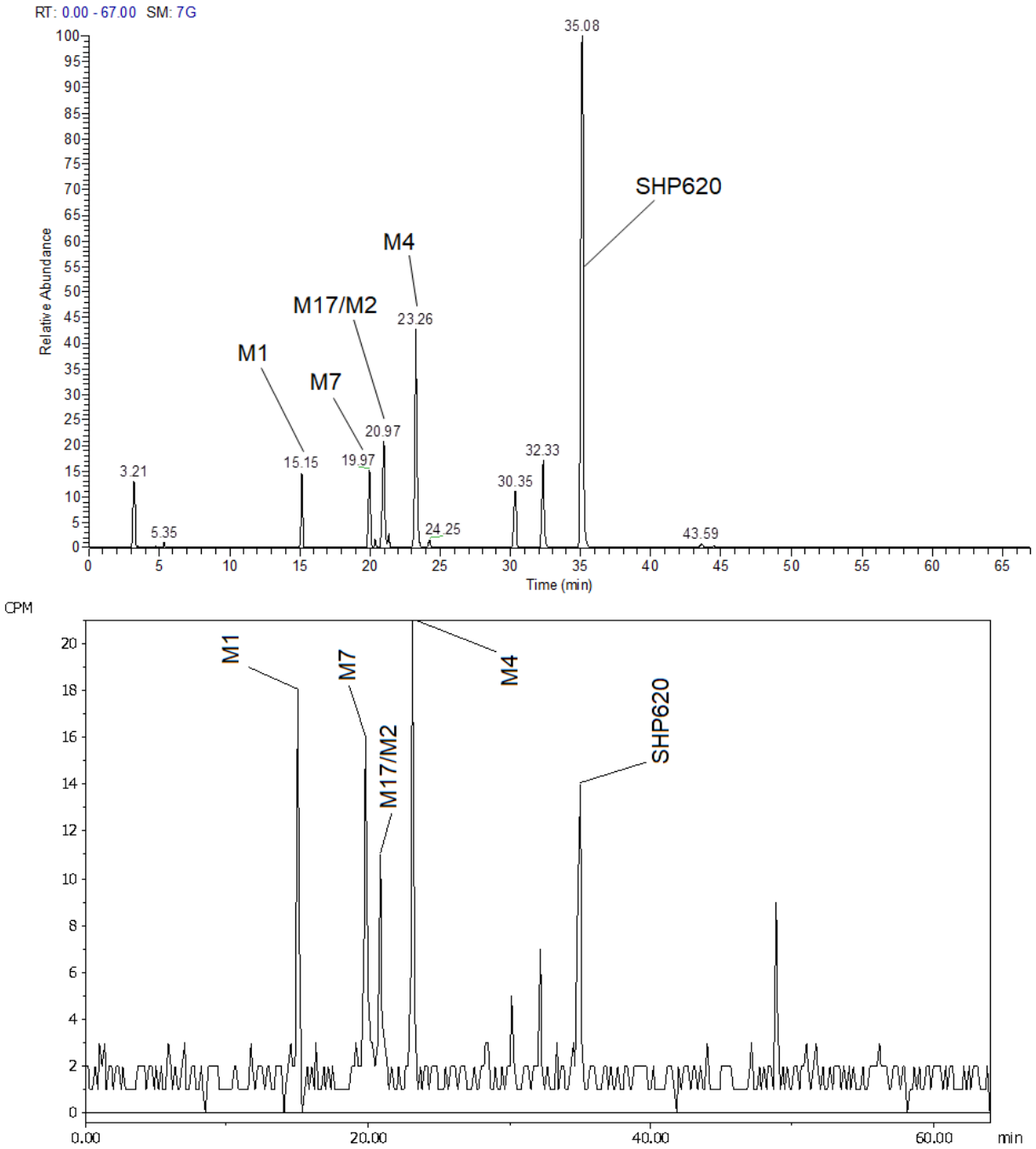

Supplemental Fig. 23. Reconstructed ion chromatogram and radiochromatogram from analysis of a 120- to 144-hour pooled urine sample after a single intravenous dose of ^{14}C-maribavir to intact male monkeys (Group 1, 13 mg/kg).

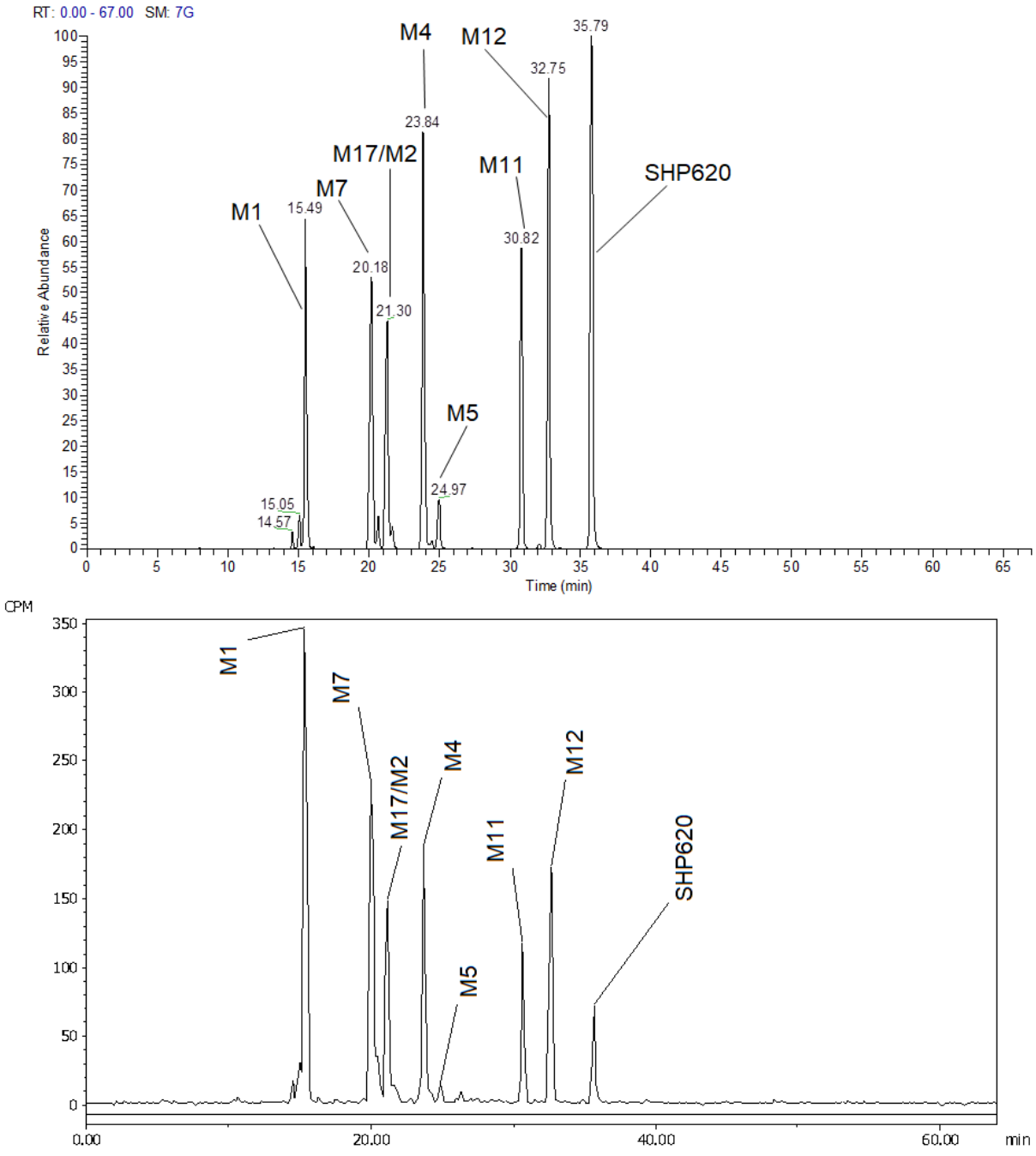

Supplemental Fig. 24. Reconstructed ion chromatogram and radiochromatogram from analysis of a 0- to 24-hour pooled urine sample after a single intravenous dose of ^{14}C-maribavir to male bile-duct cannulated monkeys (Group 2, 13 mg/kg).

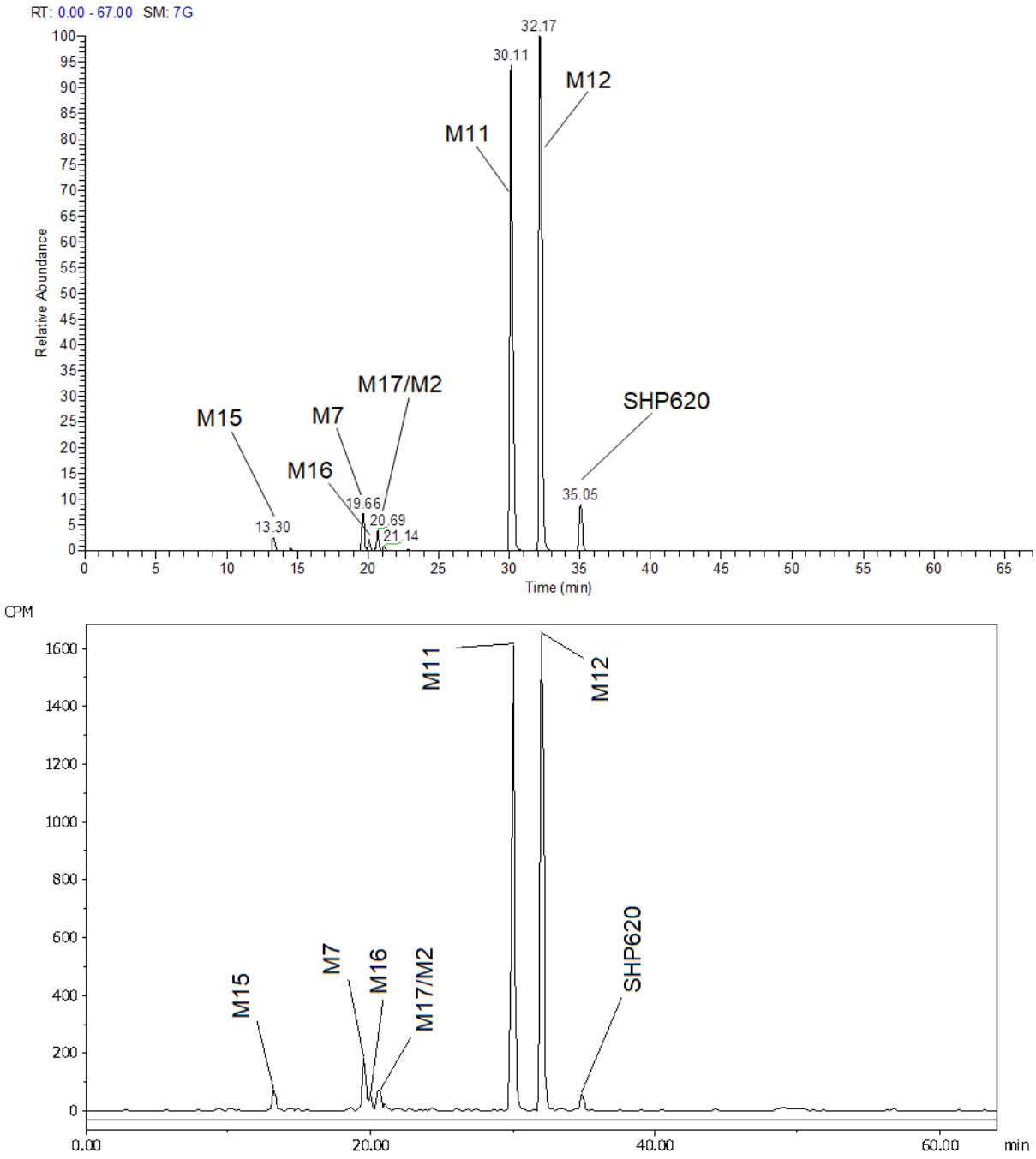

Supplemental Fig. 25. Reconstructed ion chromatogram and radiochromatogram from analysis of a 0- to 8-hour pooled bile sample after a single intravenous dose of ^{14}C-maribavir to male bile-duct cannulated monkeys (Group 2, 13 mg/kg).

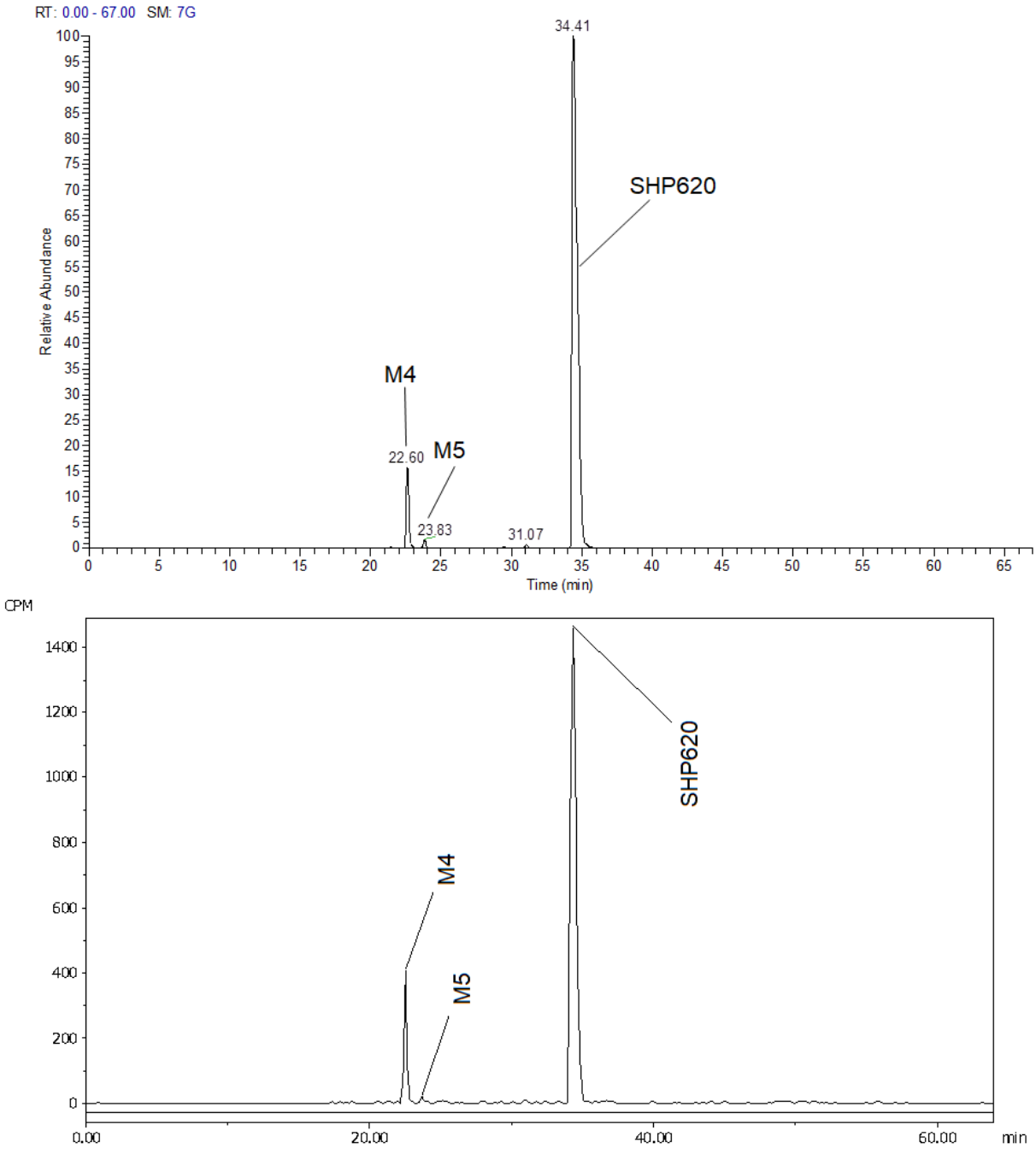

Supplemental Fig. 26. Reconstructed ion chromatogram and radiochromatogram from analysis of a 0- to 120-hour pooled feces sample after a single intravenous dose of ^{14}C-maribavir to male monkeys (Group 1, 13 mg/kg).

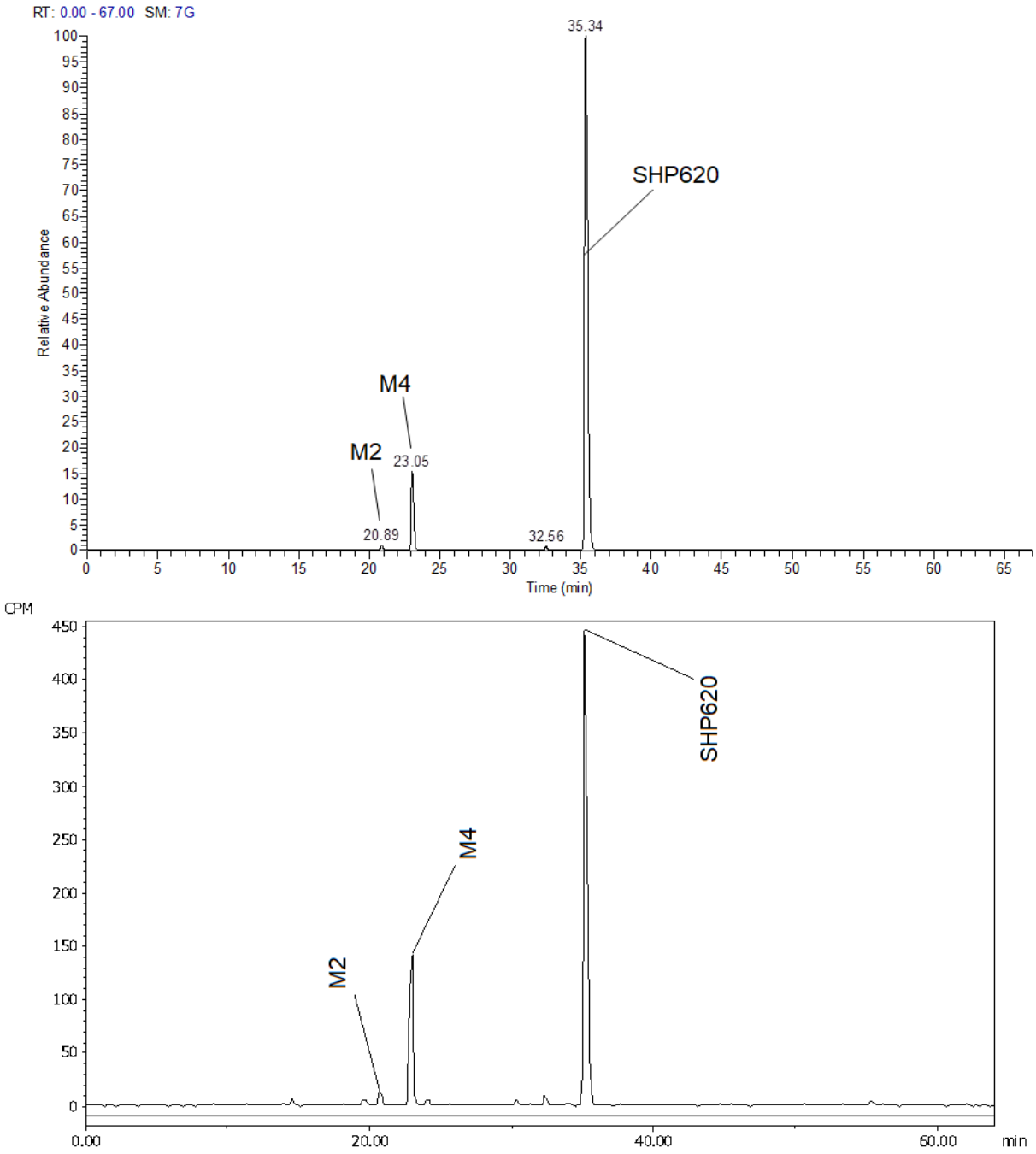

Supplemental Fig. 27. Reconstructed ion chromatogram and radiochromatogram from analysis of a 0- to 24-hour pooled feces sample after a single intravenous dose of ^{14}C-maribavir to male bile-duct cannulated monkeys (Group 2, 13 mg/kg).

A

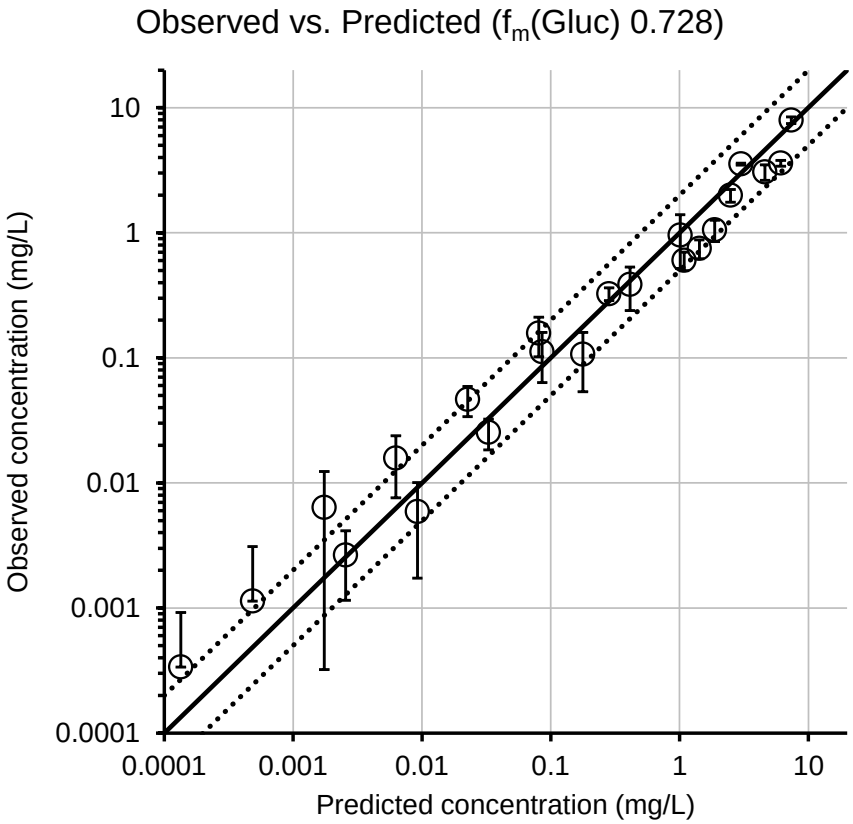
Observed vs. Predicted (f_m(Gluc) 0.728)
Observed concentration (mg/L)
Predicted concentration (mg/L)
10
1
0.1
0.01
0.001
0.0001
0.0001
0.001
0.01
0.1
1
10

B

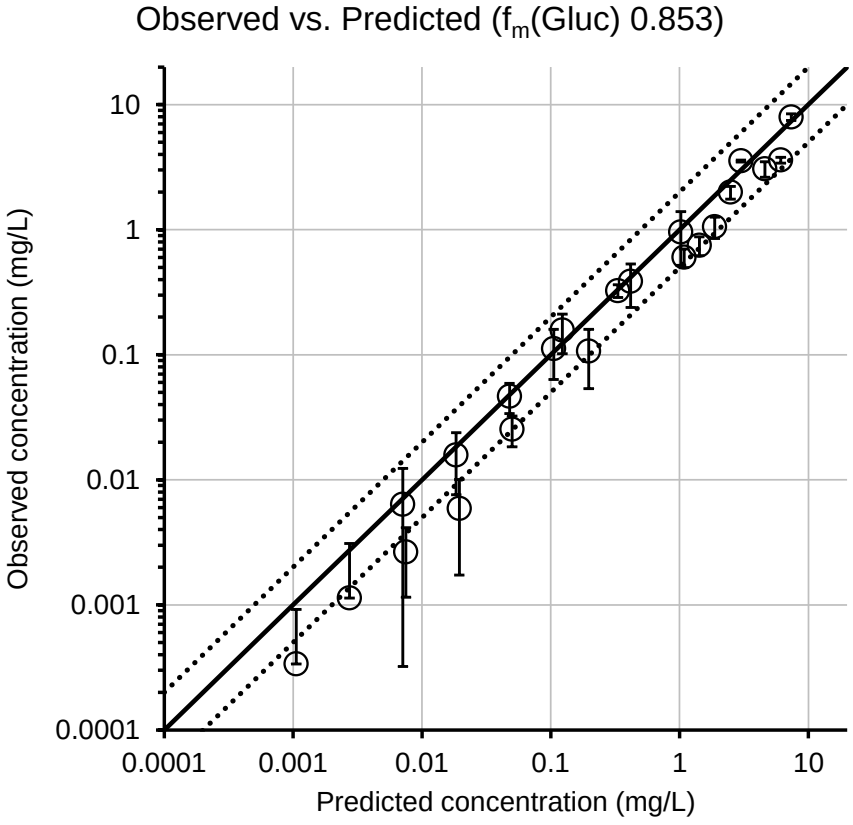
Observed vs. Predicted (f_m(Gluc) 0.853)
Observed concentration (mg/L)
Predicted concentration (mg/L)
10
1
0.1
0.01
0.001
0.0001
0.0001
0.001
0.01
0.1
1
10

Supplemental Fig. 28. Observed versus PBPK model-predicted concentration plots for plasma concentration data in 13 mg/kg ^{14}C-maribavir and 5 mg/kg maribavir intravenous bolus administration in intact cynomolgus monkeys using (A) f_m(Gluc) = 0.728 or (B) f_m(Gluc) = 0.853 for the prediction. Each plot contains the same mean observed concentration data (LC-MS/MS) from both dose groups (circles) and the y error bars denote standard deviation. The BLQ concentrations at 120- and 144-hour samples in the two 13 mg/kg ^{14}C-maribavir-dosed animals were treated as zeros. The solid line represents unity and the two dotted lines represent 0.5x and 2x Observed / Predicted ratios.

A

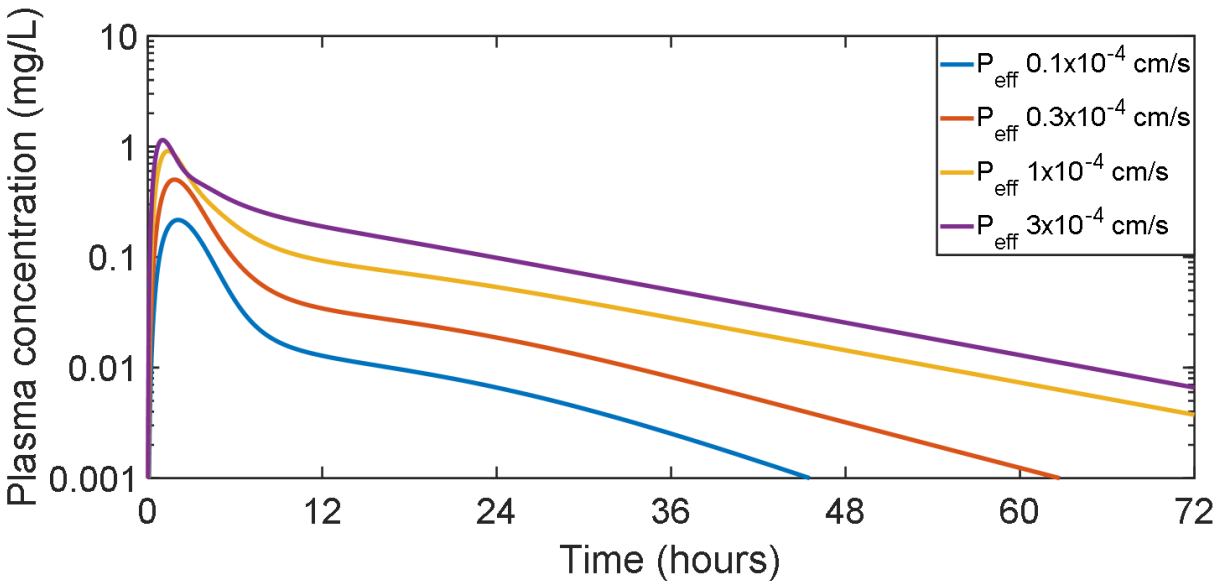
Plasma concentration (mg/L)
10
1
0.1
0.01
0.001
0
12
24
36
48
60
72
Time (hours)
P eff 0.1x10-4 cm/s
P eff 0.3x10-4 cm/s
P eff 1x10-4 cm/s
P eff 3x10-4 cm/s

B

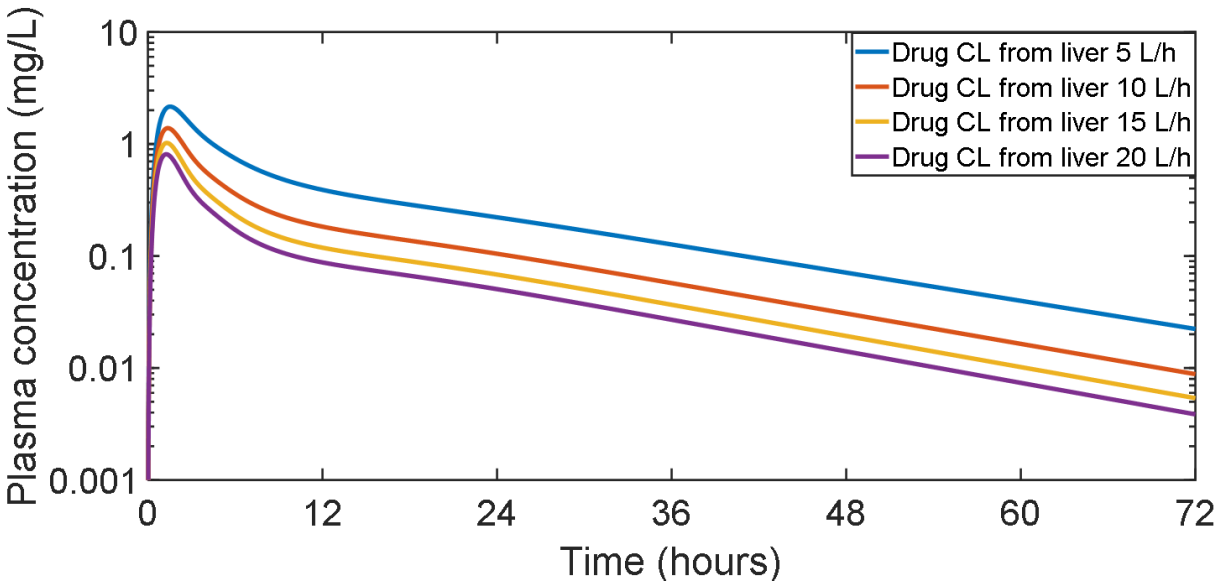
Plasma concentration (mg/L)
10
1
0.1
0.01
0.001
0
12
24
36
48
60
72
Time (hours)
Drug CL from liver 5 L/h
Drug CL from liver 10 L/h
Drug CL from liver 15 L/h
Drug CL from liver 20 L/h

C

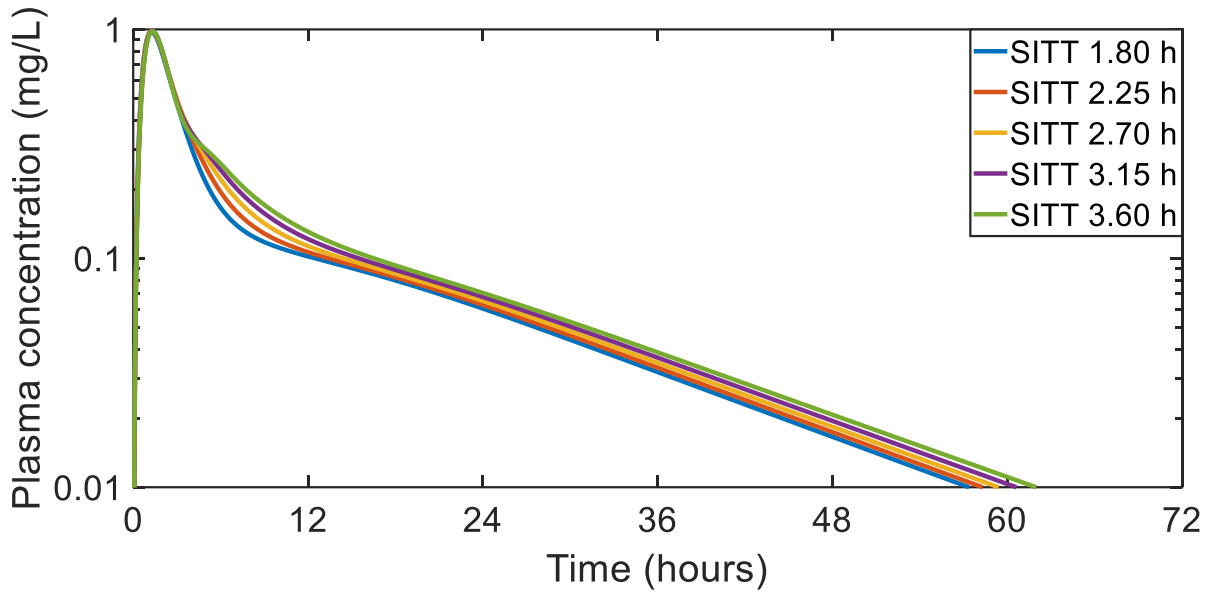
Plasma concentration (mg/L)
1
0.1
0.01
0
12
24
36
48
60
72
Time (hours)
SITT 1.80 h
SITT 2.25 h
SITT 2.70 h
SITT 3.15 h
SITT 3.60 h

D

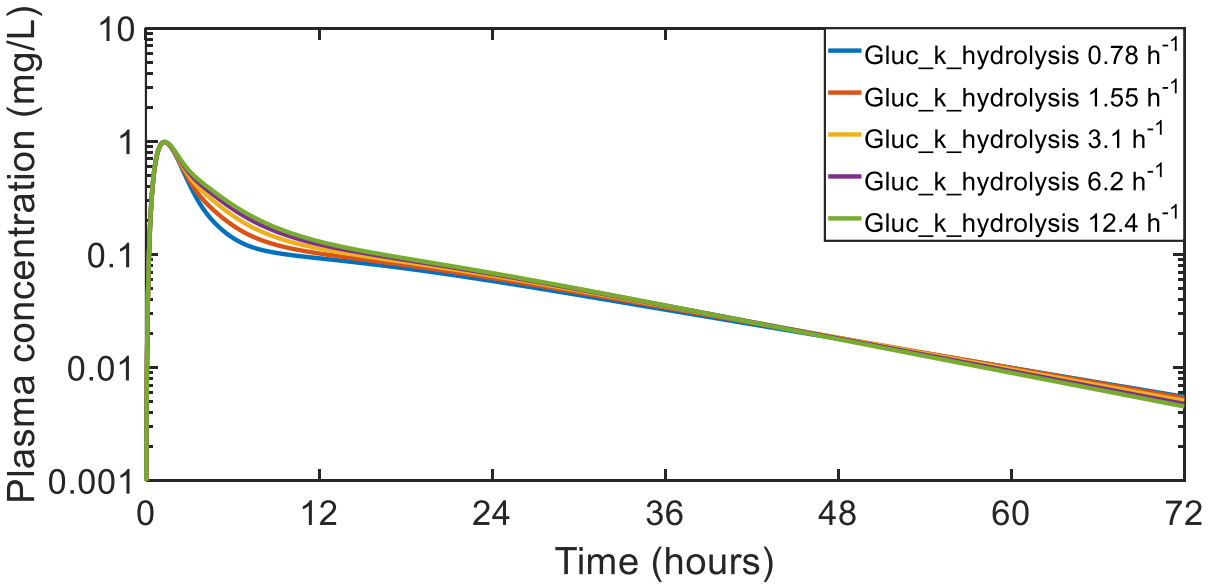
Plasma concentration (mg/L)
10
1
0.1
0.01
0.001
0
12
24
36
48
60
72
Time (hours)
Gluc_k_hydrolysis 0.78 h-1
Gluc_k_hydrolysis 1.55 h-1
Gluc_k_hydrolysis 3.1 h-1
Gluc_k_hydrolysis 6.2 h-1
Gluc_k_hydrolysis 12.4 h-1

E

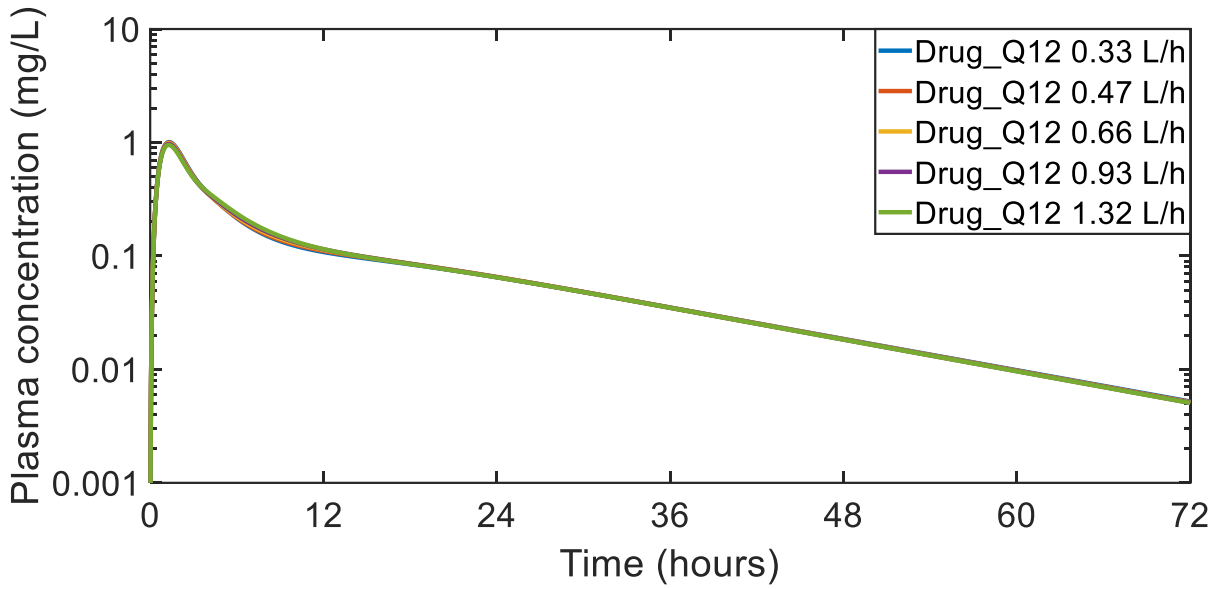

Supplemental Fig. 29. Additional sensitivity analyses for effects of parameters in the semi-physiologically based pharmacokinetic model on simulated maribavir plasma pharmacokinetic profile after a single 10 mg/kg oral dose. Parameters analyzed included (A) intestinal P_{eff}, (B) Drug_Liver_CL, (C) SITT, (D) rate of hydrolysis of maribavir glucuronides (Gluc_k_hydrolysis), and (E) intercompartmental drug clearance between the central and peripheral compartments (Drug_Q12).

SITT, small intestine transit time.

Supplemental References

Alsenz J and Haenel E (2003) Development of a 7-day, 96-Well Caco-2 Permeability assay with high-throughput direct UV compound analysis. *Pharm Res* **20:** 1961-1969.

Hamilton RA, Garnett WR, Kline BJ (1981). Determination of mean valproic acid serum level by assay of a single pooled sample. *Clin Pharmacol Ther* **29**(3):408-13.

Ikegami K, Tagawa K, Narisawa S, and Osawa T (2003) Suitability of the cynomolgus monkey as an animal model for drug absorption studies of oral dosage forms from the viewpoint of gastrointestinal physiology. *Biol Pharm Bull* **26:** 1442-1447.

Kim DH and Jin YH (2001) Intestinal bacterial beta-glucuronidase activity of patients with colon cancer. *Arch Pharm Res* **24:** 564-567.

Larregieu CA and Benet LZ (2014) Distinguishing between the permeability relationships with absorption and metabolism to improve BCS and BDDCS predictions in early drug discovery. *Mol Pharma* **11:** 1335-1344.

Li C, Liu T, Cui X, Uss AS, and Cheng KC (2007) Development of in vitro pharmacokinetic screens using Caco-2, human hepatocyte, and Caco-2/human hepatocyte hybrid systems for the prediction of oral bioavailability in humans. *J Biomol Screen* **12:** 1084-1091.

Olivares-Morales A, Lennernäs H, Aarons L, and Rostami-Hodjegan A (2015) Translating human effective jejunal intestinal permeability to surface-dependent intrinsic permeability: a pragmatic method for a more mechanistic prediction of regional oral drug absorption. *AAPS J* **17:** 1177-1192.

Peters SA (2012) Appendix A physiological parameters in preclinical species, in: *Physiologically-Based Pharmacokinetic (PBPK) Modeling and Simulations: Principles, Methods, and Applications in the Pharmaceutical Industry,* pp 408-413, John Wiley & Sons, Inc., New Jersey.

Sender R, Fuchs S, and Milo R (2016) Revised estimates for the number of human and bacteria cells in the body. *PLoS Biol* **14:** e1002533.

Sugano K (2012) Chapter 6.1.1 length and tube radius, in: *Biopharmaceutics Modeling and Simulations: Theory, Practice, Methods, and Applications,* pp 160, John Wiley & Sons, Inc., New Jersey.

Yu LX and Amidon GL (1999) A compartmental absorption and transit model for estimating oral drug absorption. *Int J Pharm* **186:** 119-125.